Controls on the development and distribution of K-feldspar megacrysts: Evidence from the Shap granitoid.

by
Richard A. Cox.

Thesis submitted for the degree of Master of Science (by research) at the Department of Geology and Applied Geology, University of Glasgow.

April 1994.

Declaration

The material presented in this thesis is the result of independent research undertaken by the author between October 1993 to April 1994, at the Department of Geology and Applied Geology, University of Glasgow. Any published or unpublished material from other works has been fully acknowledged in the text.

Richard A. Cox.

Acknowledgements

I wish to thank the following people;

My family Mum, Alison, Graeme, Grace, Alan, Andrene, Jim and Ann, for both financial and moral support throughout my academic career so far without which this project would never have happened.

Jenny, Jamie and Lindsay for many pleasant and not so pleasant hours of distraction.

Dr. Tim Dempster and Dr. Brian Bell, my supervisors, for suggesting the project and for their invaluable advice during its duration.

Bill Higginson, Dougie Turner and Murdo Mcleod, for technical assistance during the laboratory preparation and analyses, particularly during the mineral separation and A.A./A.E. analyses section of my work.

Pete Ainsorth, Dr. Colin Braithwaite, Robert MacDonald and Jim Gallacher for help during the S.E.M., C.L., microprobe and XRF investigations which form a large part of this thesis.

Douglas Mclean for his exceptional photographic skill.

Dr G. Rogers, Ann Kelly and Vincent Gallacher for assistance and advice while undertaking Rb/Sr isotope work at S.U.R.R.C. at East Kilbride.

Vojta Janousek for access to his extensive library of references.

Jeremy Preston, John Hughes and most of the post-graduate fraternity in the department for listening to long hours of "self-debate" while I was carrying out various parts of my project.

Contents

Declaration	page ii
Acknowledgements	page iii
Contents	page iv
Abstract	page vii
The occurrence of K-feldspar megacrysts in granitoids and associated rocks	page 1
1.1 Introduction	page 1
1.2 The characteristics of magmatic megacrysts	page 1
1.3 Evidence for porphyroblasts in granitic rocks	page 2
1.4 Megacrysts in enclaves	page 4
1.5 Megacrysts in country rocks	page 6
1.6 Evidence of K-feldspar megacryst growth from the Shap granitoid	page 7
The petrography of the Shap granitoid and K-feldspar megacrysts	page 11
2.1 Introduction	page 11
2.2 Basic petrographic description of the K-feldspar megacrysts in the Shap granitoid	page 13
2.3 Microscopic features of the Shap granitoid K-feldspar megacrysts	page 15
2.4 C.L. and S.E.M. imaging of the K-feldspar megacrysts	page 21
2.5 Petrography of the Shap granitoid matrix minerals	page 37
2.6 Basic Petrography of the megacrysts and matrix of the mafic enclaves of the Shap granitoid	page 42
2.7 Microscope observations on polished, etched and stained sections of K-feldspar megacrysts within the mafic enclave	page 45
2.8 C.L. and S.E.M. imaging of the K-feldspar megacrysts in the mafic enclave	page 48
2.9 Microscope observations on the enclave matrix and other crystals	page 49
2.10 Discussion	page 55
2.11 Conclusions	page 63

Electron-microprobe investigations of textures in the Shap granitoid megacrysts: some petrological implications page 65
3.1Introduction page 65
3.2 Chemical characteristics of oscillatory zones in the K-feldspar megacrysts page 65
3.3 Ternary growth and un-mixing of the K-feldspar megacrysts page 72
3.5 Discussion page 79
3.6 Conclusions page 84

Major-element, trace-element and Rb/ Sr isotope studies of the Shap granitoid to investigate K-feldspar megacryst distributions page 85
4.1 Introduction page 85
4.2 Shap Granitoid: A review of petrogenetic models page 85
4.3 Crystallisation, mixing and hybrid granitoid production page 86
4.4 Rb/Sr isotope analyses page 93
4.5 Discussion page 99
4.6 Conclusions page 100

The distribution of Li in the main minerals of the Shap granitoid and it's use as an indicator of H_2O influence on mineral growth page 102
5.1 Introduction page 102
5.2 H_2O in granitic melts: some general considerations page 102
5.3 The geochemical behaviour of Li page 103
5.4 Li in minerals page 104
5.5 The mobility of Li at lower temperatures page 105
5.6 Discussion of data page 106
5.7 The isotopic composition and distribution of Li page 110
5.8 Conclusions page 112

Interpretation of evidence page 114
Discussion and summary of conclusions page 114
A model for K-feldspar megacryst growth in the Shap granitoid magma page 116

Concluding statements page 119

Appendix I-Preliminary petrological techniques page 120
(i) Selection and preparation of samples page 121
(ii) Mineral separations and XRD analyses page 121
(iii) Petrographic examinations page 123

Appendix II-Analytical methods page 124
(i) Microprobe analysis page 125
(ii) Rb/Sr isotope determinations page 125
(iii) XRF major- and trace-element analyses page 128
(iv) A.A. and A.E. analyses page 128

References page 132

Abstract

The nature of the presence of K-feldspar megacrysts in granitoids and enclaves has been the source of much debate. Recent opinions hold that the presence of K-feldspar megacrysts in granitoids, are phenocrysts grown in magmatic conditions. The Shap granitoid, Cumbria, N.E. England, is an example of a (393Ma) late-Caledonian intrusion. Geochemical, isotopic and REE evidence suggests that the intrusion was emplaced with relatively little fractionation from a subduction generated melt. Structural evidence suggests that the intrusion was passively emplaced by relaxation of the end-Silurian stress field. Thus, the intrusion probably represents a near original magma composition, with fractionation and crustal contamination playing a minor role in determining the magma chemistry. The presence of K-feldspar megacrysts within the Shap intrusion, both in the granitoid, and also in the mafic enclaves which occur as xenoliths in the intrusion, provide an ideal opportunity to examine the processes controlling the development and distribution of these and also similar K-feldspar megacrysts in granitic magmas. Petrographic studies, using polarising microscope, C.L. and S.E.M. provide the basis for microprobe investigations and Rb/Sr isotope determination which show that the megacrysts were indeed formed as magmatic phenocrysts. The major- and trace-element and Rb/Sr studies show that the Shap is a hybrid granitoid and Li-distribution and isotopic composition along with petrographic and petrological studies indicate that the megacrysts grew in sub-solvus conditions with an increasing H_2O-content in the magma.

The occurrence of K-feldspar megacrysts in granitoids and associated rocks.

1.1 Introduction

The common occurrence of K-feldspar megacrysts in granitic rocks and the mafic xenoliths within granitoid intrusions (enclaves), and their reported presence in adjacent country rocks, has led to some debate as to their origin, and the conditions of their formation.

Generally, it is accepted that most K-feldspar megacrysts are formed as phenocrysts in granitic magmas (Vernon 1986). The presence of K-feldspar megacrysts in enclaves and country rocks, however, is still widely thought to point to solid-state growth (Didier 1973; Cantagrel et al 1984). Evidence, such as megacrysts transecting aplite boundaries, also suggests a similar formation in granites (Exley and Stone 1964). Thus, the investigation of K-feldspar megacrysts has either concluded that these crystals are phenocrysts or porphyroblasts.

1.2 The characteristics of magmatic megacrysts

The euhedral shape of most K-feldspars megacrysts is interpreted as evidence that they are of magmatic origin (e.g. Vernon 1986). Large, euhedral feldspar porphyroblasts are almost unknown (Vernon 1968). Thus, megacrysts which have mesoscopically euhedral shapes are much more likely to have formed as free growing magmatic phenocrysts. Simple twinning is extremely common in these crystals (Exley and Stone 1964; Kawachi and Sato 1978) which is in contrast to large metamorphic K-feldspar crystals (Vernon 1986).

Along with the predominantly euhedral nature of K-feldspar megacrysts, other textural features also point to a free-growing phenocryst origin. For example, both large scale core-to-rim, and oscillatory zoning, and zonally arranged inclusions, are all common in K-feldspar megacrysts. Mehnert and Busch (1981) and Bringham (1984) have shown that Ba generally decreases from core to rim in granitic megacrysts. This is often superimposed on finer Ba-rich and Sr-rich oscillations which are common in K-feldspar phenocrysts from volcanic rocks which have a definite igneous origin (Boettcher 1967) . Inclusions of quartz, plagioclase, biotite, hornblende, apatite, etc. are commonly aligned along these oscillatory zones, (Kawachi and Sato 1978; Bringham 1984) with the long axes of the inclusions parallel to the zone margin. Plagioclase inclusions are, themselves, often euhedral, zoned and contain biotite inclusions (Smith 1974). Groundmass crystals such

as biotite and plagioclase are usually much larger than the inclusions (Kawachi and Sato 1978) and are rarely aligned in a similar manner to the inclusions. This suggests that the inclusions are themselves magmatic and were trapped by the growing host crystal (Vernon 1986). Solid-state growth of the megacrysts would probably produce inclusions, within the megacrysts, of a similar nature in both size and orientation to the groundmass minerals, (Vernon 1986).

Megacrysts often show a strong foliation or alignment within granitoid intrusions. This alignment of megacrysts in their host granites has been ascribed to magmatic flow, (Mehnert 1968; Kawachi and Sato 1978; Le Bas 1982). This is the most likely explanation for the alignment of undeformed megacrysts, but does not rule out growth or alignment of the megacrysts in a stress field, in common with other minerals growing in metamorphic environments. Similar megacrysts to those which occur aligned in granite intrusions also occur in volcanic rocks associated with both the granite and shallow minor intrusions (Pitcher and Berger 1981; Mehnert and Busch 1981; Balducci and Leoni 1981). This association suggests that the crystals in the host granite are magmatic and thus, flow alignment is the most likely explanation for their preferred orientation.

If megacrysts display one or more of these features i.e. simple twinning, large scale core-to-rim and oscillatory zones, along with zonally arranged inclusions which are themselves of magmatic origin, and the presence of similar megacrysts in related volcanic or hypabyssal rocks, then a magmatic origin for such K-feldspar megacrysts is the most likely. Such features are not common in metamorphic K-feldspars (e.g. Vernon 1968). However, in some instances, megacrysts with these features occur in such unusual circumstances that an additional discussion is necessary to justify suggesting an igneous and not a metamorphic origin.

Evidence for porphyroblasts in granitic rocks

Stone and Austin (1961) provided descriptions of K-feldspar megacrysts cutting across the boundary of banded (layered) aplite veins and pegmatites in the Carnmenellis granite and the Tremearne complex, in western Cornwall. They note that perthitic megacrysts, which are subhedral to euhedral and up to 8cm long, with an average size range of 2-3cm, appear to cut across aplite vein boundaries. The megacrysts also contain inclusions of plagioclase, rounded quartz crystals and biotite. In some cases "saccharoidal patches of quartzo-feldspathic aplite matrix" with andalusite were present in the megacrysts. These were thought to represent matrix inclusions, trapped

by the sub-solid growth of the K-feldspar megacryst. Stone and Austin concluded that these crystals were the product of potash metasomatism. Exley and Stone (1964) noted that megacrysts cut across bands in aplite, and that the aplites have been locally distorted, due to the megacryst growth. They infer that megacryst growth was in the solid or near solid-state

Slightly different types of transgressing megacrysts have been reported in granitic rocks in the Thorr pluton, Donegal (Pitcher and Berger 1972) and the Kern Mountains, Nevada (Hibbard and Watters 1985). These megacrysts cut across the aplite veins in these intrusions, in a sub-parallel manner, rather than normal to the contact as in the Cornish examples. The aplites and mafic schlieren in these intrusions are not straight sided as in the Cornish aplites but rather irregular, indicating a very uneven fracture along which the mafic material was emplaced. However in both these examples magmatic, rather than solid state growth can account for the features described. The euhedral nature of large K-feldspar crystals, as stated previously, is not consistent with metamorphic growth (Vernon 1968). The small, often euhedral inclusions of biotite and plagioclase in the transgressing Cornish megacrysts (Stone and Austin 1961) are also more likely to represent magmatic trapping of the inclusions by a K-feldspar crystal that sub-solid replacement of the matrix by a porphyroblast. The deflected aplite layering attributed by Exley and Stone (1964) to the megacryst as it grew in the solid-state is unlikely, especially if the aplite is included in the megacryst, as represented by the saccharoidal patches in the K-feldspar crystals. The deflection of the layering by a megacryst projecting into the vein, as the aplitic magma flowed over, it is a far more acceptable explanation. The saccharoidal inclusions in this case simply represent small primary inclusions which are in fact common in magmatic K-feldspar phenocrysts (Smith 1974; Kawachi and Sato 1978; Mehnert and Busch 1981; Bringham 1984).

The fracturing of the granite when not completely crystalline, i.e. with a small proportion of the melt still present, would produce the uneven edges to the aplites observed by Pitcher and Berger (1972) and Hibbard and Watters (1985). The unconsolidated state of the granite during this fracturing would presumably allow some megacrysts to become detached and incorporated into the flowing aplite magma. Thus, the megacrysts in this instance can be explained in terms of magmatic processes, and are therefore xenocrysts within the aplite, and not porphyroblasts.

The fracturing of granite along crystal boundaries and the intrusion of aplite into incompletely consolidated granite is a preferable explanation for transgressing megacrysts, as these crystals display magmatic features

(euhedral shape, etc.). Also, the occurrence of megacrysts transgressing aplite and schlieren boundaries is rather uncommon. If these crystals had grown in solid state as porphyroblasts then transgression of aplite and schlieren boundaries would be a much more common feature in megacryst-bearing granitic intrusions.

Megacrysts in enclaves

An other argument for solid-state growth of K-feldspar megacrysts is that they often occur in enclaves within the host granitic body and occasionally are seen to cut across granitoid/enclave boundaries. These crystals are commonly regarded as porphyroblasts (e.g. Didier 1973; Cantagrel et al. 1984).

Enclaves in granitic intrusions, often referred to as mafic xenoliths, are thought to be either solid fragments of country rock, or "foreign" magmas which have been mixed with the granitic "host". This distinction is very important. Vernon (1986) pointed out that a great many so called metasedimentary xenoliths, when subjected to further examination were found to display features in common with micro-diorite or other mafic igneous rocks (e.g. Thomas and Smith 1932; Read 1942 and 1957; Perin 1954). Many authors have reported an absence of megacrysts within xenoliths of a sedimentary or metamorphic origin. For instance, Balducci and Leoni (1981) observed that gneiss and hornfels xenoliths, which were abundant in sanidine megacryst-bearing lavas from Tuscany, Italy, contain none of the sanidine crystals themselves. A similar observation for xenoliths in granites has been noted by Kleeman (1937) and Mehnert (1968). It would seem from these observations and the extensive review of a number of other examples by Vernon (1986), that megacrysts do not occur in country rock xenoliths, but only in enclaves of a magmatic origin.

Didier (1973) and Cantagrel et al. (1984) have described a hornfels xenolith transecting the margin of a micro-granitoid enclave (see **Figure 1.1**). The enclave contains megacrysts whereas the xenolith has none. This poses the question, that if the megacrysts in the enclave are porphyroblasts, then why are none present in the xenolith of sedimentary origin? The presence of metamorphic K-feldspars in sedimentary rocks is not uncommon. Therefore, it seems unlikely that the mafic enclave and not the sedementary xenolith should develope megacrysts. The overwhelming majority of the evidence would indicate that megacrysts only occur in enclaves of magmatic origin. These megacrysts are often similar if not identical to those in the host granite, being euhedral, twinned crystals (Vernon 1986) and exhibiting

normal and oscillatory zoning (Mehnert and Busch 1981). The presence of other host granitic crystals e.g. quartz and plagioclase (Vernon 1983) as well as megacrysts would point to the incorporation of these minerals as xenocrysts during the mixing of two magmas. This does not however explain the transecting of enclave boundaries by megacrysts e.g. Didier (1973), and Cantagrel et al (1984).

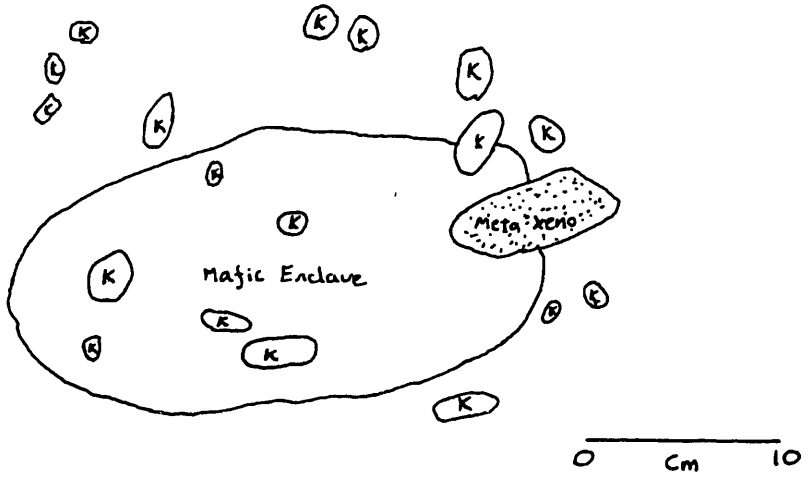

Figure 1.1. Sketch of K-feldspar megacryst and hornfels xenolith transecting the boundary of a micro-granitoid enclave (from Didier 1973). Note: the megacrysts are present only in the magmatic rock types.

The occurrence of crystals projecting from enclave boundaries into host granite, like megacrysts cutting aplite margins, is rather uncommon. Rare examples which have been identified (Didier 1973; Cantagrel et al. 1984) appear to provide evidence which supports a solid-state growth mechanism, similar to the aplite-transecting megacrysts. However, as a magma mixing event , resulting in xenocrysts of granitic phases becoming trapped in the enclave, require the enclave to be liquid, then solid crystals projecting from the enclave would not be totally unexpected. This is seen in mafic schlieren, etc. in the Thorr pluton, Donegal described by Pitcher and Berger (1972). The presence of solid metasedimentary xenoliths also projecting from enclaves (Didier 1973; Cantagrel et al. 1984, see Figure 1.1) confirms that solid fragments are capable of transecting enclave boundaries and thus, megacrysts, trapped by a globule of enclave magma show the same attributes i.e. they transect the enclave/host boundary.

It is clear that from the shape, zoning and cross-cutting relationships the megacrysts in granitic enclaves are likely to be of the same magmatic origin as the megacrysts of the host granitic intrusion.

Megacrysts in country rocks

The occasional occurrence of megacrysts in surrounding country rocks is the third argument often presented to support solid-state growth of megacrysts. These megacrysts are interpreted as porphyroblasts in metasedimentary schist (e.g. Turner and Verhoogan 1951; Smithson 1962; Cannon 1962; Wintsch 1975). Here, again, when the descriptions of these rocks and the K-feldspar megacrysts are scrutinised there is doubt about the validity of the sedimentary origin of the parent rock-type, and the solid-state growth of the megacrysts. The megacrysts described by these authors are euhedral, often simply twinned, and display magmatic zoning and inclusions. The matrix is often highly strained. Booth (1968) showed that matrices of Cornish granites are strained and that the megacrysts exhibit augen strain features, although their resistance to deformation is shown by the retention of euhedral shapes and the lack of strain deformation on the inclusions within the megacrysts. Vernon (1983; 1986) illustrated megacrysts which showed twinning and euhedral crystal form, and had rotation strain shadows, where the foliation of the granitic matrix was deflected by the megacryst, (see **Figure 1.2**).

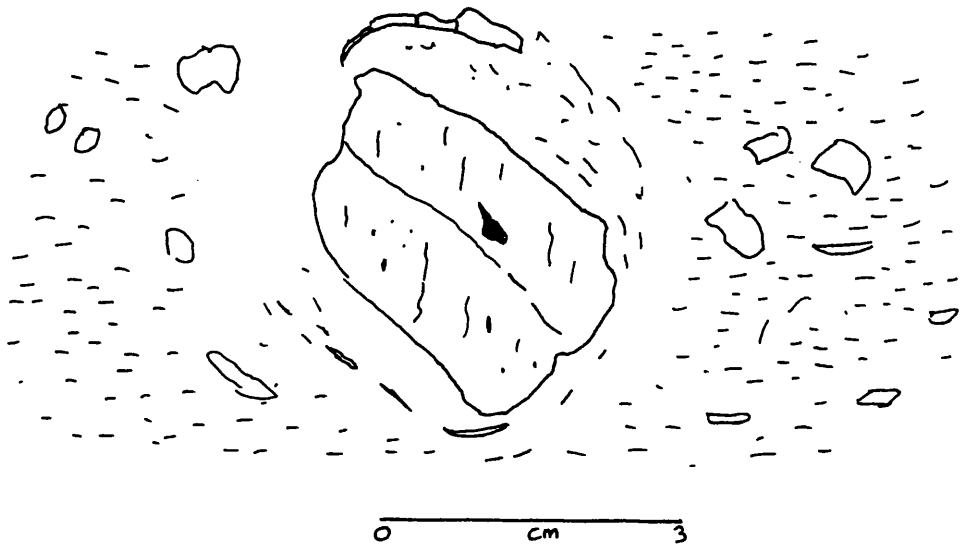

Figure 1.2. Sketch of polished slab of deformed granite from the Wologorong Batholith, N.S.W., Australia (Vernon 1983), showing the foliation deflected round the megacryst, when it was rotated in the stress field. This shows that the megacryst must have been solid when deformation took place.

In all of these cases the original rock type is of igneous (granitoid) origin. The lack of megacrysts in sedimentary wall rocks (Heald 1950; Sylvester 1964) and the clear evidence that the country rocks which do

contain megacrysts are strained (augen) granites, (Booth 1968; Vernon 1983; 1986) leads to the conclusion that the megacrysts represented in country rocks are strain-deformed phenocrysts and not porphyroblasts.

Evidence of K-feldspar megacryst growth in from the Shap Granitoid

The Shap granitoid is one of the most famous of the later Caledonian granitoids, in part due to a long history of quarrying of both the granite and the surrounding volcanic country rocks. Details of the field relationships and petrology of the Shap intrusion are presented by Harker and Marr (1981), and subsequently by Grantham (1926).

The intrusion occupies an area of about 2.5km by 2km much of which is covered by glacial boulder clay and till, and lies in the Westmoreland area of Cumbria, N.W. England, (**Figure 1.3**). It is intruded into Borrowdale Volcanic Group andesites which are often found as inclusions within the granitoid. The granitoid lies very close to the Ordovician/Silurian boundary and the sedimentary rocks of the Silurian Wenlock, (Brathay flags, Conniston grits) and the Ordovician Ashgill/Caradoc, (Coniston limestones) show contact metamorphism when near the granitoid. The intrusion has been described as a lens-shaped body with lateral density variation which corresponds to the different zones present, based on gravity survey data (Bott 1978).

The Shap intrusion has been described as an adamellite by Grantham using analyses carried out by Harwood, (in Grantham 1926) which showed that similar amounts Na_2O, K_2O and CaO were present. The general appearance of the rock is dominated by the presence of large euhedral to subhedral K-feldspar megacrysts. The megacrysts commonly display simple twinning and average 2-3cm in length, (along {001}). Harker and Marr (1891) suggested that the mafic inclusions of diorite, which also contain megacrysts, indicated that the Shap intrusion represented a residual acidic fraction from a basic magma. This implied that the megacrysts were of magmatic (phenocryst) origin. This view was supported by Grantham (1926) when he noted that the K-feldspar megacrysts in the main body of the intrusion are commonly aligned, suggestive of flow in a magmatic environment. The Shap megacrysts occasionally have mantles which could either be of magmatic origin e.g. (Hibbard 1991) or may be a strain deformation effect (e.g. Debat et al. 1978). Boulter and Soper (1973) discussed structural data from country rocks and the Shap and Skiddaw intrusions, and concluded that the Shap granitoid was intruded during the last stages of "end-Silurian" cleavage

formation. Therefore, the resulting orientation of the megacrysts may be partly produced by this stress field.

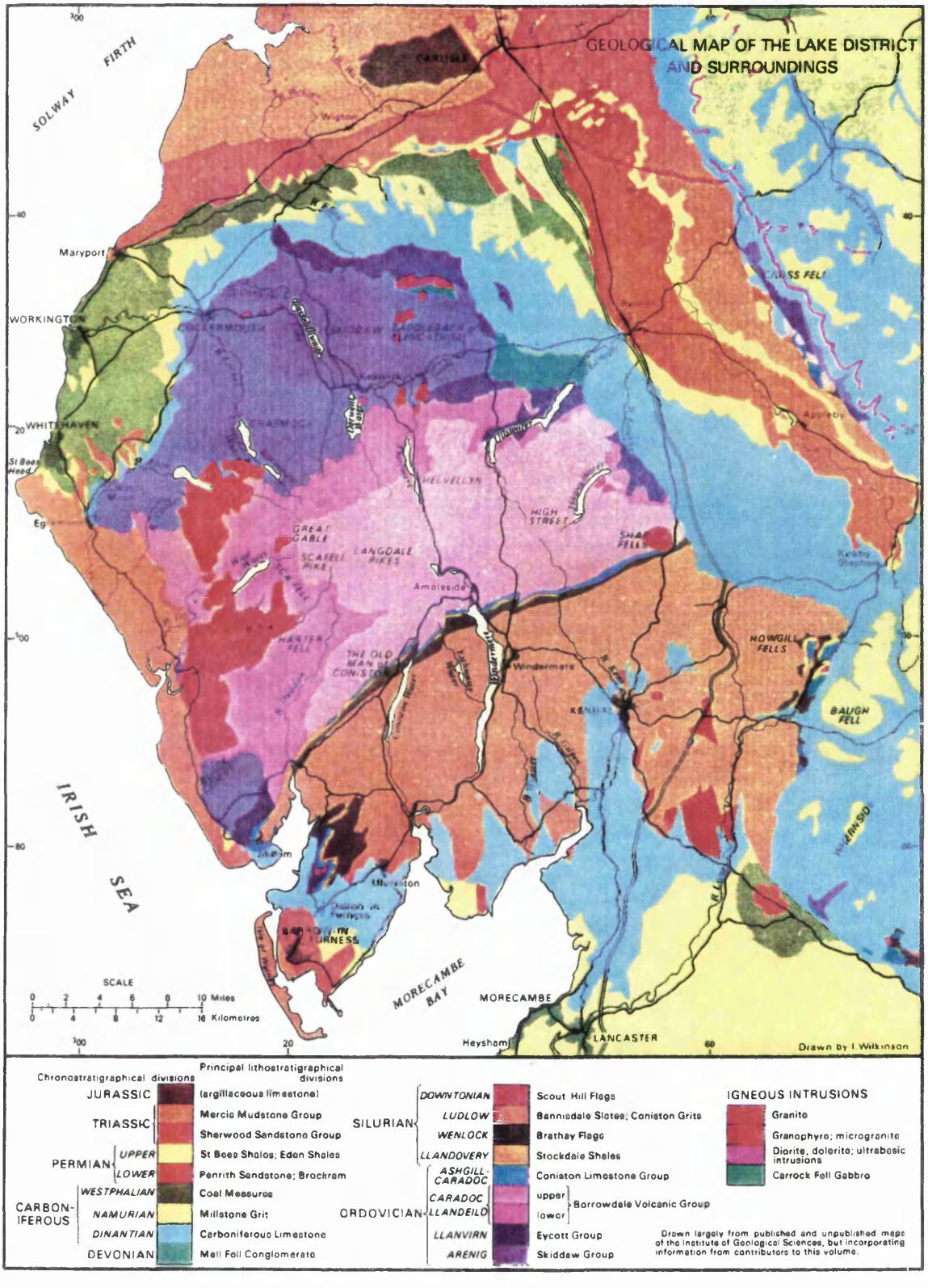

Figure 1.3. Geological map of the Shap granitoid locality (from Moseley 1978).

Grantham (1926) described the extensive pneumatolysis of the intrusion, which is generally concentrated along joint faces. The analysis by Harwood (in Grantham 1926) of the main Shap granitoid showed that Li_2O was present in fairly substantial amounts, which often indicates that pneumatolysis has taken place (Turner and Verhoogan 1960). A study of these processes carried out by Firman (1957), suggested that epidote and garnet which occurs in fissures in the country rocks surrounding the Shap intrusion, derived Ca and Fe from the granitoid. He also concluded that percolating fluids, rich in Si, K, CO_2, "hydrothermal ions", along with the Ca and Fe also caused potash metasomatism and silicification at the granitoid/country rock contact. Spiers (1961) carried out a survey of radioactivity in the Shap intrusion and found that despite making-up only 2% of the intrusion, 90% of the α-particle radiation was concentrated in the late-stage and accessory minerals, (see **Figure 1.4**).

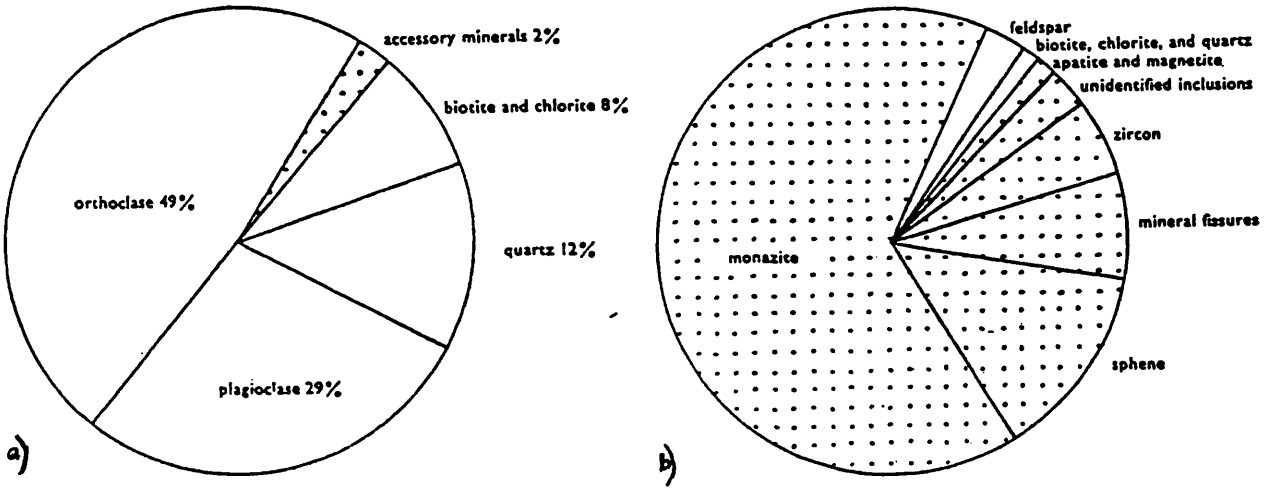

Figure 1.4. The distribution of α-particle radiation in the minerals of the Shap intrusion, from Spiers (1961), with a) the area occupied by the minerals in the sections analysed and b) the distribution of α–particle radioactivity in the sections.

It is evident that the Shap intrusion underwent prolonged cooling and possibly fluid partitioning. This may have caused the distribution pattern of the hydrothermally mobile elements described by Firman (1957) and Speirs (1961). In conclusion, during its history, both high temperature magmatic processes and lower temperature water/rock reactions are evident within the Shap intrusion.

The aim of this study is to examine the K-feldspar megacrysts of the Shap intrusion in a detailed petrographic and geochemical study, to

determine the main controls on the growth and distribution of these crystals in the Shap granitoid. This will hopefully place constraints on the models suggested for the growth and distribution of K-feldspar megacrysts in granitic rocks in general.

The petrography of the Shap granitoid and K-feldspar megacrysts

2.1 Introduction

Grantham (1926) described in detail the main divisions of the Shap granitoid intrusion, building on the earlier work of Harker and Marr (1891). Grantham divided the Shap body into three main mass types; Stage I, which lies to the west of the quarry and is transgressed by the other rocks of the intrusion. It contains only about 15% of porphyritic K-feldspar megacrysts. Stage II, which occupies about 25% porphyritic K-feldspars, which are often aligned. The appearance of this under the microscope and the analysis of the rock by Harwood (Grantham 1926) shows that it is very similar in composition to Stage I. Stage III, occupies a large dyke-like body which cuts through both Stage I and Stage II. It has over 50% K-feldspar phenocrysts. The groundmass is coarser grained than either Stage I or Stage II. In addition to the main mass types, Grantham describes the occurrence of an early basic type of granitoid which occurs as xenoliths and in small outcrops which are surrounded by the other granitoid types.

The main deduction that can be drawn from Grantham's descriptions is that the phenocrysts and groundmass were able to grow longer or faster, in the later stages of the intrusion, hence the increase in grain size and abundance of phenocrysts from the Stage I to Stage III granitoids. Grantham also described the minor intrusions within the granitoid as schlieren, aplites and coarse pegmatites.

The schlieren are streaky in appearance, with an extremely biotite-rich matrix. The aplites, which can be seen cutting the schlieren, have a more acid composition, similar to the granitoid and have very sharp contacts with the host rock either the schlieren or the granitoid. The schlieren almost certainly represent the remains of an intrusion into a poorly consolidated granitic host, whereas the aplites with have straight contacts (**Figure 2.1**) and were probably emplaced by fracturing of an almost solid body, i.e. the host Shap intrusion. The presence of K-feldspar megacrysts, in both the schlieren and aplites, is explained by Grantham (1926) as "floated off wall rock" and he also states that such a process "can be seen in operation". Small K-feldspars within the aplite intrusions are thought to be indigenous to the aplite magma.

The occurrence of megacrysts in the enclaves as well as the host Shap granitoid has been described as the result of magma mixing, (Harker and Marr 1891). They pointed to the adamellite composition of the Shap granitoid as showing a dioritic affinity. The enclaves were thought to be the result of re-

mixing of an early, more mafic fraction of the intrusion with the host granitoid which also accounts for K-feldspar megacrysts within them.

Figure 2.1. Photo of aplite/granite contact on a sliced rock sample. Scale shown is in mm's.

The lack of K-feldspar megacrysts within the country-rock xenoliths (Harker and Marr 1891; Grantham 1926), supports the idea that magma mixing rather than the porphyroblastic growth occurred to account for the presence of the megacrysts within the enclaves. Grantham however was of the opinion that the different shapes and textures displayed by the megacrysts, and altered nature of the dioritic xenoliths, pointed to a metamorphic growth for the megacrysts in these xenoliths.

By looking at the petrography of the K-feldspar megacrysts, and other petrographic features, of both the host granitoid and dioritic enclaves in the Shap intrusion, a possible origin for these crystals may be discovered.

2.2 Basic petrographic description of the K-feldspar megacrysts in the Shap granitoid.

The examination of the Shap megacrysts in this study focused on those in the Stage II granitoid as this part of the intrusion occupies 90% of the mass of the Shap intrusion.

The Stage II Shap granitoid has 25-30% K-feldspar megacrysts with a matrix of approximately equal amounts of quartz, K-feldspar and albitic plagioclase, with smaller amounts of biotite and accessory apatite, calcite and other minerals. The crystal properties i.e. shape, size, twinning and orientation of the K-feldspar megacrysts were assessed using a large flat slab of the Stage II granitoid (**Figure 2.2**).

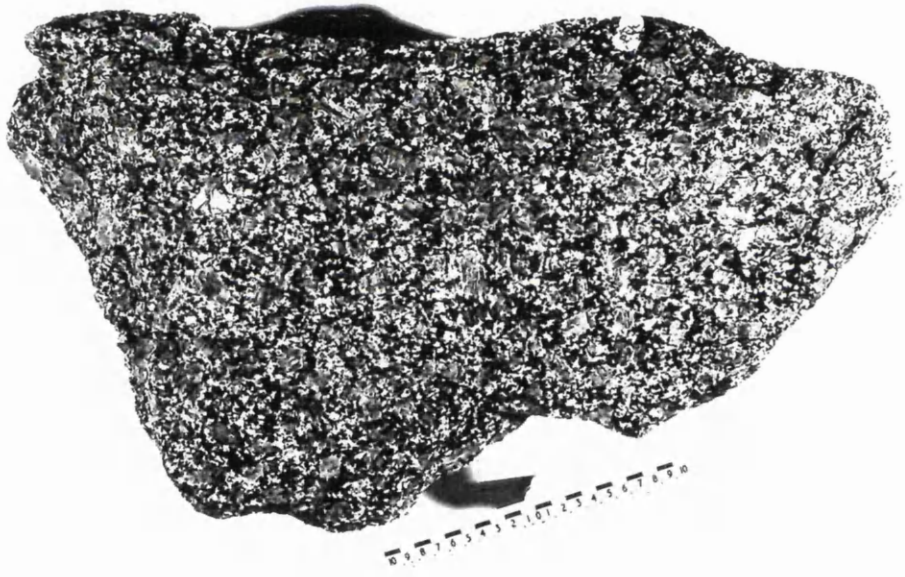

Figure 2.2. Photograph of the slab of Stage II Shap granitoid rock from which the size, shape, twinning and orientation of the megacrysts was assessed.

The slab was photographed as shown above but on to an A3 sized print and the crystal shapes traced onto a computer, using a digital tablet. The photograph was used to identify the features which were examined, and the digital images were illustrated accordingly. Comparisons were then made to assess any correlation between the shape, size, etc. of the K-feldspar megacrysts in this representative sample.

(a)

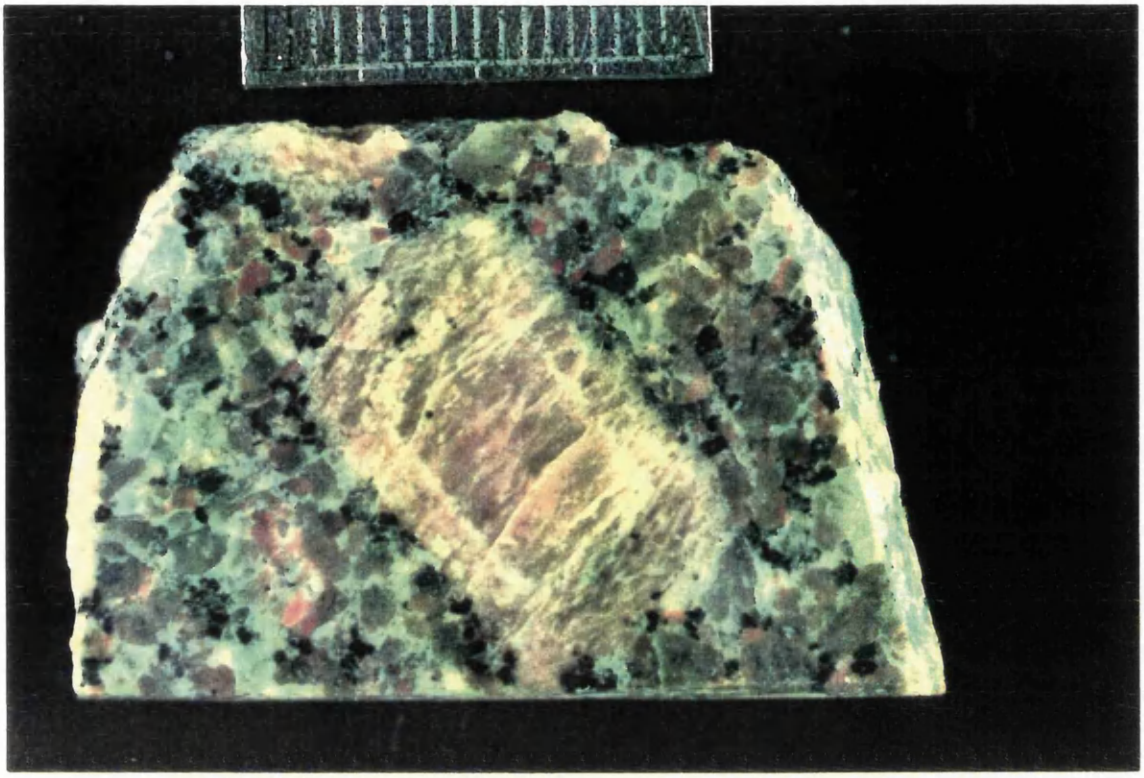

(b)

Figure 2.4. Photographs of sliced **(a)** euhedral, and **(b)** subhedral K-feldspar megacrysts showing zones and zonally arranged biotite (black) inclusions. Note the truncation of the zone against the crystal edge in the subhedral type.

	Euhedral	Subhedral
Shape	49%	51%
Grain size		
0-1cm	3%	4%
1-3cm	20%	21%
>3cm	77%	75%
Twinned crystals	68%	72%
Oriented crystals	71%	14%

Table 2.1. Table of data obtained by digital image analyses of slab of Shap (Stage II) granitoid from the photograph (**Figure 2.2 & 2.3**).

From the table of data (**Table 2.1**) it would appear that general crystal shape, is unrelated to the size or twinning of these megacrysts. In other words these two mesoscopic features of the K-feldspar megacrysts, which relate to magmatic growth (Vernon 1986), are not related to the production of subhedral megacrysts. However, euhedral crystals are much more likely to be oriented along their {001}-axis than subhedral crystals. It may be that the orientation of the megacrysts and shape of the crystals are in some way linked.

The megacrysts, particularly the ones with euhedral forms, often show one very prominent oscillatory zone, round the centre of the crystal, when sliced (**Figure 2.4**). Occasionally small biotite inclusions are visible, normally arranged around this zone. The subhedral megacrysts show an oscillatory zone and similar small biotite inclusions, but very often these zones are slightly truncated against, or restricted to, the rim of the megacryst, (**Figure 2.4(b)**).

The slight truncation of the zones and random orientation of subhedral megacrysts suggests that a dissolution process may be involved in controlling the euhedral or subhedral shape of these crystals. If such a process was magmatic then most megacrysts would be expected to show zone truncation. The similar percentages of twinned megacrysts of each shape and the similarity in grain size distribution may indicate that for the most part the growth conditions for all the megacrysts were the same. All the megacrysts examined as sliced pieces show a coarse, often turbid appearance, with small K-feldspar sub-grains, outlined by light coloured K-feldspar, near the rims of the megacrysts, often visible.

2.3 Microscopic features of the Shap granitoid K-feldspar megacrysts

Under a petrological polarising microscope, with crossed-polars, and either x5 or x10 magnification a number of textures and features in the Shap

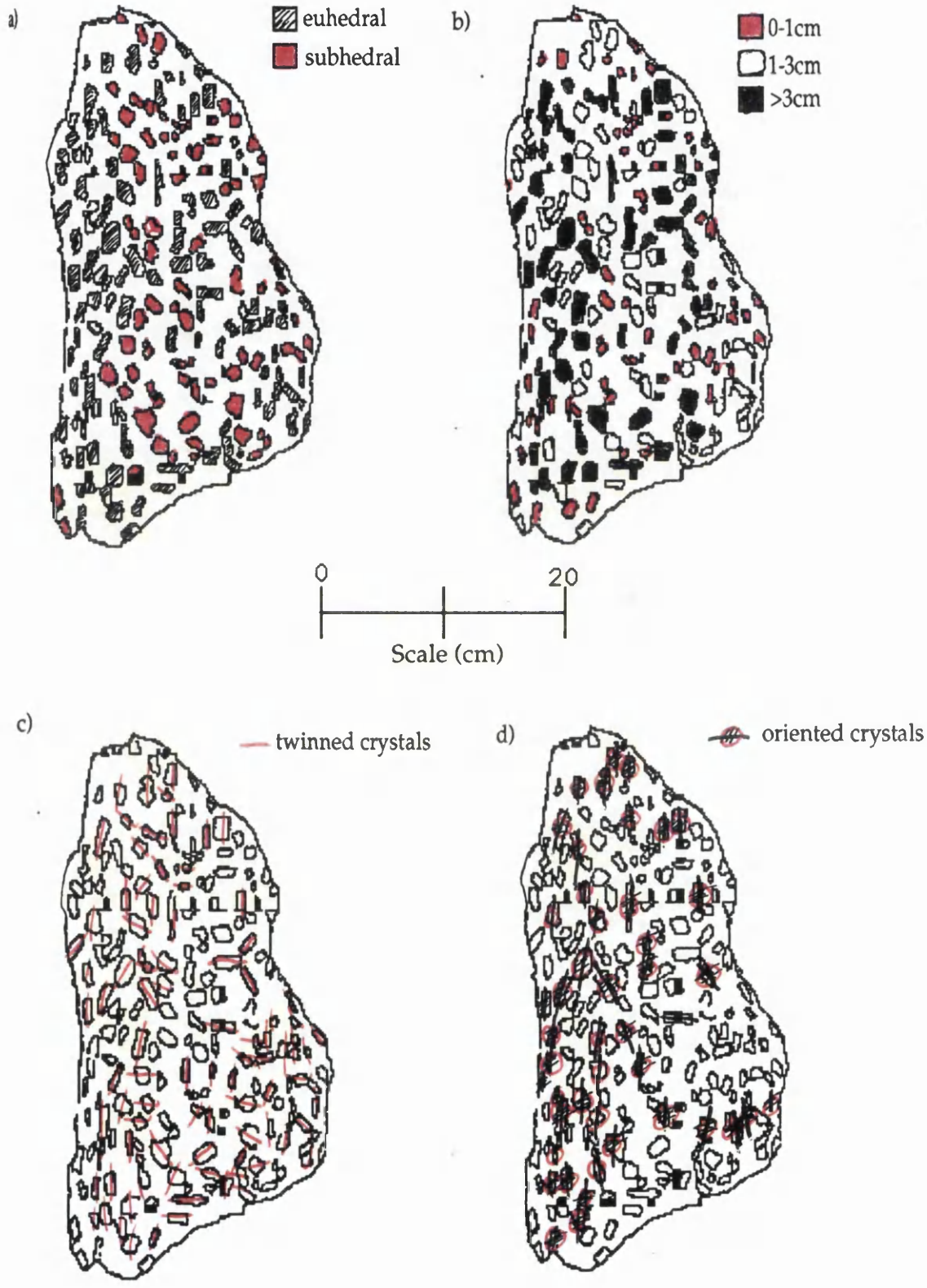

Figure 2.3. Digital images of a slab of Stage II, Shap adamellite, showing the relative proportions of a) euhedral and subhedral megacrysts, b) size of the megacrysts, (along {001}), c) twinned megacrysts and d) megacrysts which are oriented within 30 degrees of the vertical direction of the image along the main {001} axis.

megacrysts can be seen. Apart from the general crystal shape, twinning and zoning which was observed in the large slab and slices (**Figures 2.2, 2.3, and 2.4**), it is obvious that the K-feldspar megacrysts are not optically continuous i.e. different parts of the megacrysts go into extinction at different positions. This is due to a) twinning, b) zoning, c) inclusions, d) perthites and e) sub-grains.

(i) zoning

There would appear to be three different types of zoning in the in the K-feldspar megacrysts. The first of these, is the oscillatory zones observed in the sliced crystals (**Figure 2.4**). These vary from mostly, extremely fine to approx. 0.1mm thick, and appear to run continuously round the megacryst, mirroring the euhedral nature of the crystal. They also seem to be truncated against, or refracted by, the sub-grains of K-feldspar within the megacrysts (**Figure 2.5**).

The second type of zoning present can be observed by the different extinction positions of the crystal from core to rim, which is independent of the fine oscillatory zones present. This may indicate a larger scale zoning from core to rim, (Mehnert and Busch 1981; Gribble and Hall 1985; MacKenzie et al. 1987).

The third form of zoning is seen as higher birefringence patches of K-feldspar (apart from the oscillatory zoning), which give the megacrysts a coarse, patchy appearance, when under crossed polars. The higher generally silvery/grey, first order, birefringence colours, tend to be concentrated along cracks and coarse, irregular perthites which are common in the megacrysts.

(ii) inclusions

All the megacrysts have numerous inclusions of plagioclase, biotites and some quartz, generally increasing in both size and quantity from the core outwards. The long axes {001} of the inclusions, particularly of the plagioclase inclusions, are often aligned parallel to the oscillatory zoning (**Figure 2.6**). Invariably the inclusions have a high birefringence zone surrounding them, with similar optical properties to the patchy zones around the coarse perthites. The plagioclase inclusions often showed multiple twins but zoning within them was not observed. Biotite inclusions were chloritised to some extent, although this seemed to be less than in the surrounding matrix biotites. Grantham (1926), pointed to the lack of quartz inclusions within the Shap K-feldspar megacrysts as evidence that the quartz phase of growth of the granitoid was a late event in the crystallisation history of the intrusion. However, small quartz crystals are indeed present along the inner oscillatory

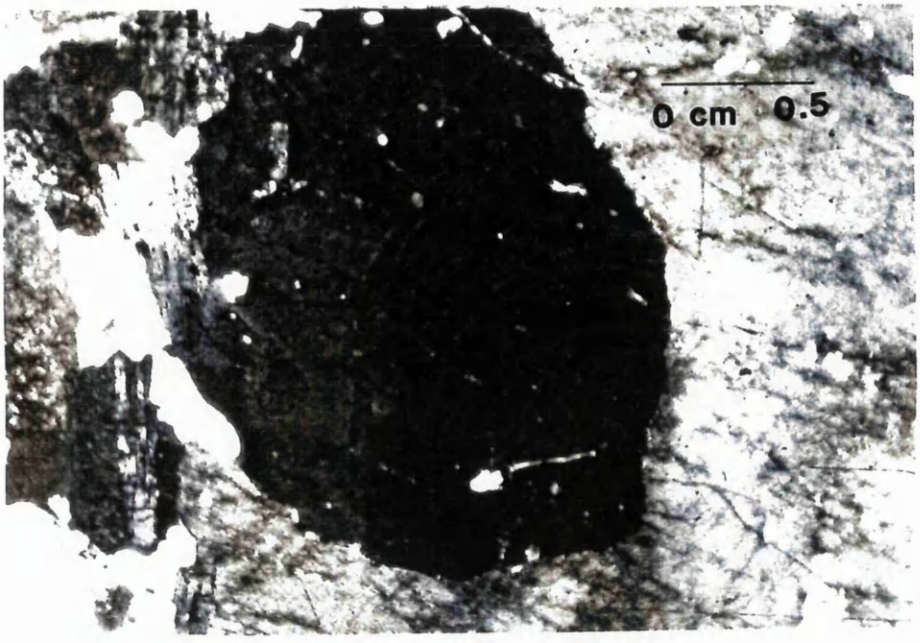

Figure 2.5. Xpls photomicrograph of a K-feldspar megacrysts from the Shap granitoid. The presence of sub-grains of K-feldspar within the host megacryst can be seen with fine oscillatory zones also visible. The presence of a coarse perthite can be seen cutting across the crystal, zoning and sub-grain boundaries. The zoning refracts or truncates against the sub-grain/host crystal boundary edge. A high birefringence rim can be seen surrounding the sub-grain.

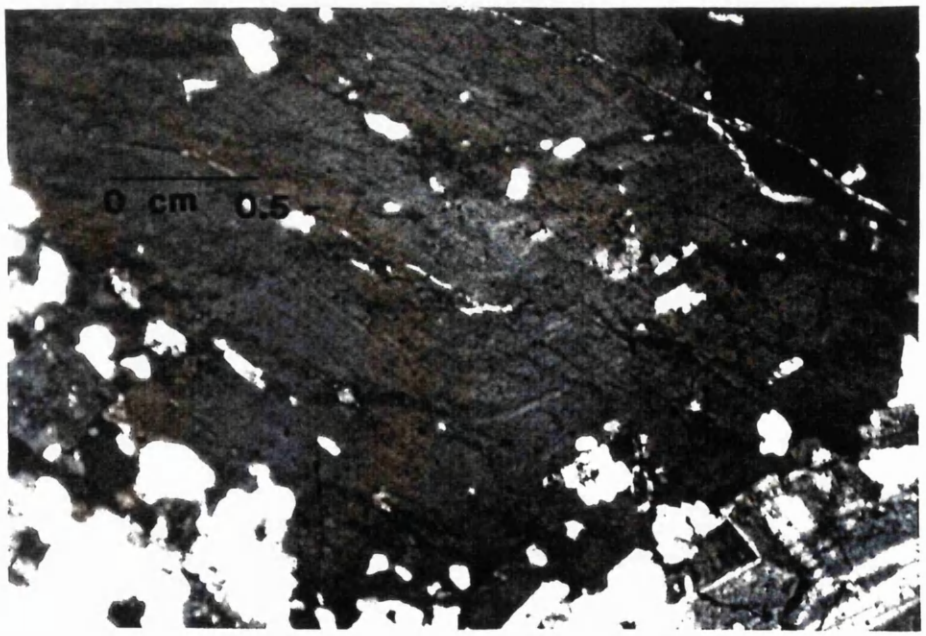

Figure 2.6. A K-feldspar megacryst showing similar zones and sub-grain features to the crystal in **Figure 2.5**, but note also the zonally arranged inclusions in the megacryst.

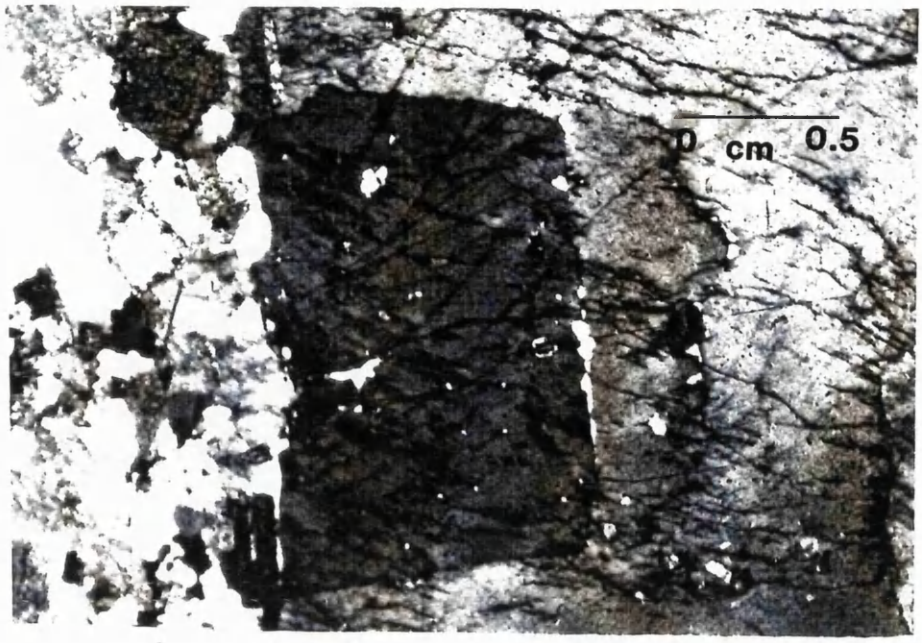

Figure 2.7. A K-feldspar megacryst from the Shap granitoid showing a euhedral sub-grain of K-feldspar with oscillatory zoning just visible. The coarse perthites are also apparent in the section. Note the presence of biotite and plagioclase inclusions at the sub-grain/megacryst boundary.

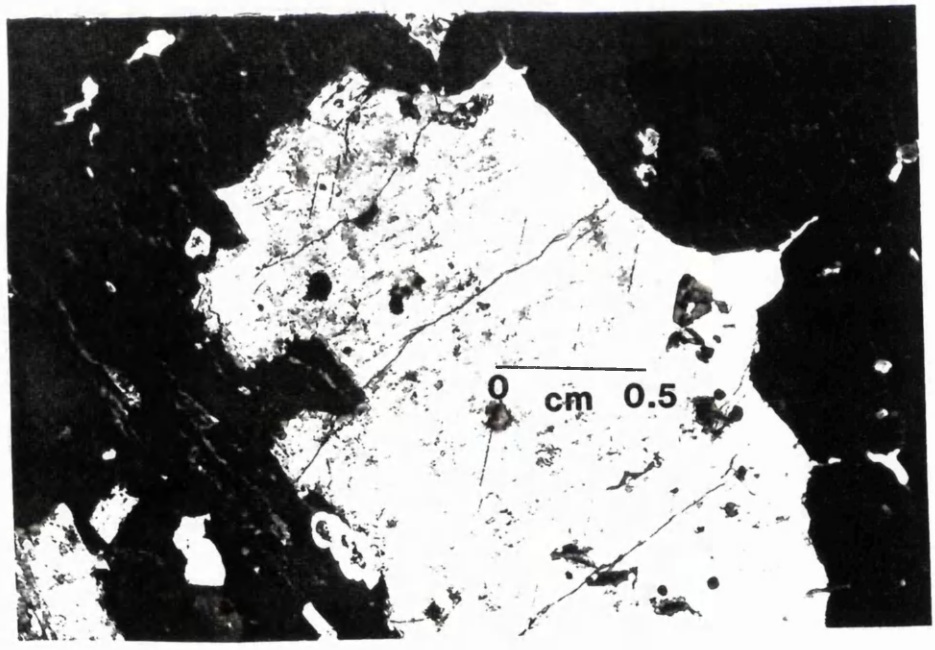

Figure 2.8. An anhedral sub-grain of K-feldspar within a megacryst. Note the high contrast in extinction angles giving a bright birefringence for the sub-grain while the host crystal is in complete extinction. A high birefringence rim surrounding the sub-grain is also apparent. The perthites of the sub-grain are normal to the perthites in the host megacryst.

zones and core regions of most megacrysts. These quartz inclusions are generally well formed and would appear to be primary rather than the result of secondary processes. Some small inclusions mostly of apatite, are noticeably absent from the core regions of the megacrysts. All the megacryst inclusions, although displaying magmatic characteristics such as euhedral shape and zonal alignment are smaller than their matrix equivalents. This indicates a shorter growth period for the inclusions before they were trapped by the growing megacryst.

(iii) perthites

The megacrysts also show evidence of two perthite exsolutions under the microscope. With low power magnification (x5) a coarse relatively regular perthite fabric which cuts sub-grain boundaries and is variably continuous to the edge of the megacryst is apparent (**Figures 2.5, 2.6, 2.7, & 2.8**). This perthite exsolution appears parallel to {001}-face of most of the megacrysts. Under much higher (x10) magnification, a very fine crypto-perthite is present. The size ranges of these two different types are of a sub-1mm scale for the coarse micro-perthites and appears to be only 10's of μm's for the crypto-perthites. The orientation of the crypto-perthites is similar to the micro-perthites, but is far more regular and cuts the boundaries of the boundaries of the sub-grains and the micro-perthites in all the megacrysts. Both these perthites would appear to be generally albitic in composition but accurate extinction angle determination is almost impossible due to the rather fine scale of these micro -textures.

(iv) sub-grains;

Another feature of the megacrysts, which was apparent in sliced specimens, is the presence of K-feldspar sub-grains within the megacrysts. These range in shape from euhedral to subhedral and in orientation, with most showing similar extinction angles to the main megacryst (**Figures 2.5 & 2.7**), but some are obviously in a different orientation This is shown by the different extinction angles of these sub-grains and the coarse perthites (which have {011} orientation), running almost at right angles to the coarse perthites in the host megacryst (**Figure 2.8**). The oscillatory zoning which is visible in these crystals can be seen to pass with a slight distortion through the boundaries of most of these sub-grains (**Figures 2.5 & 2.7**), although this feature seems to be restricted to those sub-grains which are euhedral and/or those which have a similar orientation to the main megacryst. The sub-grains are

often quite large in comparison to the inclusions of plagioclase, quartz, etc. and are almost exclusively restricted to the rim areas of the megacrysts.

To help determine the nature of the sub-grains within the megacrysts, a measurement of their orientation in relation to the host crystal was made, using a U-stage microscope, and following the extinction method to find the angle of the {001} axes of both megacryst and sub-grains in a number of these crystals. The results of these measurements are shown in the Wulf stereo-net orientation diagram shown below (**Figure 2.9**).

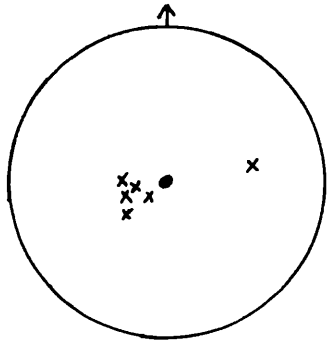

Figure 2.9. Wulf stereo-net orientation diagrams showing the orientation of the {001}-axes of both the host megacrysts and associated sub-grains.

Most of the sub-grains are in relatively close orientation to their host megacrysts (**Figure 2.9**), despite showing different extinction angles. The presence of a high birefringence rim to the sub-grains, in both oriented and non-oriented types, is a common feature (**Figure 2.5, 2.6, 2.7, 2.8**). This appears to be similar in nature to the coarse, micro-perthites and cracks which appear in the main megacryst. The plagioclase present within these areas is generally albitic in nature with quartz also present. This change from K-feldspar crystals to sub-grained boundaries may well mark a change in growth conditions of the megacrysts.

2.4 C.L. and S.E.M. imaging of the K-feldspar megacrysts

(i) C.L. imaging

Cathodo-luminescence and back-scattering S.E.M. microscopy greatly enhance many of the features of the K-feldspar megacrysts, observed under the polarising microscope, described above. C.L. in particular enhances the large scale core-to-rim zoning and the oscillatory zoning, inclusions and areas of secondary calcite infill along cracks.

The method involves using an incident beam of electrons aimed at the surface of a polished section, which causes activation of the electrons within the atoms of the section to higher energy states. On return to lower energy states, these electrons emit photons of light which are seen as the observed luminescence colours. Mariano et al. (1973) used doped plagioclase crystals to show the colours produced by trace element activators. Plagioclase can accept sufficient quantities of all the activator elements (**Table 2.2**) and therefore, can emit all the colours shown, whereas K-feldspars were showed either blue (Ti^{4+}, Cu^{2+}) or red (Fe^{3+}), (Mariano 1983). Quartz is often observed to change colour during a short period of bombardment (Marshal 1991), and for the purposes of this study is useful only in differentiating between the smoky quartz C.L. colours and the black, non-emitting biotite.

Activator	Colours	Minerals
Ti^{4+}	Blue	Quartz, K-feldspar, Plagioclase
Mn^{2+}	Green-Yellow	Plagioclase
Fe^{2+}	"	Quartz, Plagioclase
Fe^{3+}	Red	Quartz, K-feldspar, Plagioclase
Cu^{2+}	Blue	K-feldspar, Plagioclase

Table 2.2. C.L. activator elements and associated colours and minerals.

Accessory minerals, calcite and apatite, showing orange and yellow C.L. colours respectively, can also be clearly seen in the sections. Calcite identification was used mainly in finding areas to avoid when analysing using the electron microprobe or when removing samples from the thin slices for Rb/Sr isotope measurements.

Figure 2.10 shows a single megacryst, 1.2cm by 0.75cm in size, which was photographed at x6.5 magnification using the C.L. technique described above. One of the most striking features of the zoning, which oscillates from pale to bright blue in colour, is the presence of both regular and disrupted oscillatory zones. These zones show as the brightest blue in the crystal and appear to run concentrically around the megacryst and seem to be the same oscillatory zones as those observed in transmitting light (**Figures 2.5, 2.6, 2.7, 2.8**). The disrupted zones (**Figure 2.10(a)**), are generally much wider than the regular oscillations. The regular zones are common showing up as a sudden increase in colour intensity, then decrease to normal blue colour, whereas the disrupted zones are sparse. In both **Figure 2.10(a)** and **Figure 2.11(a)** the crystals show one very large disrupted irregular zone, which shows a sudden increase in brightness followed by a gradual change to the background colour. This

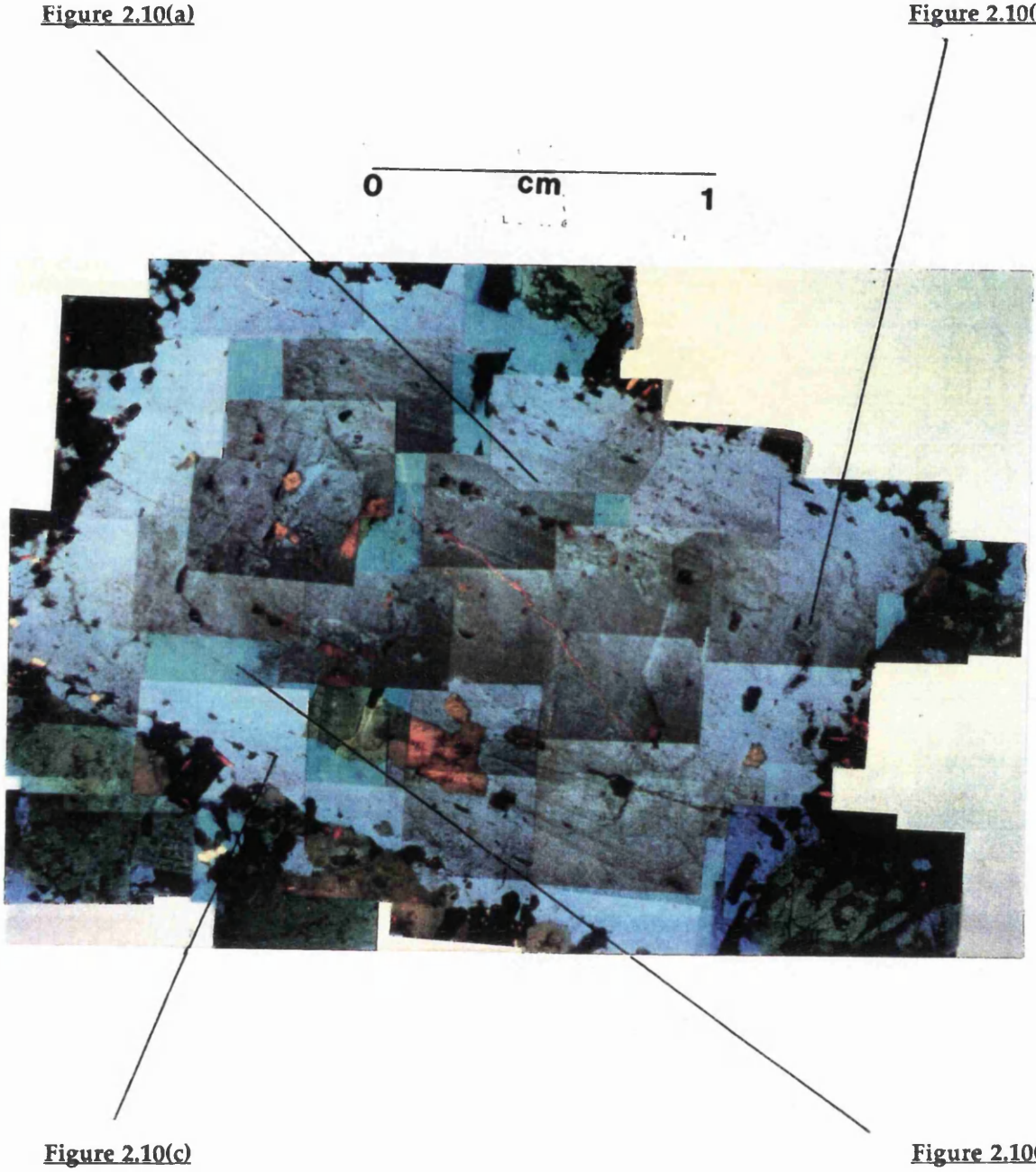

Figure 2.10. A photographic reduction of a C.L. montage of a megacryst and surrounding matrix from the Shap granitoid. The positions of the full-sized reproductions are shown (**Figures 2.10(a-d)**). Note the blue (Ti^{4+} activator) colours of the K-feldspars and green (Mn^{2+} or Fe^{2+} activators) colours of the plagioclase inclusions and matrix crystals. The biotites are generally black and the quartz crystals are dull colours giving a smoky appearance.

(a)

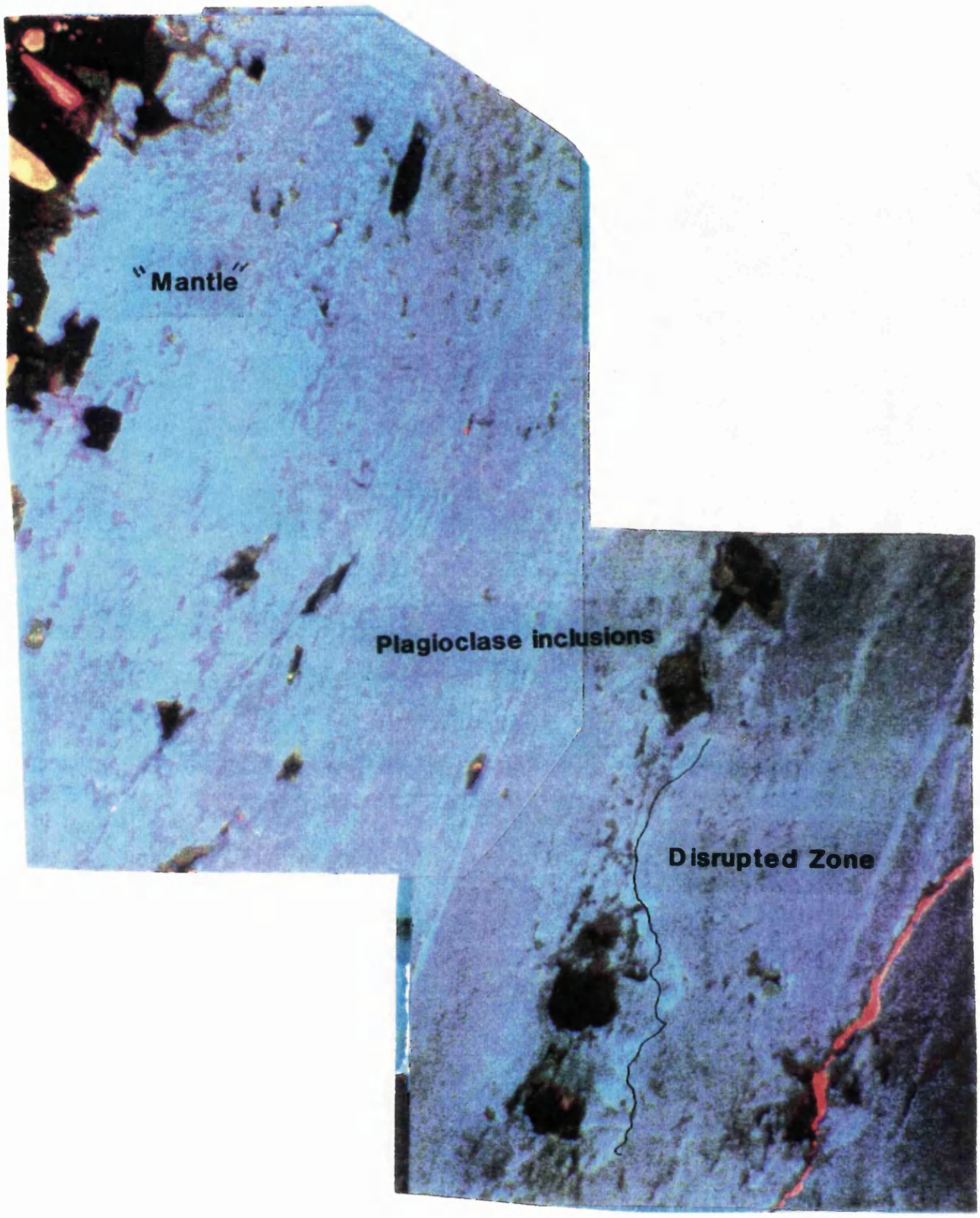

(b)

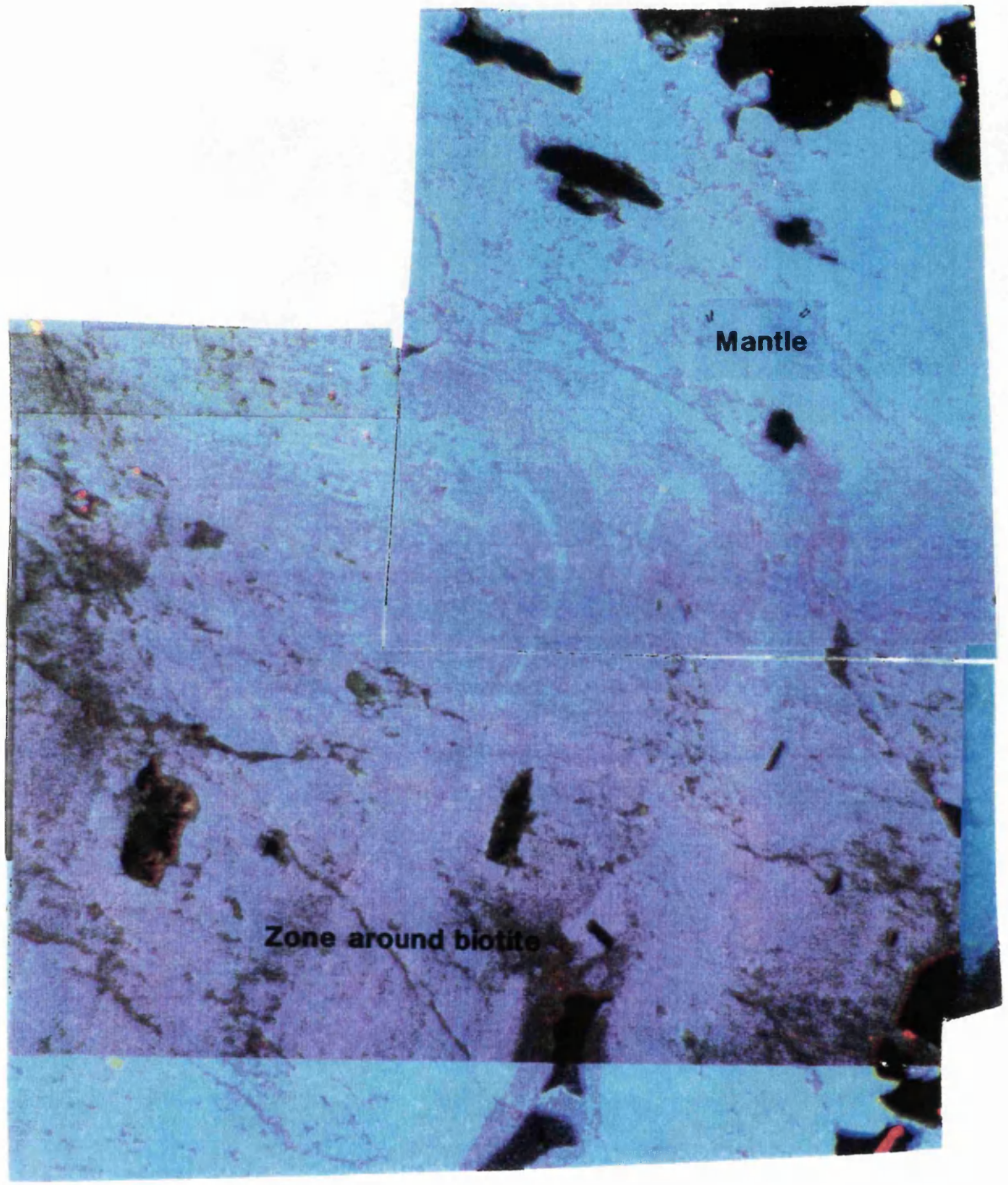

(c)

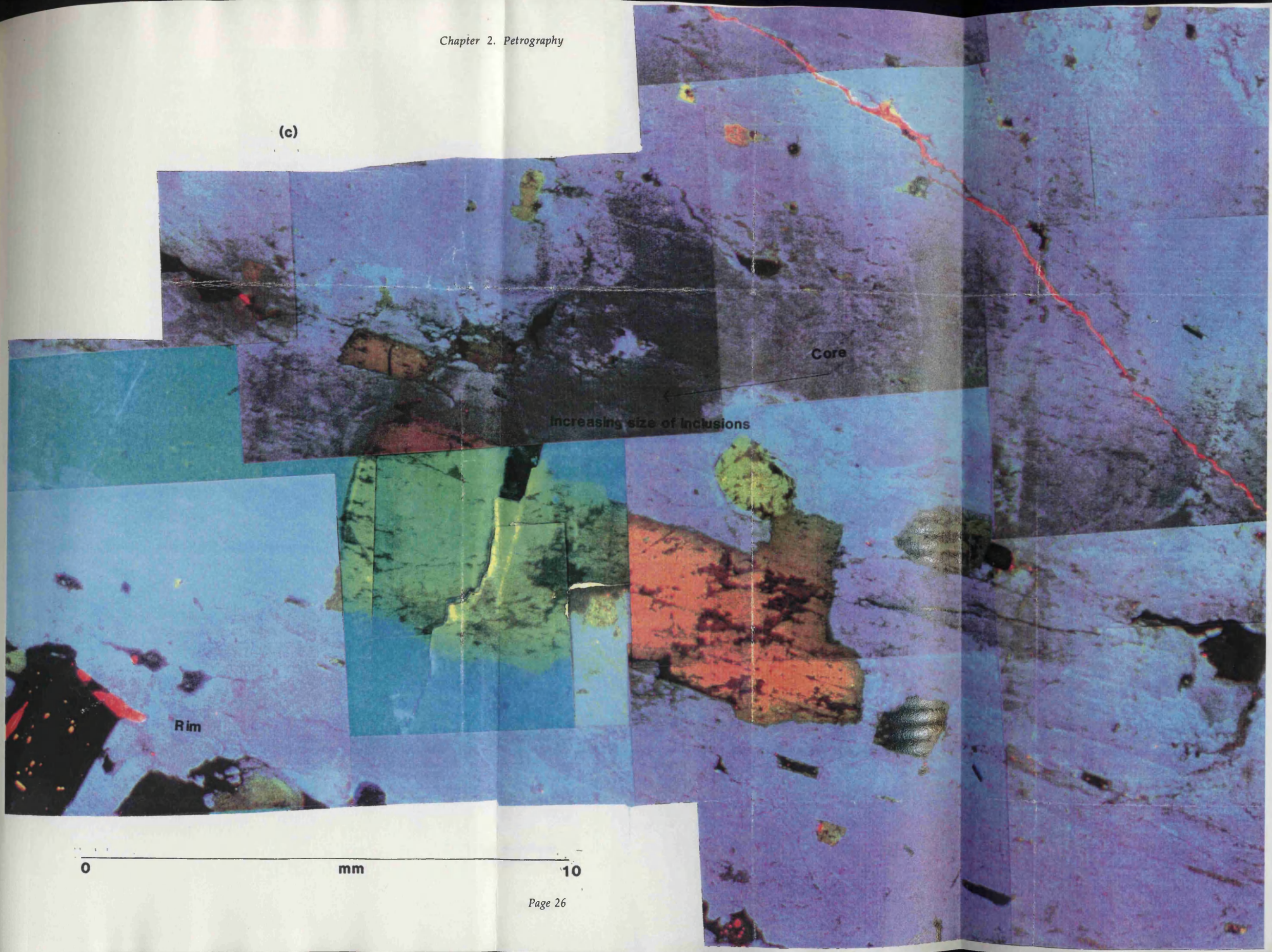


Disrupted zone
Plagioclase inclusions
Quartz
Plagioclase matrix
Zone
(d)
0
mm
10

Figure 2.11(a)

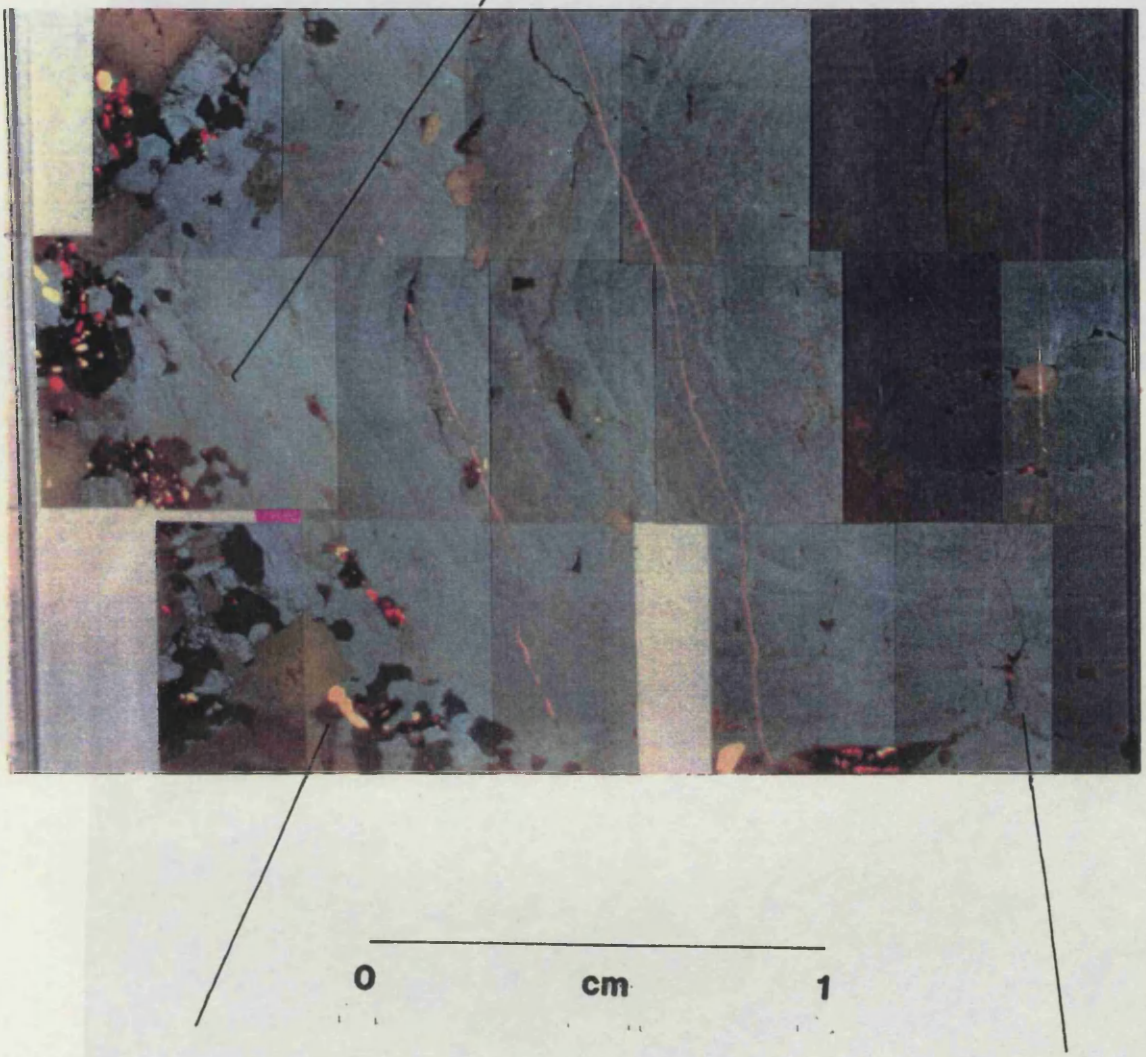

Figure 2.11(b)

Figure 2.11(c)

Figure 2.11. A photographic reduction of a C.L. montage of the edge of a large K-feldspar megacryst with the positions of the full-sized reproductions shown (**Figures 2.11(a-c)**). The activators and colours are the same as for **Figure 2.10** and shown in **Table 2.2**.

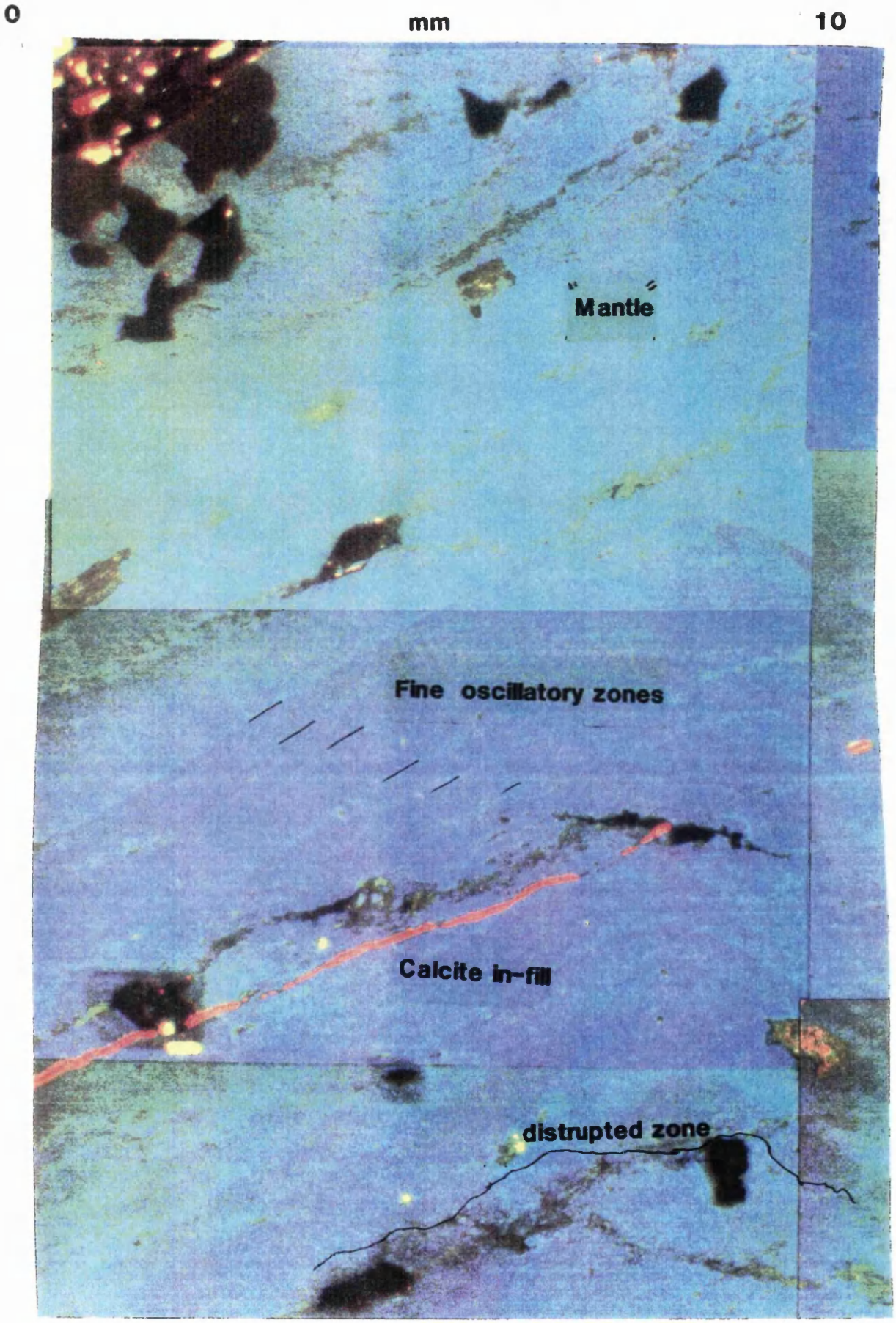
0
mm
10
Mantle
Fine oscillatory zones
Calcite in-fill
distrupted zone

(a)

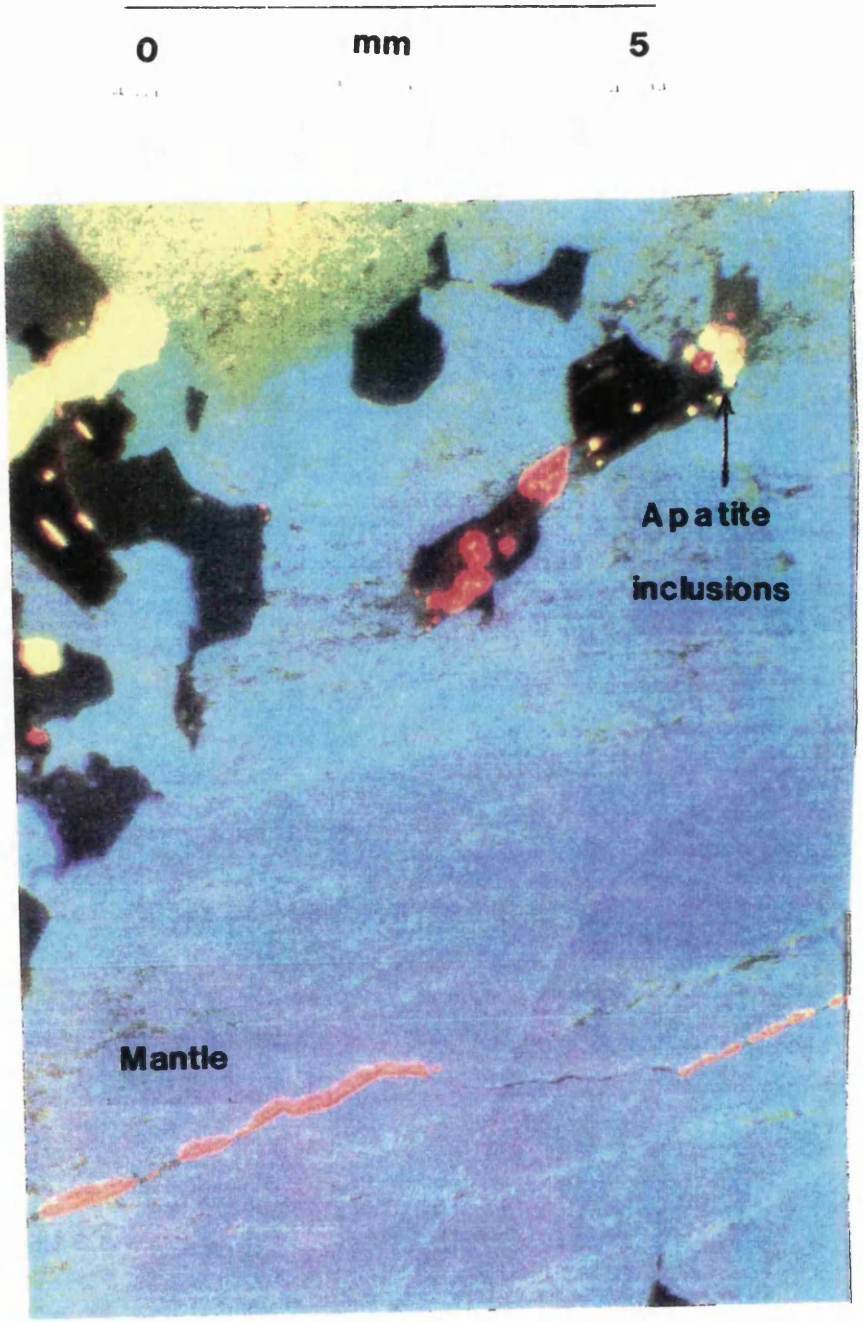

(b)

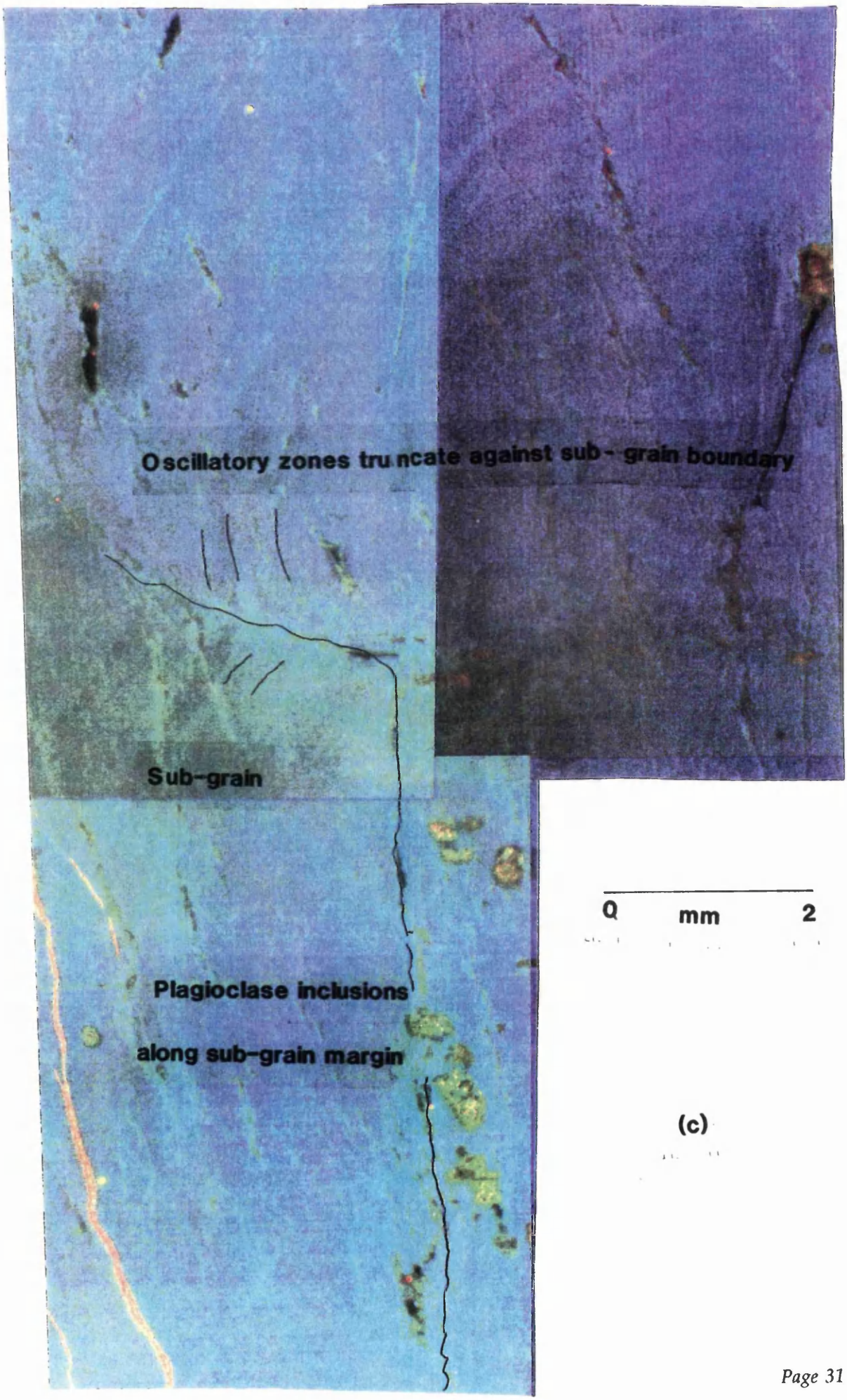
Oscillatory zones truncate against sub-grain boundary
Sub-grain
Plagioclase inclusions
along sub-grain margin
Q
mm
2
(c)

large irregular zone corresponds to the large zone which can be seen in the thin slices of the megacrysts (**Figure 2.4**).

Nearer the rim of the crystal, proceeding outwards from the large disrupted zone, the megacrysts show a marked increase in brightness and the rims of the crystals are largely unzoned, and uniformly bright blue in colour. This gives a mantled appearance to the megacrysts (**Figures 2.10(a)** and **2.11(a)**). The rim area of the megacrysts is also marked by the presence of the sub-grains of K-feldspar, within the megacrysts (**Figure 2.11(c)**). The apparent "refraction" of the small scale regular zoning appears much clearer in C.L., and the zones terminate against the sub-grain/K-feldspar boundary, although the zones within both the sub-grain and the megacryst, are parallel.

Inclusions, of plagioclase (yellow) and dark quartz and biotite are obvious in the C.L. images of the megacrysts. Both the size and abundance of the inclusions, particularly the plagioclase (**Figure 2.10(c)**), increases from the core to the rim in the megacrysts. Apatite (bright yellow) inclusions are present but almost exclusively in the outer rims of the megacrysts, (**Figure 2.11(b)**). The plagioclase inclusions are predominantly euhedral and are zonally arranged (**Figure 2.10(c)**), with the long axes {001} of the plagioclase inclusion crystals aligned parallel to the adjacent oscillatory zones. Some small inclusions biotite and quartz are present in the larger plagioclase inclusions (**Figure 2.11(b)**). The quartz and biotite inclusions, within the megacrysts are zonally arranged in the same manner as the plagioclase inclusions (**Figure 2.10(c)**). Quartz and biotite are generally well-formed, but quartz inclusions also occupy cracks in the megacryst, often joining inclusions (**Figures 2.10(d)** and **2.11(c)**).

Calcite appears as a secondary mineral, in-filling cracks in the megacryst (**Figure 2.11(c)**). The calcite was not considered further, apart from where sampling the megacrysts, when they were avoided when possible.

K-feldspar zones which are bright blue, were observed around the plagioclase inclusions, and similar, although dark blue zones, occurred around some biotite inclusions (**Figures 2.10(b)** and **(c)**). These zones appeared to correspond to areas of bright birefringence, in transmitted light.

(ii) S.E.M. imaging

Back-scattering S.E.M. imaging further enhances these features in two ways. Firstly, the resolution is increased, with very fine scale observations possible, and secondly S.E.M. images give a qualitative indication of the chemical nature of these features.

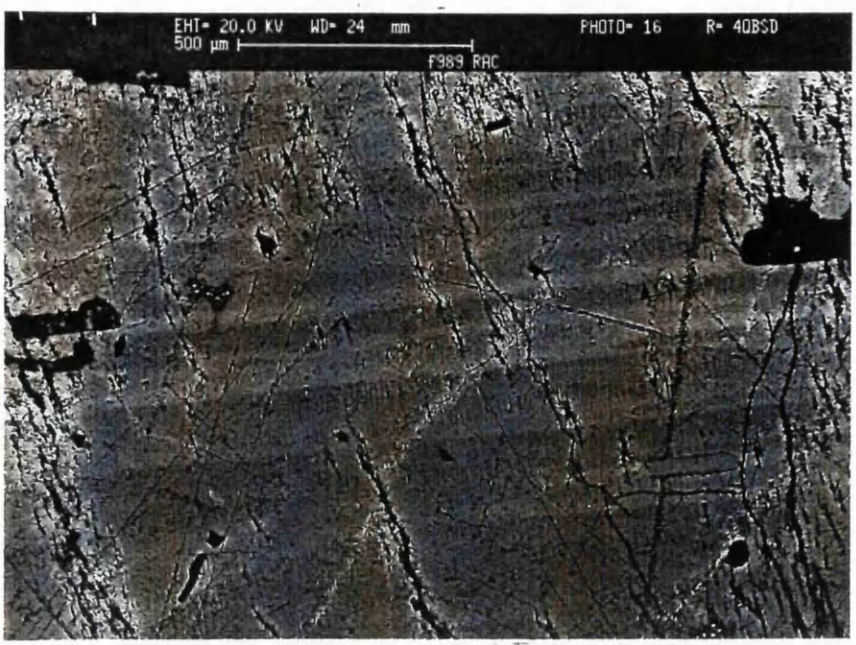

Figure 2.13(a) Back-scattering S.E.M. photomicrograph of a K-feldspar megacryst from the granitoid showing fine-scale, high-mass oscillations in the crystal.

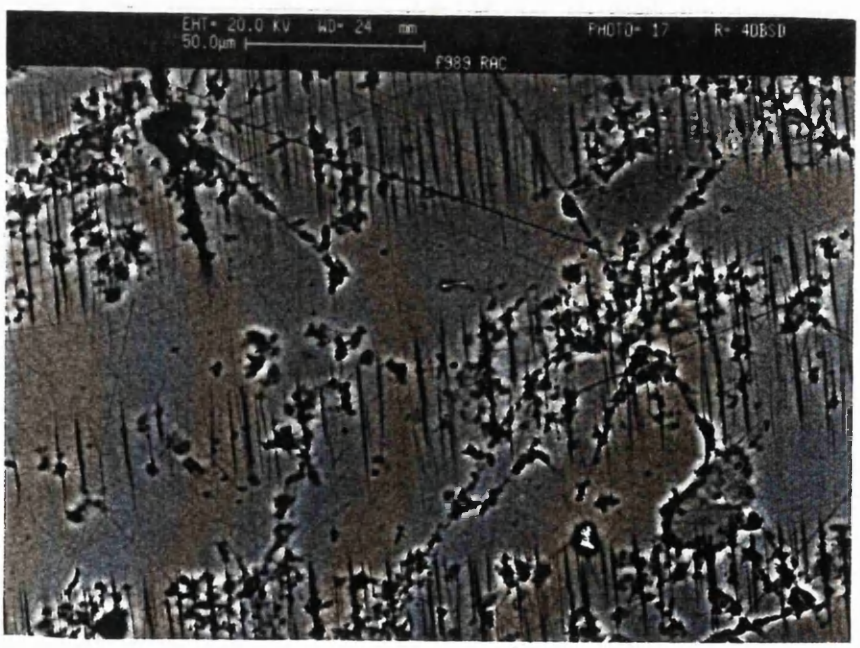

Figure 2.13(b) Back-scattering S.E.M. photomicrograph showing a high magnification image of the detailed morphology of the fine-scale oscillations.

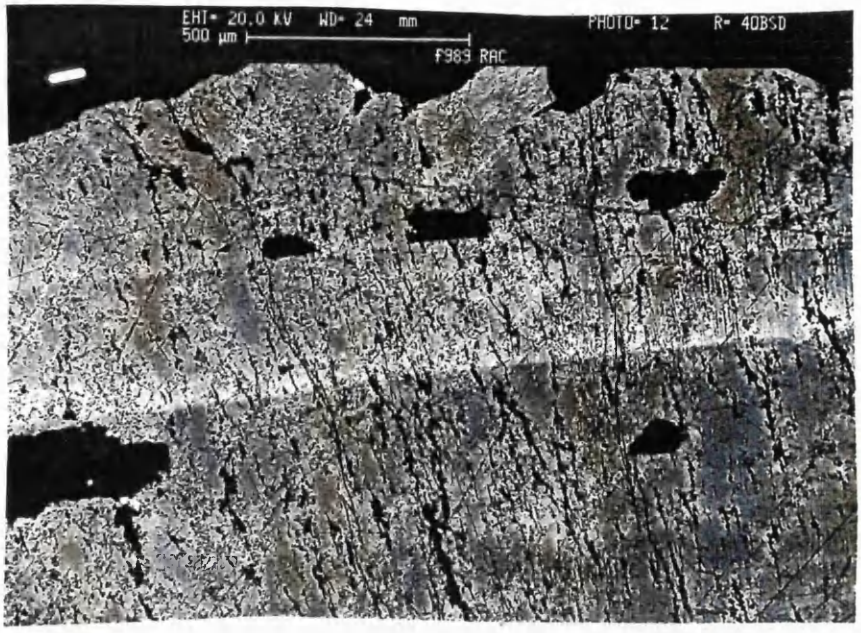

Figure 2.14(a) Back-scattering S.E.M. photomicrograph showing the large-scale zone parallel to the {001} axis. Note the high mass (bright image) of the zone in comparison to the normal brightness of the megacryst, which occupies the lower half of the picture.

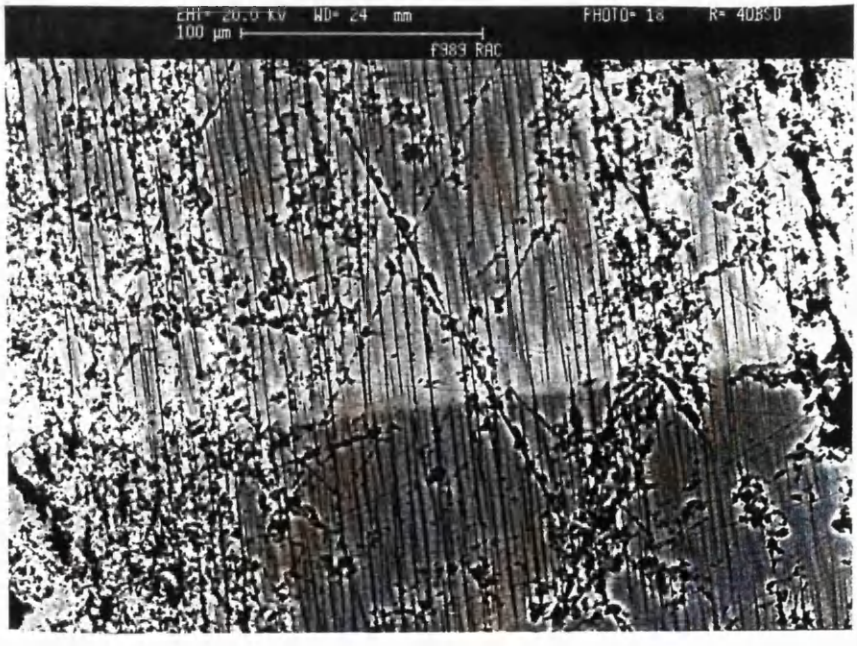

Figure 2.14(b) A Back scattering S.E.M. image of the same zone as shown above in **Figure 2.14(a)** but at higher magnification to show more detailed morphology.

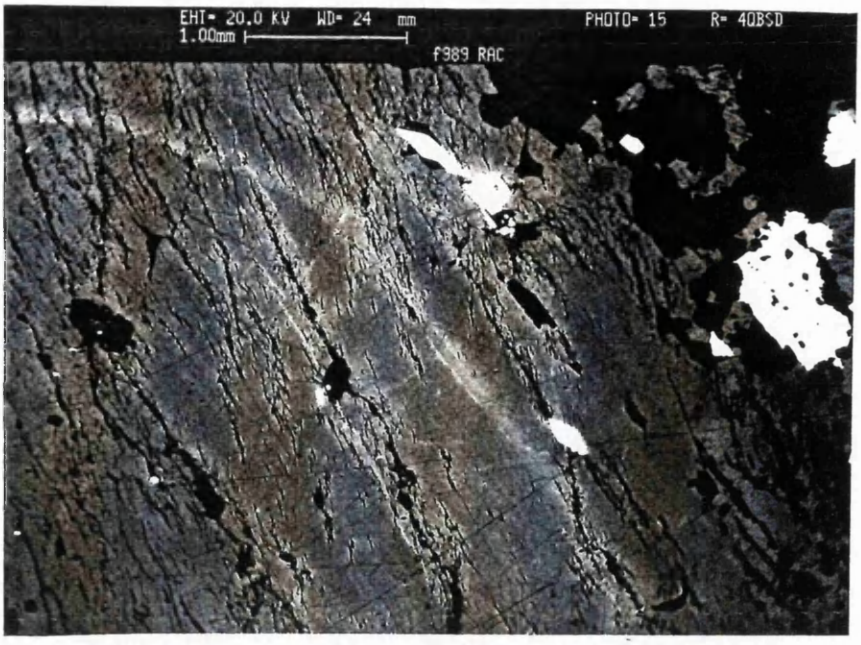

Figure 2.15(a) A back-scattering S.E.M. photomicrograph of the {101} and {201}-parallel areas of the disrupted, large-scale oscillatory zone of a K-feldspar megacryst. Note the more complex morphology of this part of the zone in comparison to the {001}-parallel section, (**Figure 2.14(a)**).

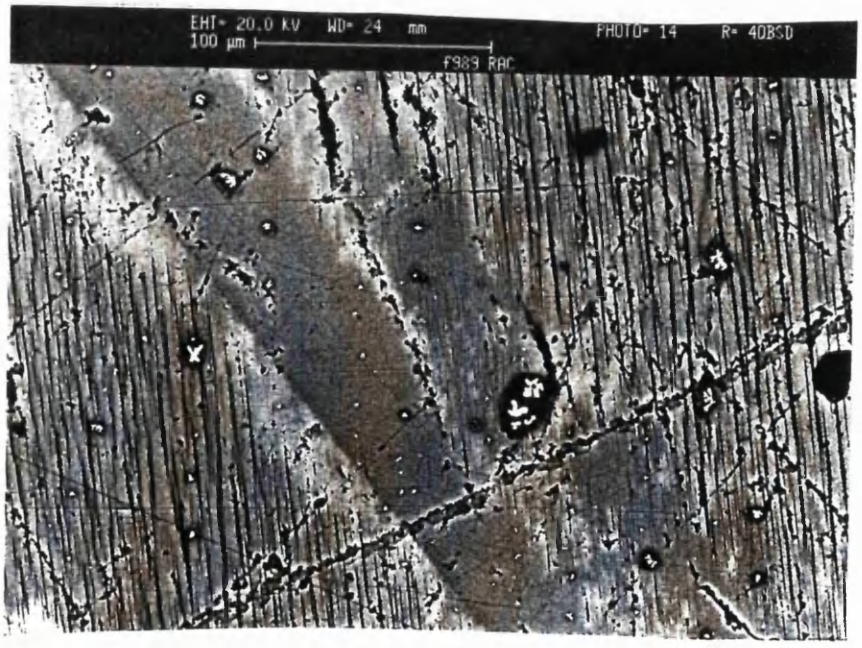

Figure 2.15(b) Back-scattering S.E.M. photomicrograph, at high magnification, of the large-scale, disrupted zone ({101}-parallel) showing more detailed morphology.

The principle behind back-scattering electron imaging is very similar to the C.L.-method but with a higher incident-electron beam current. This causes more electrons to be scattered, i.e. liberated from the outer shells of the atoms. As more massive elements have more outer shells, with a correspondingly lower electro-static attraction, they will produce more back-scattered electrons from a given beam current. This translates into the brightest area of a back-scattered image, and subsequent photomicrograph, (Newbury et al. 1987).

The textures which the back-scattering S.E.M. imaging reveal most about in these samples, can be divided into primary (growth features, essentially the zoning), and secondary features.

The large-scale zoning from core to rim, which can be seen by the variable extinction of the megacrysts, the change from dark to bright C.L. colours (**Figure 2.10(b)** and **2.11(b)**) is apparent using back-scattering S.E.M. images (**Figure 2.12**) but only as a subtle darkening of the image towards the rim, indicating an overall decrease in average mass towards the rim of the crystal. This is often easier to see in the smaller megacrysts (<0.5cm) where smaller numbers of oscillatory zones occur, and because the whole crystal can be imaged, albeit at low magnification (**Figure 2.12**).

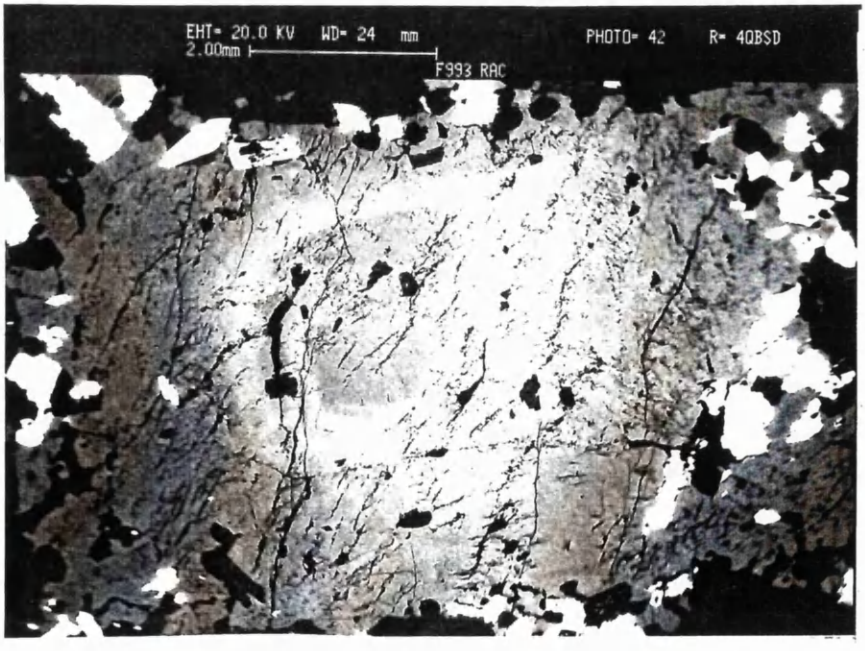

Figure 2.12. Back-scattering S.E.M. image of a small K-feldspar megacryst from the Shap granitoid. Note the general core-to-rim zoning, and the presence of a prominent oscillatory zone in the crystal.

In the larger megacrysts, both the fine and large-scale oscillatory zones are visible as very bright, fairly regular stripes which run continuously round the crystal. The fine oscillations however are not quite as regular as they appear in C.L., with some merging into each other, and some being slightly discontinuous (**Figure 2.13(a)**). The larger oscillatory zones are considerably wider than these fine zones generally >100μm as compared to 5-30μm. The fine-scale oscillatory zones show an increased brightness (mass) which in high magnification (**Figure 2.13(b)**), has no detailed structure, other than a lack of fine perthite within the zone itself. The larger scale oscillatory zones are more complex and show both more variation in morphology along their length and detailed internal variation.

The {001}-parallel zones show a sharp inner boundary with a generally dark (low-mass) transition (**Figure 2.14(a)** and **2.14(b)**). This pattern is identical on the opposite side of the megacryst. The crypto-perthites have been exsolved in all but the brightest (highest mass) areas across these zones. At the edges of the megacrysts, when zones are parallel to the {101} or {201} crystal faces, a more complex internal zone-structure exists (**Figure 2.15(a)**). Here the zone has an irregular contact with a high-mass area followed by a low-mass area similar in morphology to the smaller oscillations shown in **Figure 2.13(b)**. There is then a graduated high- (inner) to low- (outer) mass part as in the {100}-parallel parts of the zone, with crypto-perthites being exsolved in all but the brightest (high mass) areas and the low mass cores as in the smaller oscillations (**Figure 2.13(b)** and **Figure 2.15(b)**).

The most prominent feature of the exsolution of the perthites, revealed by these back-scattering S.E.M. images, is the concentration of high-mass (bright) areas around the coarse micro-perthites (**Figure 2.13(a)** and **2.14(b)**). These are absent from the crypto-perthites and any fluctuation in brightness on the rims of these smaller exsolutions, is due to surface effects only visible under high magnification (**Figure 2.13(b)** and **2.14(b)**).

2.5 Petrography of the Shap granitoid matrix minerals

The matrix of the Shap granitoid is composed essentially of equal amount of K-feldspar, plagioclase and quartz, with about 5% of the matrix consisting of biotite. The grain size is quite uniform with crystals generally 1-2mm in size, although quartz and plagioclase are slightly larger than the matrix biotite and K-feldspar crystals. The matrix is not obviously foliated and matrix crystals show no apparent alignment in hand specimen (**Figure 2.2**).

Figure 2.16(a) Xpls photomicrograph of fractured biotite (bright birefringence), quartz (in extinction), plagioclase, (twinned) and turbid K-feldspar, which is both in extinction and showing first order birefringence, in the matrix of the Shap granitoid. Note the fractured pieces of the biotite can be matched-up with a quartz occupying the space. The biotite show lower birefringence along the fracture where it has undergone retrogression to chlorite.

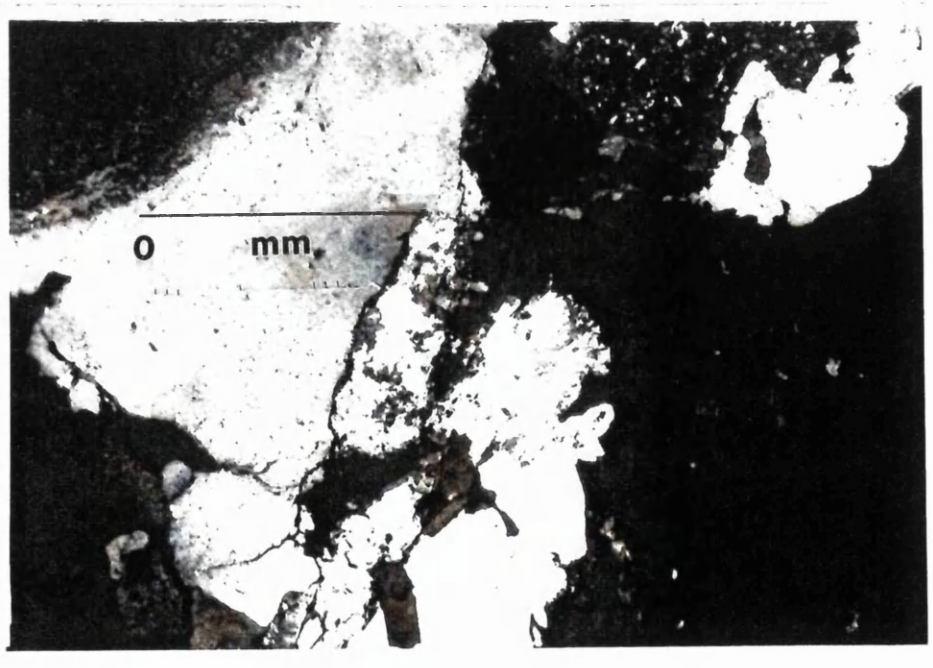

Figure 2.16(b) Xpls photomicrograph of a fractured biotite (bright birefringence) in the matrix of the Shap granitoid. The fracturing had occurred at the edge of a K-feldspar megacryst with one half of the biotite occurring as an inclusion in the megacryst.

Virtually all the biotite crystals have undergone retrogression to chlorite. Biotite is found as inclusions within the quartz plagioclase and K-feldspar matrix. In addition to this biotites are also found to be fractured, with opposite sides of the crystal being separated by other matrix crystals such as quartz (**Figure 2.16(a)**) or occasionally by the edges of a megacryst (**Figure 2.16(b)**). Chlorite alteration occurs along these fractures, or along the areas of more ductile deformation, in the biotites. This ductile deformation of the biotites is seen as a contortion of the cleavage and can be seen in many of the matrix biotite crystals.

The matrix plagioclases show sericite alteration in many of the crystals and often secondary calcite. However, some are fresh and show high albite to oligoclase extinction angles (7^{o}-15^{o}) measured on the multiple twins. In addition to the twinning many crystals show very clear oscillatory zoning where the zones have different extinction positions (**Figure 2.17**). Clear truncation of the zones against the outer edges of the plagioclase crystals is apparent, where the rims of the plagioclase crystals display an apparently corroded or dissolved appearance.

Matrix quartz shows two different morphologies. The first is the subhedral to euhedral form which can be up to 2mm in diameter. The second form is an interstitial quartz which can be easiest seen where it occupies spaces between low relief minerals, namely the plagioclase and K-feldspars.

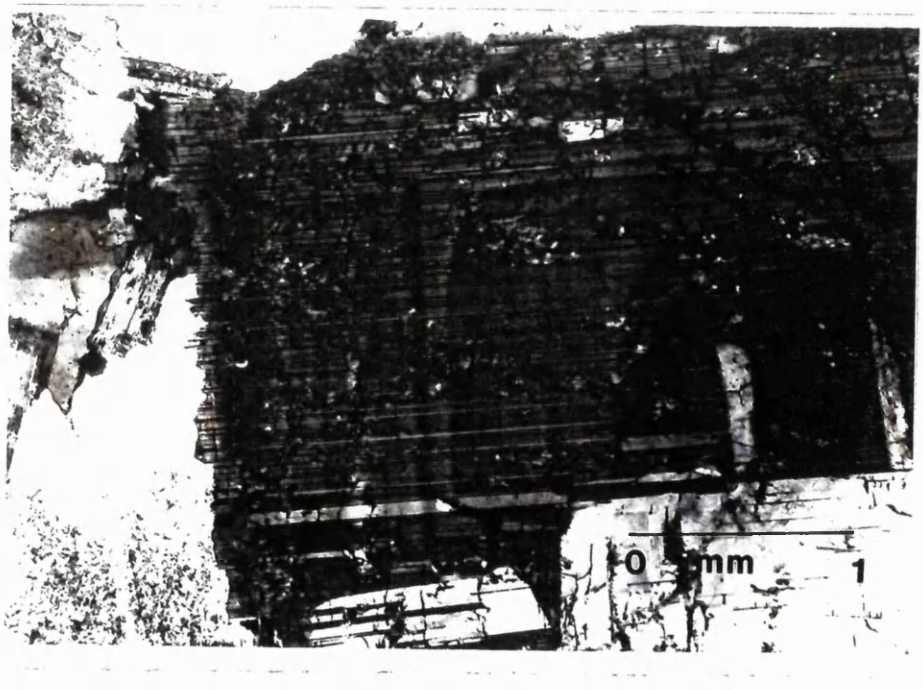

Figure 2.17. Xpls photomicrograph of oscillatory zoning in a matrix plagioclase crystal. Zone truncation and slight corrosion of the rim can be seen.

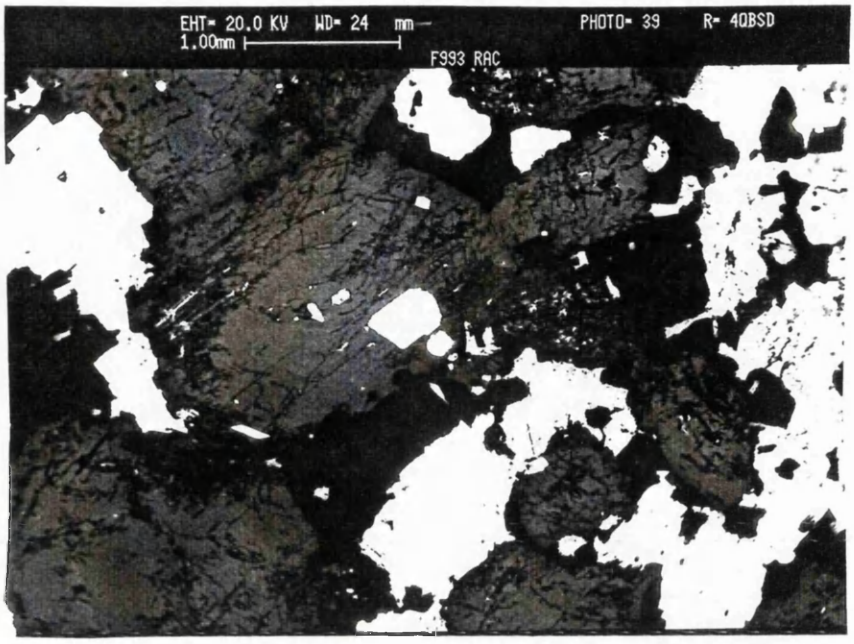

Figure 2.18. Back-scattering S.E.M. image of a plagioclase crystal in the Shap granitoid. Note the fine concentric oscillatory zones and the zonally aligned biotite inclusions (bright birefringence). The zones are truncated at the corroded/dissolved edge of the crystal.

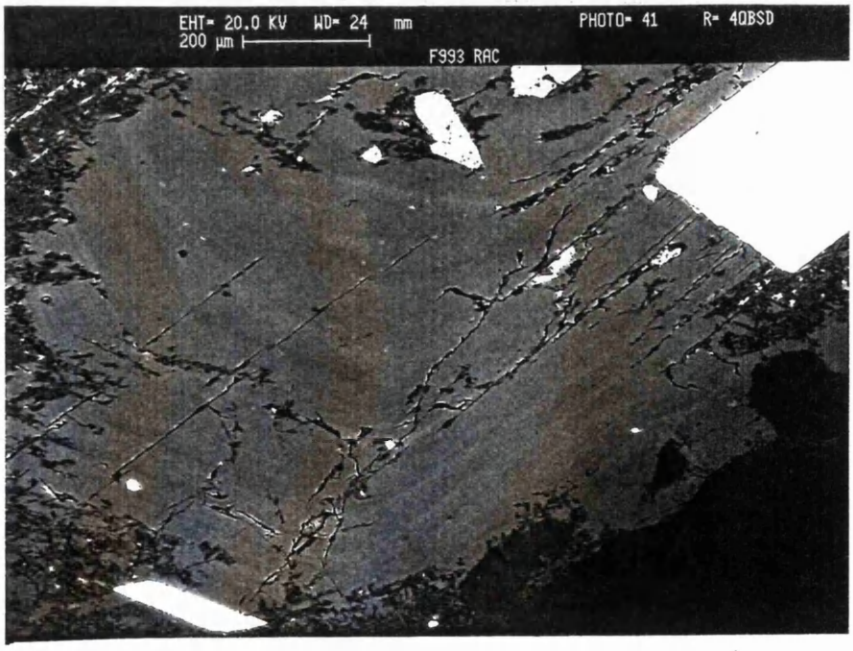

Figure 2.19. Back-scattering S.E.M. image of the same plagioclase crystal in **Figure 2.18** but at higher magnification to show the detailed morphology of the zones. Note the high to low mass fluctuations of the oscillations, and the various widths of the zones on the different crystal faces.

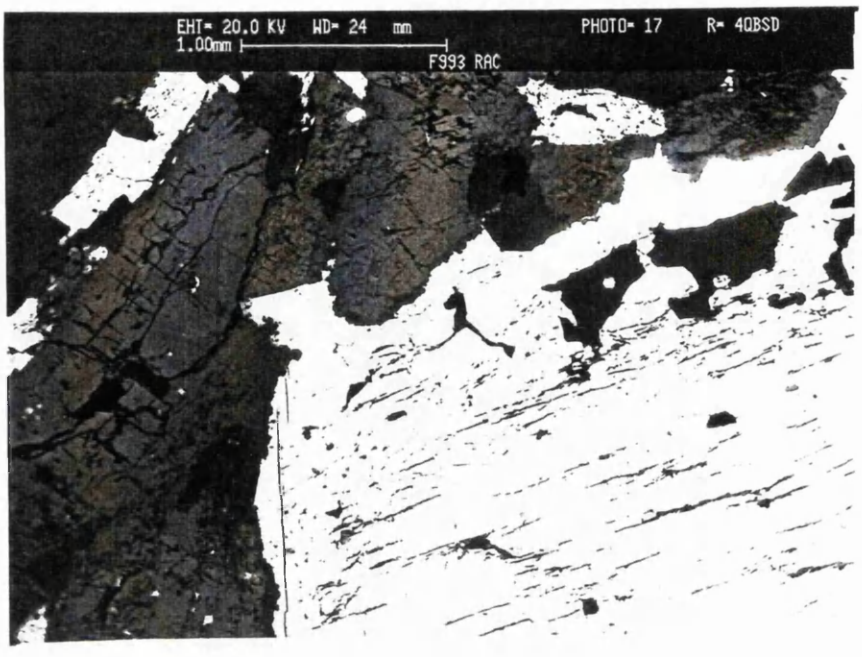

Figure 2.20. Back-scattering S.E.M. image of the edge of a K-feldspar megacryst in contact with plagioclase, biotite, and quartz matrix crystals.

Figure 2.21. High magnification back-scattering S.E.M. photomicrograph of the edge of the K-feldspar megacryst shown in **Figure 2.20**, with a plagioclase matrix crystal displaying a dark (low mass) rim where it is in contact with the megacryst.

Under C.L. microscope the plagioclase matrix crystals show a relatively uniform yellow colour, (with either Fe^{2+} or Mn^{2+} activation), but the zoning shows-up relatively poorly. This indicates that although chemical fluctuations are present, as indicated by the oscillatory zones in **Figure 2.17**, these zones do not correspond to trace element C.L. activator fluctuations. However, often there is a blue C.L. zone within the normally uniform yellow plagioclases, (**Figure 2.10(c)**). This may correspond to the large disrupted zone in the K-feldspar megacrysts, as it appears to be similarly disrupted in nature. The most likely chemical changes in these matrix plagioclases is in the Ca/Na ratio, i.e. the total An-content (MacKenzie et al. 1982).

Back-scattering S.E.M. images enhance some of the above observations considerably. In particular, the zoning and chemical composition of the plagioclase crystals is revealed by this technique. **Figures 2.18** and **2.19** show a typical plagioclase matrix crystal. At lower magnification, (**Figures 2.18**) oscillatory zones can be seen, with small scale brightness fluctuations, which are truncated against the irregular edge of the plagioclase crystal. Another feature which can be observed in these plagioclase matrix crystals is a dark (lower mass) rim around almost all the matrix plagioclases, (**Figures 2.18, 2.19**). The change from bright (high mass) to dark (low mass) is generally restricted to the outer 0.1mm of these plagioclases. The size of the darkest rims are particularly noticeable at the plagioclase/K-feldspar or plagioclase/biotite boundaries where the contrast in brightness of the images is greatest, (**Figures 20, 2.21**).

It seems from these textures that the Shap granitoid matrix, particularly the plagioclase has undergone a complex growth, which may also be reflected by the K-feldspar megacryst growth in this rock.

2.6 Basic petrography of the megacrysts and matrix of the mafic enclaves of the Shap granitoid

The occurrence of mafic enclaves within the Shap intrusion, is a feature shared with many granitoid bodies, e.g. Querigut complex, France (Fourcade and Allegre 1981), Petford granite, Queensland, Australia (Bailey 1984), Hercynian belt granitoids, Spain (Castro et al. 1990), Massive Central intrusions, France (Pin 1991). Harker and Marr (1891) and Grantham (1926) suggested that the presence of enclaves within the Shap intrusion indicated mixing of two magmas. The presence of K-feldspar megacrysts and other minerals in both the enclaves and the granitoid seems to support this view, although Grantham (1926) was of the opinion that the K-feldspar megacrysts

were of metamorphic origin. A detailed look at the textures of these enclaves and the so called "alien minerals" within them may help to clarify their origin.

The mafic enclave investigated (**Figure 2.22**) is a xenolith of micro-diorite, about 30cm in diameter, and is typical of enclaves from the Shap intrusion. The diorite matrix was fine to medium grained (<0.5mm) and an overall grey colour, apart from subhedral K-feldspar, plagioclase and quartz (2mm to 8mm in size) and K-feldspar megacrysts which were also subhedral and generally 0.5cm to 2cm in size. The hand specimen was sliced into 2cm thick slabs to reveal more of the K-feldspar megacrysts, and other textural features within the dioritic enclave. The granitoid surrounding the enclave is of the Stage II type (Grantham 1926) although it is noticeably paler in it's overall colour than the normal Stage II granitoid in **Figure 2.2**.

Figure 2.22. Photograph of a hand specimen showing the mafic enclave surrounded by the host Stage II Shap granitoid.

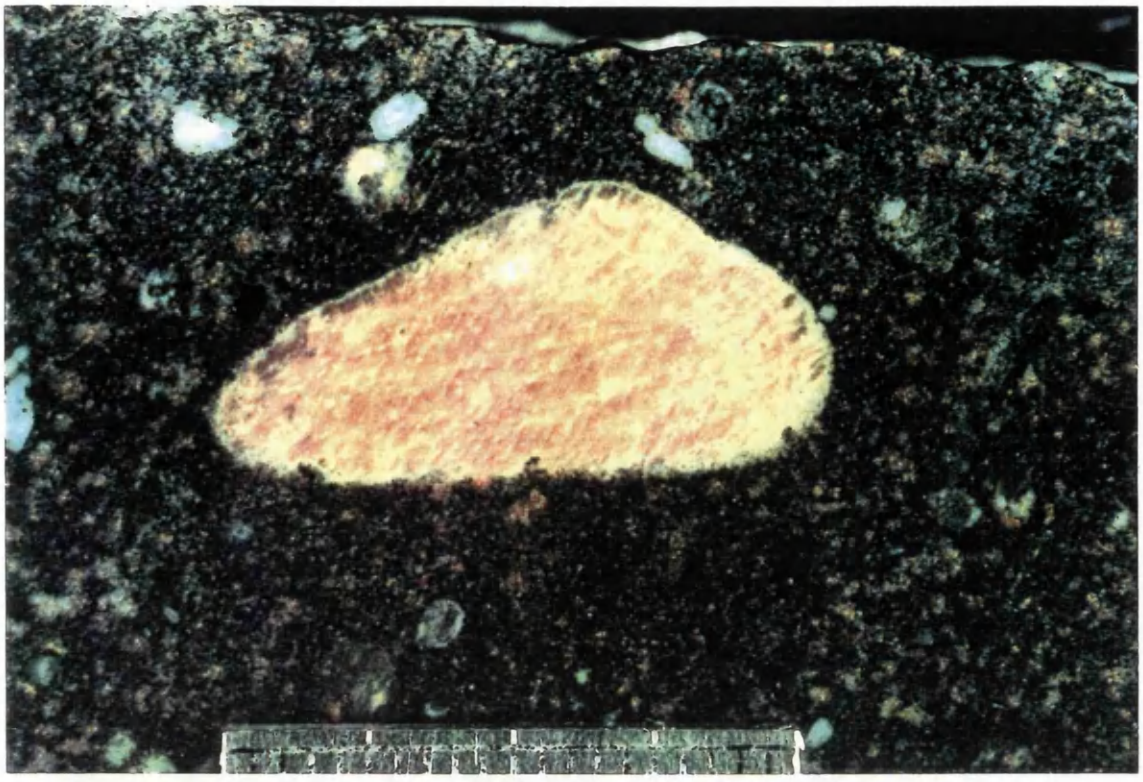

Figure 2.23. Colour photograph of a sliced slab of the enclave examined from the Shap granitoid (**Figure 2.22**) with a subhedral, K-feldspar megacryst, and larger plagioclase and quartz crystals in the enclave (quartz microdiorite) matrix.

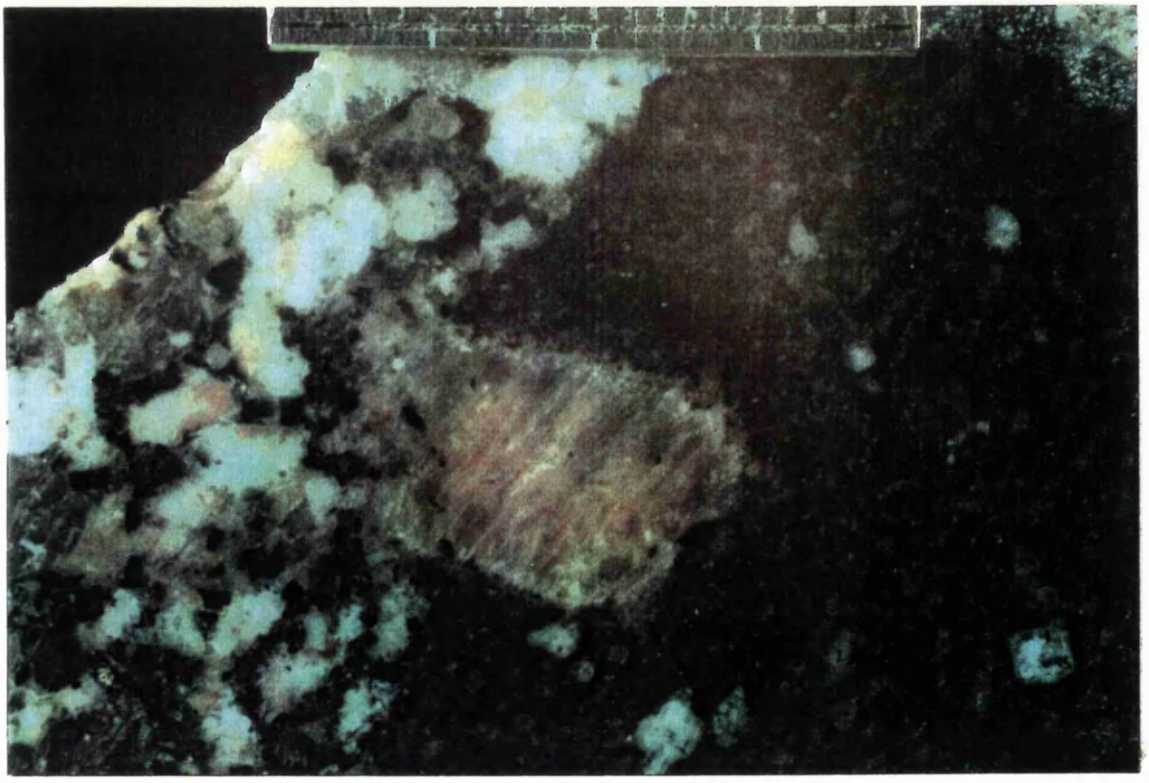

Figure 2.24. Colour photograph of a sliced slab of the enclave examined from the Shap granitoid (**Figure 2.22**) with a K-feldspar megacryst in contact with the surrounding host granitoid. Note the megacryst has undergone abrasion and dissolution at the contact with the host granitoid. An asymmetrical shape to the dissolved megacryst edge is visible.

The slabs of the diorite reveal a number of subhedral to anhedral K-feldspar megacrysts within the enclave. These range from 0.5 to 2cm, considerably smaller than the granitoid equivalents. The megacrysts within the enclave often show embayed, irregular edges, and are occasionally mantled by plagioclase (**Figures 2.23** and **2.24**). The enclave matrix surrounding the K-feldspar megacrysts is often darker than the normal matrix material (**Figure 2.23**). Rarely, K-feldspar megacrysts occur at the granitoid/enclave boundary (**Figure 2.24**). In such cases, it is apparent that the megacryst has undergone extensive dissolution at the boundary as the dioritic matrix is partly distorted outwards around the megacryst and the boundary appears to display an asymmetrical rotation along the edge of the megacryst (**Figure 2.24**).

Larger plagioclase and quartz grains within the enclave, generally 2-3mm (but up to 8mm) are common. The matrix of the diorite is very fine grained plagioclase, quartz, biotite and some apatite which is 0.1mm or smaller, but slightly larger crystals of K-feldspar (0.5mm) often mantled by plagioclase are abundant (**Figures 2.23** and **2.24**). The matrix and larger crystals (K-feldspar, etc.) are quite strongly aligned in the enclave. This, along with the suggestion of rotational strain of the megacryst at the boundary (**Figure 2.24**) seems to indicate that foliation of the enclave after partial crystallisation, may have taken place. This may be related to the orientation process of the megacrysts in the granitoid (**Figure 2.3**).

The margin of the enclave is generally darker in colour which probably represents a higher proportion of mafic minerals and/or a finer grain-size caused by rapid chilling of the enclave liquid when mixed with the granitoid.

2.7 Microscope observations on polished, etched and stained sections of K-feldspar megacrysts within the mafic enclave

The K-feldspar megacrysts within the mafic enclave appear to show very few of the features of their granitoid counterparts. It is clear that their growth histories have been different in some respects. However, in transmitted light with Xpls it is possible to begin to identify shared textural characteristics between the granitoid and enclave K-feldspar megacrysts. There is, firstly, twinning of the enclave megacrysts, (**Figure 2.25**). This feature is not normally associated with metamorphic K-feldspar (Vernon 1986). Zoning which would appear to be oscillatory and zonally arranged inclusions are also visible in some of the enclave megacrysts (**Figure 2.26**) although these are less common than in the granitoid megacrysts. K-feldspar sub-grains at the rims of the enclave megacrysts are also present, (**Figure 2.26**).

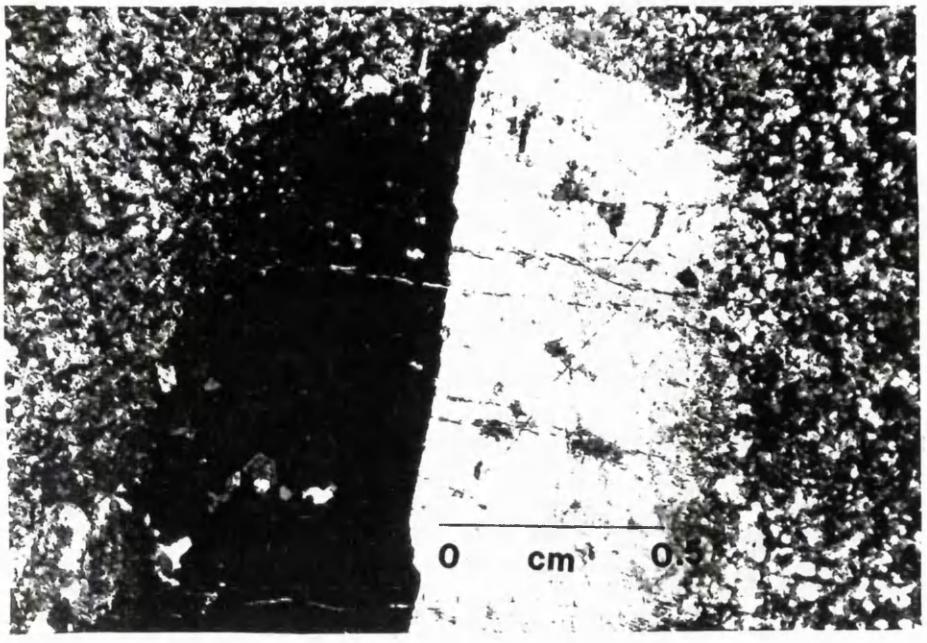

Figure 2.25. Xpls photomicrograph of a K-feldspar megacryst in a quartz microdiorite enclave from the Shap granitoid. The megacryst shows clearly simple twinning.

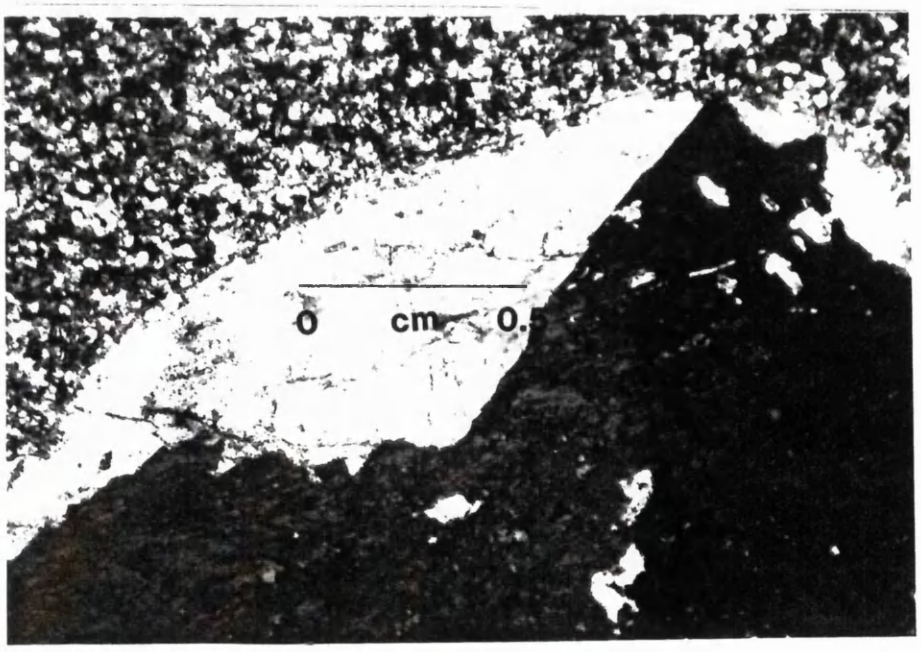

Figure 2.26. Xpls photomicrograph of a K-feldspar megacryst in a quartz microdiorite enclave from the Shap granitoid. The megacryst shows K-feldspar sub-grains, plagioclase, quartz and biotite inclusions, which appear to aligned along faint oscillatory zones in the megacryst.

There are however, extensive differences between the granitoid and enclave megacrysts. The size range (0.5 to 2mm) and predominantly subhedral (rounded) shape of the enclave megacrysts are shared by only 40% (**Table 2.1**) of the granitoid megacrysts. The subhedral enclave megacrysts show extensive embayments and reaction textures including mantling of the crystal rims, which is a feature none of the subhedral megacrysts in the granitoid appear to share.

To attempt to highlight the textural features of the megacrysts within the enclave, some of the enclave megacryst sections were etched in flouroboric acid which may accentuate feldspar zoning (Pearce and Clark 1989). Other sections were stained using the method outlined by Hutchison (1974) and Houghton (1980) which gives red coloured plagioclase and yellow or unstained K-feldspars.

The etched sections of enclave K-feldspar megacrysts show the nature of the oscillatory zoning (**Figures 2.27** and **2.28**). The etching of K-feldspars in flouroboric acid will tend to enhance the Ba- and Ca- rich zones (Clark et al. 1986). The sections shown (**Figures 2.27** and **2.28**) show that fine oscillatory zoning, very similar in morphology to those in the granitoid megacrysts (**Figures 2.5, 2.6, 2.7, 2.8, 2.10, 2.11, 2.13(a)** and **2.13(b)**) occur in the megacrysts in the micro-diorite enclave. Not only do the zones run concentrically round the megacrysts in the enclaves by also in euhedral sub-grains as well (**Figure 2.28**).

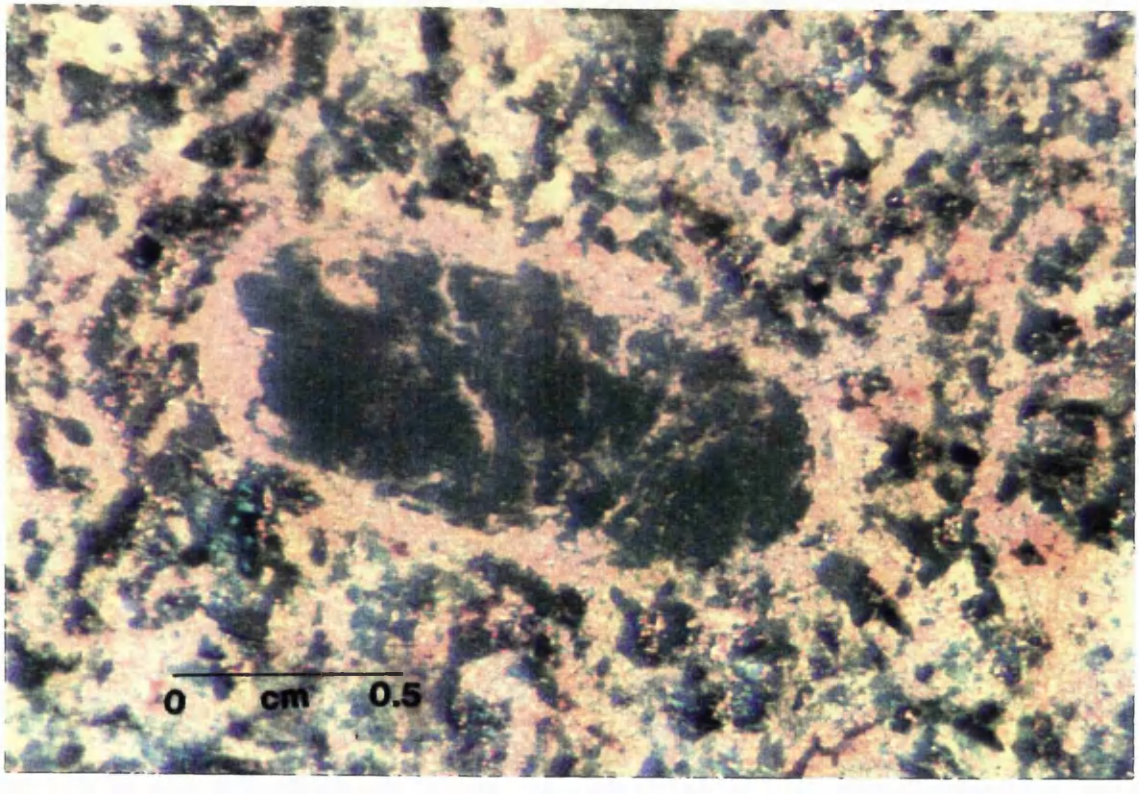

Figure 2.29. Photograph of the surface of a stained section showing a K-feldspar megacryst (unstained) mantled by plagioclase (red).

The enclave megacrysts which were stained show the chemical nature of the reaction zone and mantle round the K-feldspar crystal, (**Figure 2.29**). The red plagioclase overgrowth can be clearly seen around the generally unstained, subhedral, K-feldspar megacrysts. The mantling of K-feldspar by plagioclase, (i.e. rapakivi texture *(sensu lato)*) is thought to be caused by mixing of xenocrysts in a "foreign" magma (Vernon 1986; Hibbard 1991) or by complex sub-solvus plagioclase exsolution (Dempster et al. 1994).

2.8 C.L. and S.E.M. imaging of the K-feldspar megacrysts in the mafic enclave

C.L. images of the mafic enclave megacrysts (**Figure 2.30**) show the same Ti^{4+} activated blue colour as the granitoid examples (**Figure 2.10** and **2.11**). Euhedral, yellow inclusions, black biotite and smoky quartz inclusions are present and appear to be zonally arranged, (**Figure 2.30(a)**). The size and frequency of these inclusions show similarities to the core regions of the granitoid megacrysts, (**Figure 2.10**). The zoning, which is only faintly visible (**Figure 2.26** and **2.30(a)**), appears to be truncated against one edge of the crystal (**Figure 2.30(b)**). The crystal is also surrounded by a very bright blue C.L. mantle, and is embayed along this mantle, with more patchy and paler blue mantling beyond this rim (**Figure 2.30(b)**). This may correspond to the plagioclase mantle in **Figure 2.29**.

Back-scattering S.E.M. images of this embayed margin show its exact morphological nature and extent. The rim of the crystal is full of {010}-parallel embayments (**Figure 2.31(a)**) which extend to about 0.5mm into megacryst, beyond the mantled area. The K-feldspar margin, which appears bright blue in C.L. images (**Figure 2.30**) is about 0.5mm beyond and is represented by a bright (high mass) irregular zone. The plagioclase mantle is a dark (low mass) 0.25mm thick rim around the megacryst, and clearly the same material fills the {010}-parallel embayments (**Figure 2.31(b)**). The mantle appears as a series of twinned high and low mass plagioclase crystals with some quartz. Thus, the mantle appears to consist of two plagioclase compositions, the brightest being more massive and therefore probably more Ca-rich, although both are much less bright (lower average mass) than the K-feldspar and are both probably low An-plagioclases.

2.9 Microscope observations on the enclave matrix and other crystals

The observations made on the enclave matrix using a hand lens on the sliced hand specimen slabs (**Figures 2.23** and **2.24**) can be added to little by normal ppl or Xpls microscopy, in either transmitted or reflected light, other than to give the proportions of the main minerals. There is about 40% plagioclase, 25% biotite and 25% quartz, with around 10% of the matrix consisting of apatite, K-feldspar and opaque ore minerals. The grain size (0.1mm) generally restricts any more detailed observations on individual grains. Based on these approximate proportions the enclave could be classed as a quartz-microdiorite.

In C.L. the plagioclase matrix is always blue (i.e. Ti^{4+} activated) unlike the plagioclase inclusions in the megacrysts and matrix plagioclases in the granitoid (**Figures 2.10, 2.11** and **2.30**). Some of the bright blue feldspars in the C.L. photomicrograph of the enclave matrix, would appear to mantle darker blue crystals (**Figure 2.32(a)**). The relative abundance of apatite (bright yellow) is shown clearly by the C.L. images of the enclave matrix. The whole matrix shows the strong foliation, observed in the slabs (**Figures 2.23** and **2.24**).

Large crystals of plagioclase and quartz within the enclaves were also microscopically examined. The subhedral plagioclase crystals showed extreme alteration, particularly around the rims (**Figure 2.33**). The presence of oscillatory zoning was visible in these crystals, with high and low birefringence zones truncated against the corroded rims.

Quartz crystals up to 3mm across are also quite common. These show subhedral oscelli-type shapes, which generally have an embayed rim with more mafic crystals nucleating on this margin. In this case the quartz oscelli have plagioclase and biotite crystals growing along their corroded and embayed margins (**Figure 2.34**).

Glomerocrysts of K-feldspar, quartz and plagioclase crystals are also present and these are often mantled by plagioclase-rich quartz-microdiorite matrix (**Figure 2.35**). The glomerocrysts are up to 7mm in diameter and consist mainly of crystals which are euhedral, except where individual crystal edges within the glomerocryst are in contact with the enclave matrix.

C.L. and back scattering S.E.M. imaging of the large plagioclase crystals within the enclave show the chemical nature of the zones and their truncation, quite clearly. The C.L. colours of the plagioclase crystals are similar (yellow) to the matrix plagioclase crystals in the granitoid (**Figure 2.36**) and show light to dark yellow oscillations.

The zones within the plagioclases in the enclave which appear in Xpls and in C.L. are shown by back-scattering S.E.M. images to be high to low mass

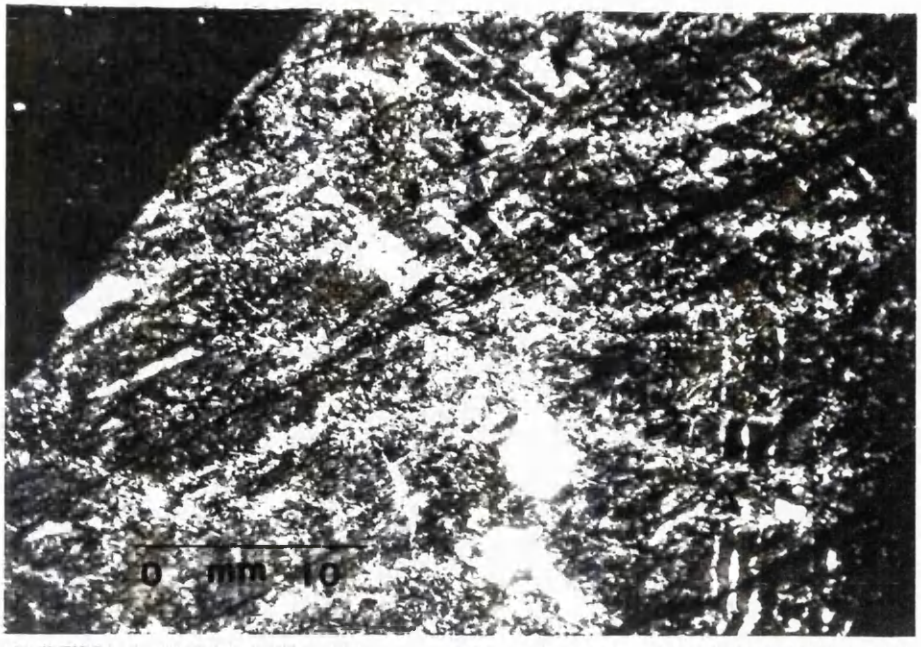

Figure 2.27. Xpls photomicrograph of an acid-etched section of a K-feldspar megacryst from a quartz microdiorite enclave. The Ca- and Ba-rich oscillatory zones are enhanced and appear as bright lines running concentrically around the megacryst.

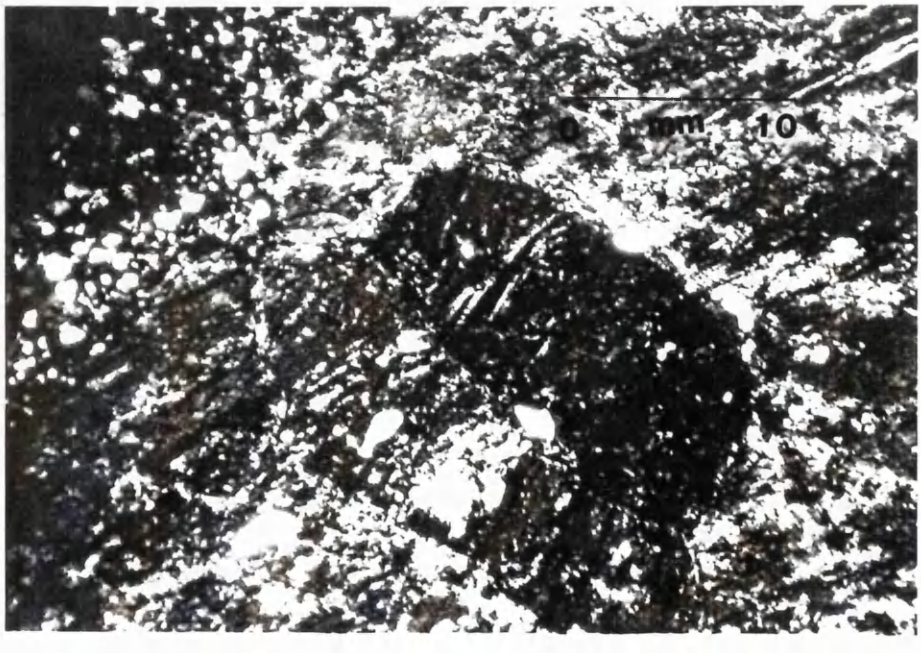

Figure 2.28. Xpls photomicrograph showing euhedral sub-grain in an etched K-feldspar megacryst. Note the oscillatory zoning which is present in both the sub-grain and the megacryst.

Figure 2.30(a)

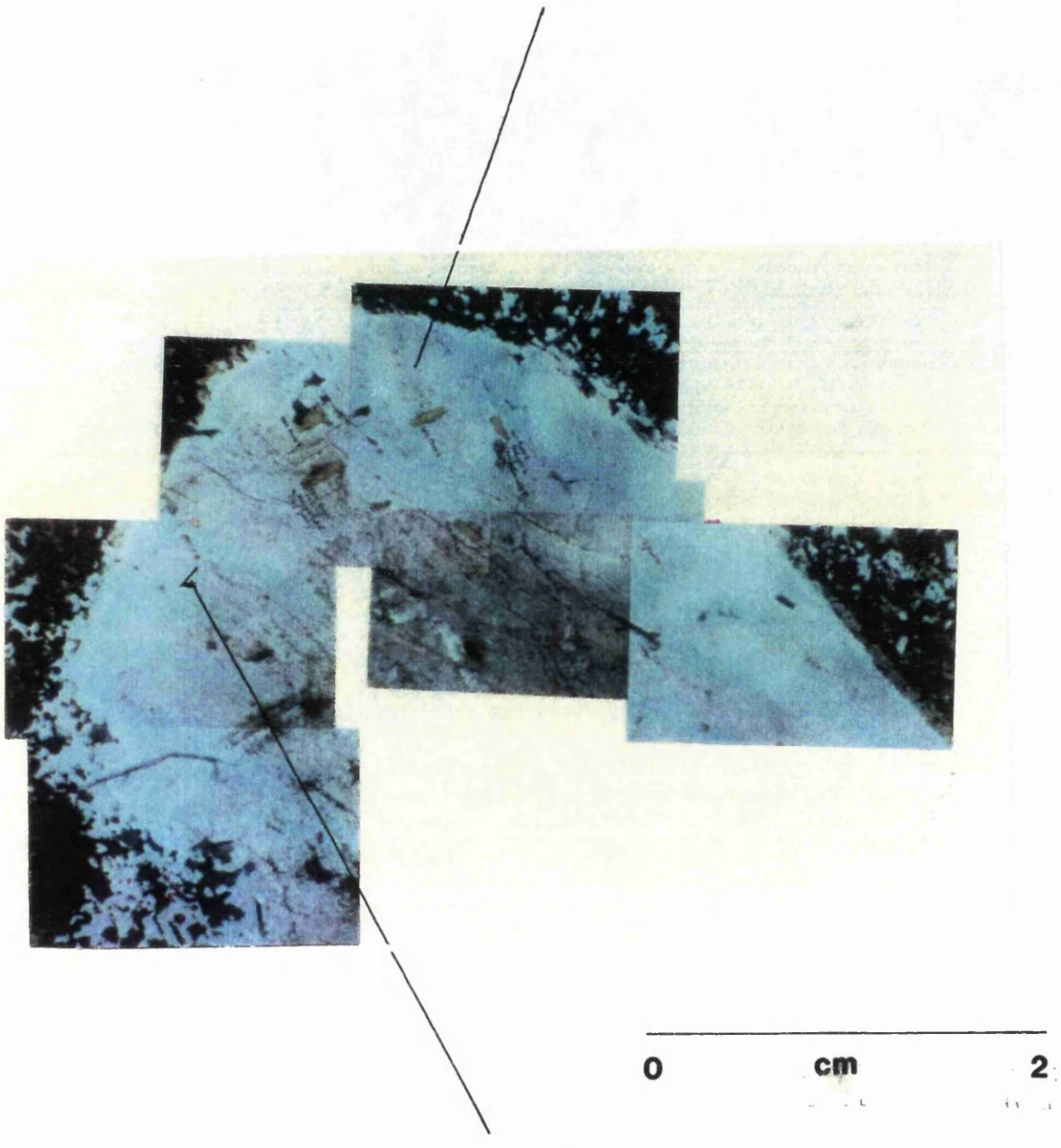

Figure 2.30(b)

Figure 2.30. C.L. montage showing a K-feldspar megacryst from the enclave. The position of the full-scale pictures are shown.

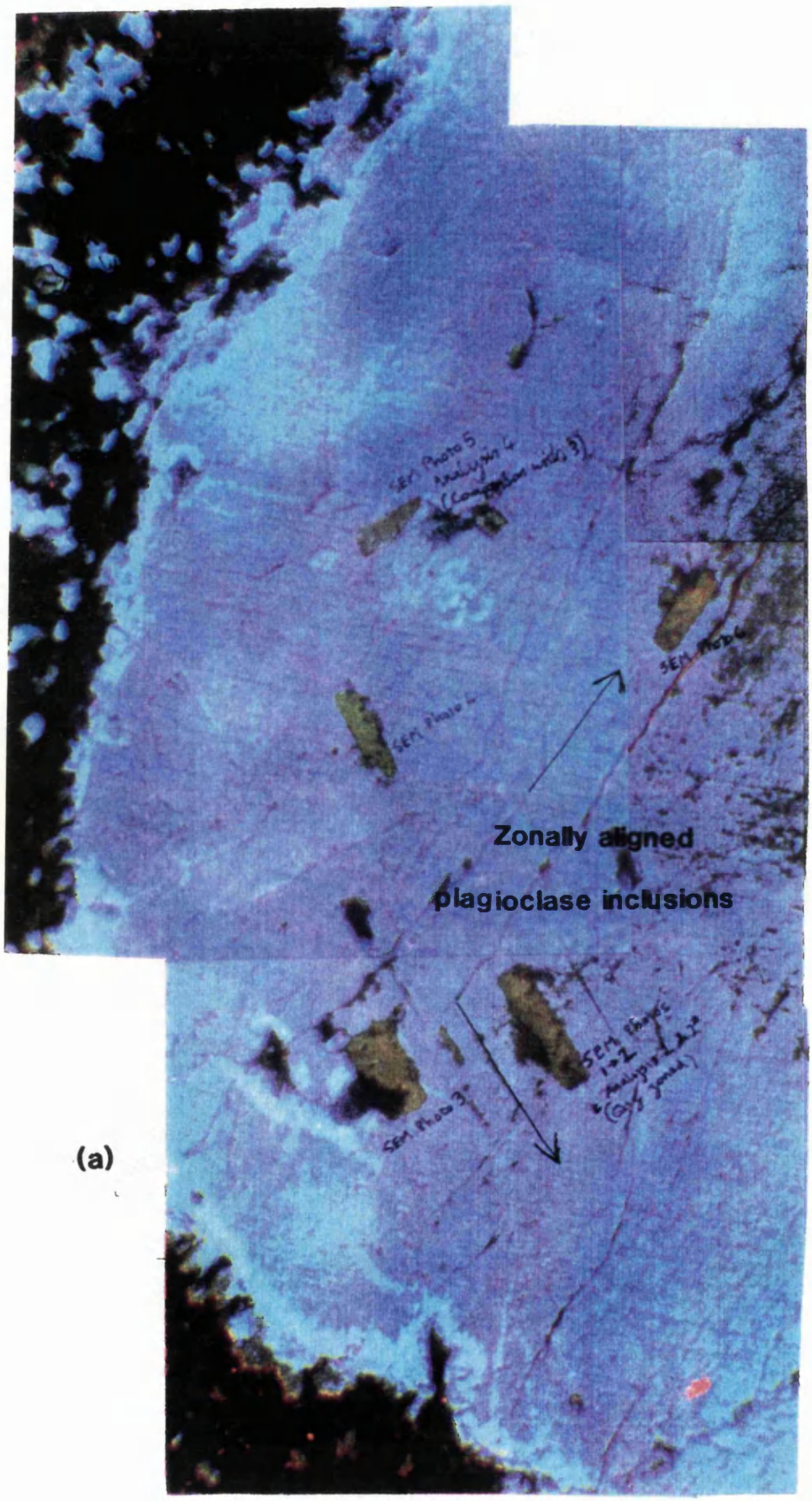
Zonally aligned
plagioclase inclusions
(a)
0
cm
0.5

(b)

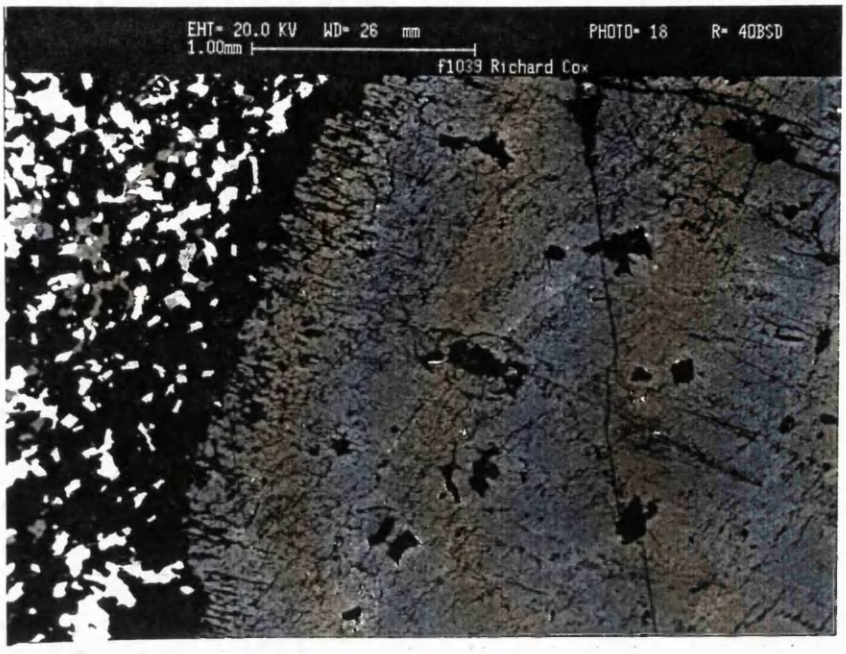

Figure 2.31(a) Back-scattering S.E.M. image of a mantled K-feldspar from the quartz microdiorite enclave. Note the embayed margin to the megacryst and the lower mass of the mantle. The bright rim to the megacryst observed in C.L. images (**Figure 2.30**) shows a higher mass then the megacryst in general.

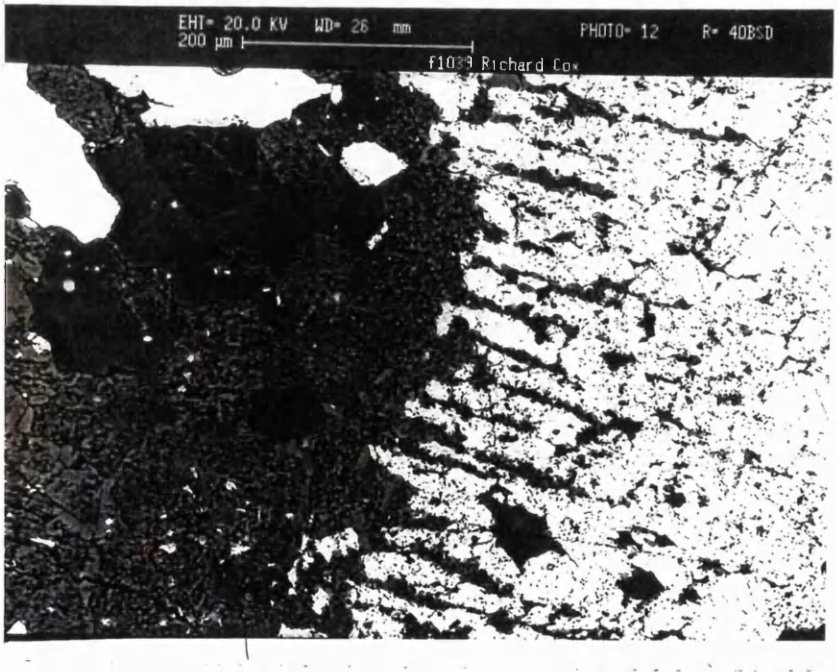

Figure 2.30(b) Close-up back-scattering S.E.M. image of the mantle surrounding the K-feldspar megacryst in **2.30(a)**. The mantle has a complex twinned appearance which is due to it's plagioclase composition. Note the presence of two different compositions of plagioclase in the mantle and the bladed appearance to the embayed K-feldspar.

(bright to dark) zones which are clearly truncated and dissolved at the edges of the crystal (**Figures 2.37(a)** and **2.37(b)**). Small biotite inclusions are present in the plagioclase crystal. The biotite inclusions appear to be zonally arranged with the {001}-axis parallel to the oscillations. The rims of the plagioclase crystals have quite high concentrations of bright biotite matrix crystals, particularly on the flattest edges (**Figure 2.37(a)**) forming a "mafic-mantle" effect, with the biotites.

2.10 Discussion

From the preceding descriptions of the of the minerals in the Shap intrusion, a number of processes appear to be involved in the growth of both the megacrysts, and the matrix minerals.

The first of these processes identified, and probably the least important as far as overall mineral growth is concerned, is the "tectonic" activity indicated by the fracturing of biotites, rotation of megacrysts and foliation of the enclave matrix. It is apparent from the data in **Table 2.1** that the size and twinning of the K-feldspar megacrysts is independent of whether they are sub- or euhedral. The close-aligned orientation of the megacrysts would appear to be largely restricted to the euhedral forms. Harker and Marr (1891) suggested that the orientation was due to magmatic flow but this would clearly affect all the megacrysts and not just the euhedral types. It is unlikely that euhedral megacrysts would be five times more likely to be closely oriented than subhedral forms, i.e. 71% to 14%, (see **Table 2.1**). Poli and Tommasini (1990), Castro et al. (1990) and John and Blundy (1993), illustrated some typical petrographic relationships between enclaves and host granitoids. In most cases the enclaves were flattened and elongated in a "flow" direction. Often mechanical fragmentation of this type of enclave can be observed (Poli and Tommasini 1990).

In the enclave studied here, there is clear foliation of the enclave matrix and megacrysts, and some rotation may have occurred as shown by the megacryst near the boundary of the enclave (**Figures 2.23, 2.24** and **2.32**). The presence of a chilled margin around the edge of the enclave may have helped restrict it's mechanical fragmentation during foliation.

Rotation of the K-feldspar megacrysts during foliation of the enclave and during the alignment of the megacrysts in the granitoid may have contributed to their subhedral nature, by mechanical attrition of the crystals. Smaller scale rotation of the biotites, quartz, etc. in the matrix may have

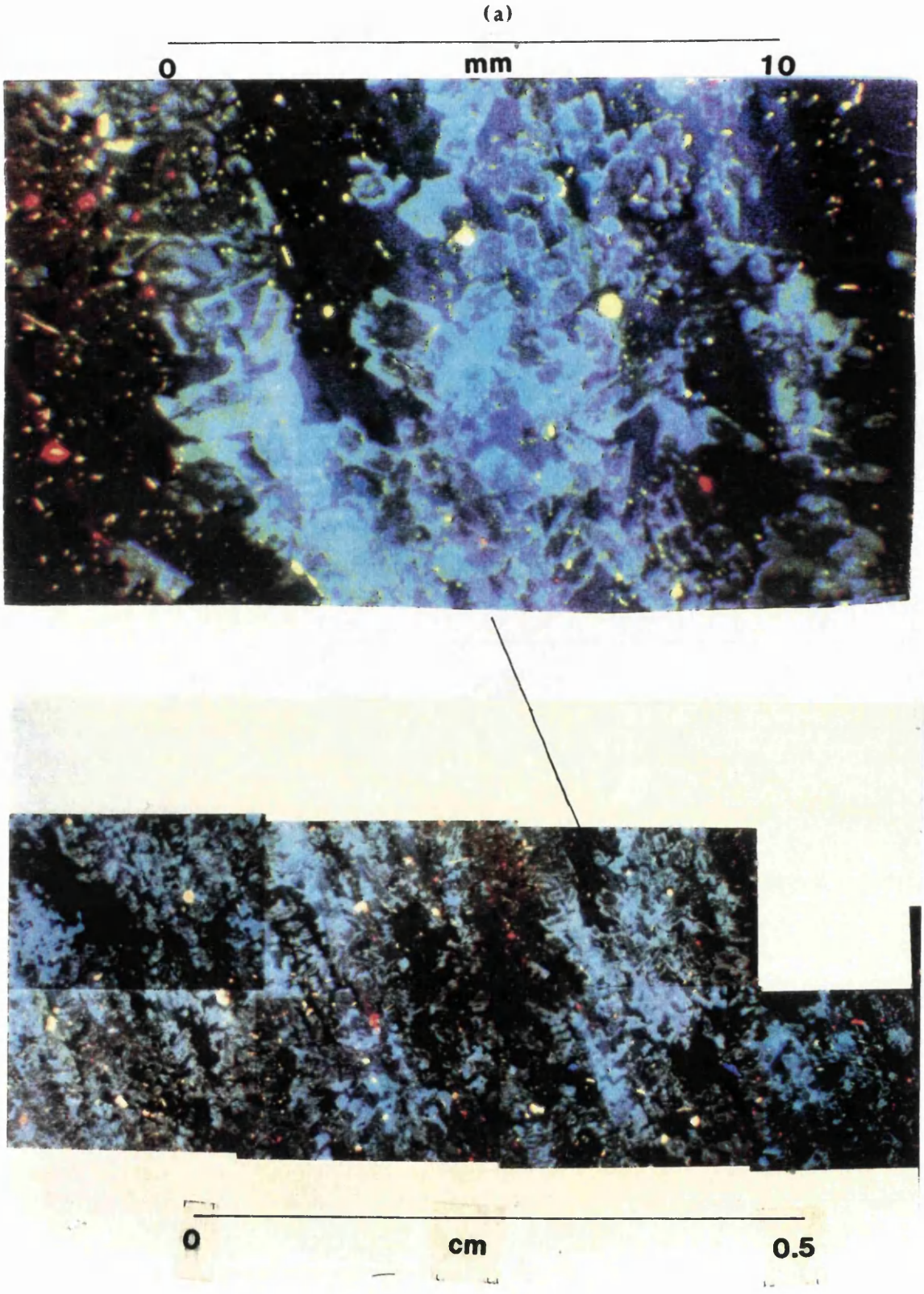

Figure 2.32 C.L. montage of the matrix of the dioritic enclave with (a), a close up showing the blue C.L. plagioclase mantling on a dark C.L. mineral. The foliation of the matrix is also quite apparent.

Figure 2.33. Xpls photomicrograph of a large zoned plagioclase from the enclave matrix. The crystal appears altered and extensively corroded particularly around the margins.

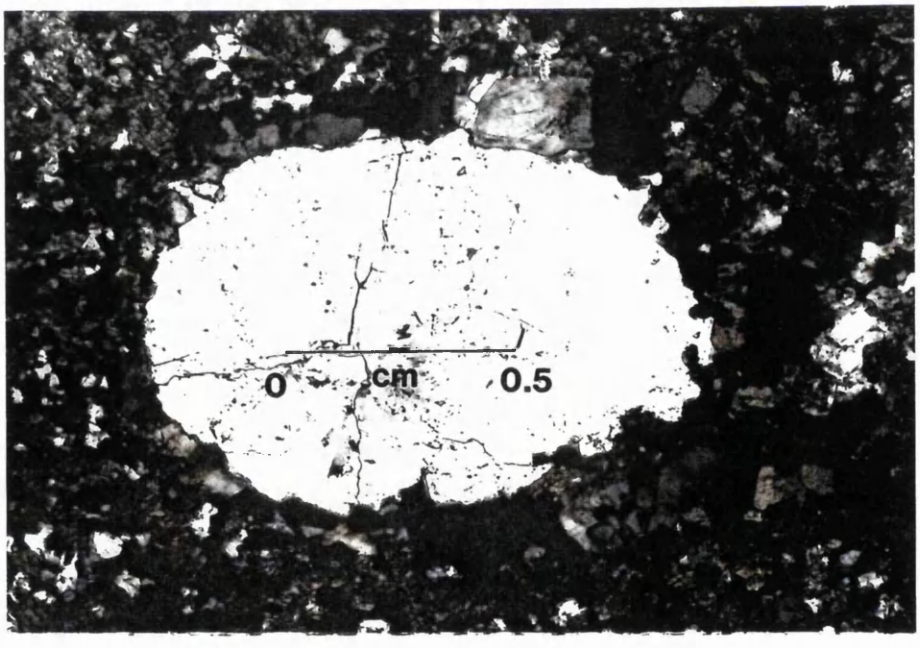

Figure 2.34. Xpls photomicrograph of a large quartz oscelli from enclave. Note the rounded embayments and the "clotting" of plagioclase and biotite around the margin of the crystal.

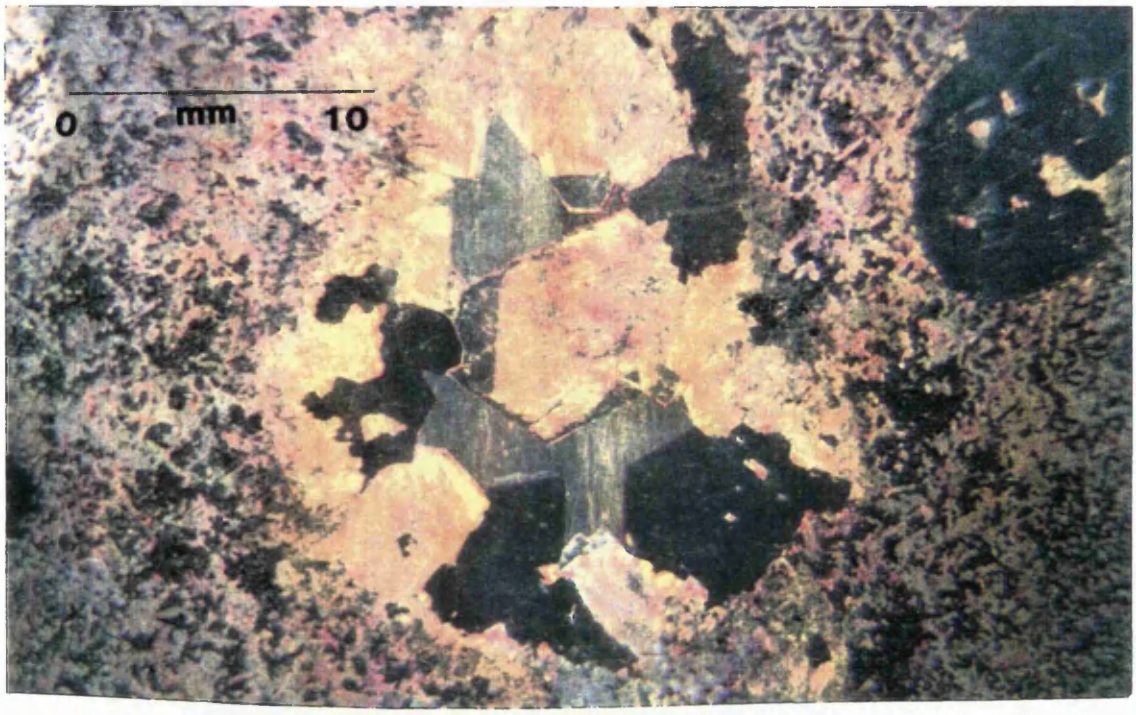

Figure 2.35. Colour photograph of the surface of a stained section of enclave material which shows a K-feldspar (yellow), plagioclase (red) and quartz (clear) granitoid matrix clot which forms a glomerocryst in the enclave matrix. The dissolution of the glomerocryst can be seen around the margin in contrast to the normally euhedral crystals which make up the glomerocryst.

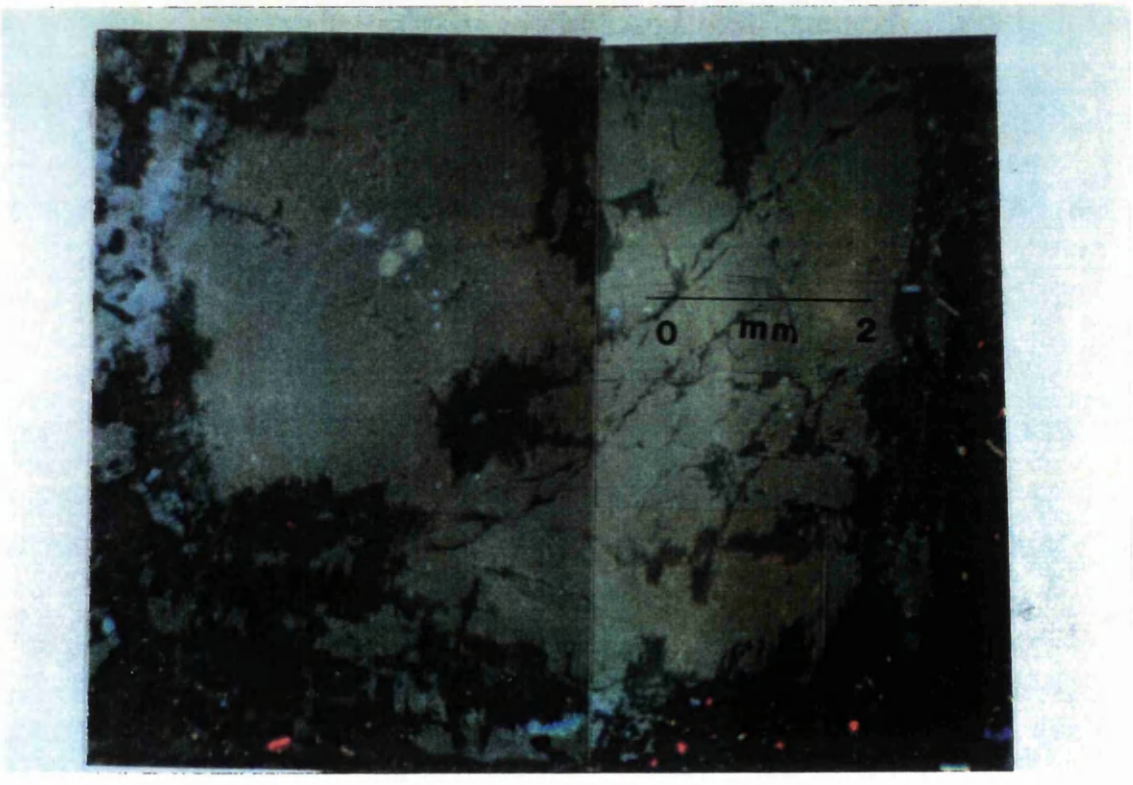

Figure 2.36. C.L. montage of plagioclase crystal shown in **Figure 2.33**. The zoning and truncation of the zones are very clear in this image.

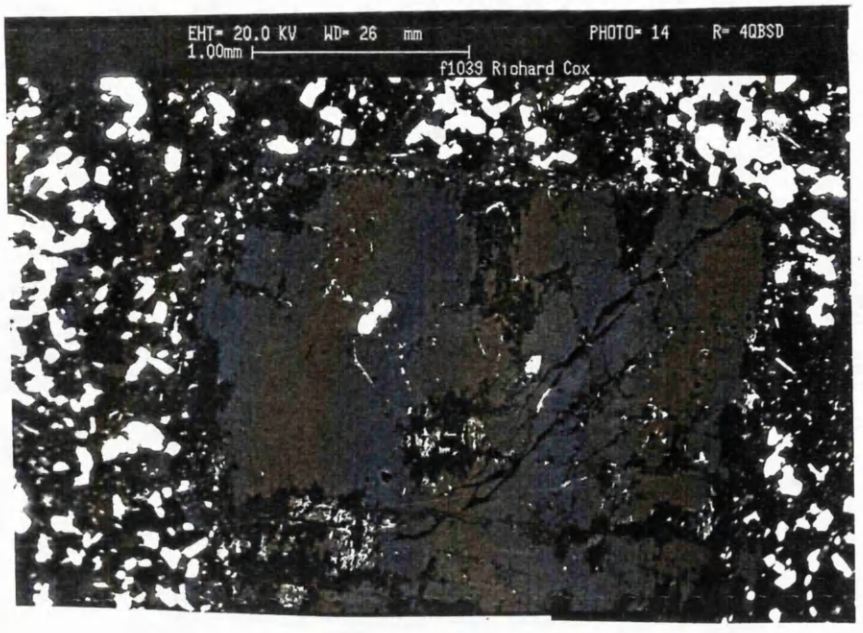

Figure 2.37(a) Back-scattering S.E.M. image of the plagioclase crystal shown in **Figures 2.33** and **2.36**. Note the zonal alignment of the biotite inclusions, and the semi-mantling effect of the biotites along the dissolved margins of the plagioclase.

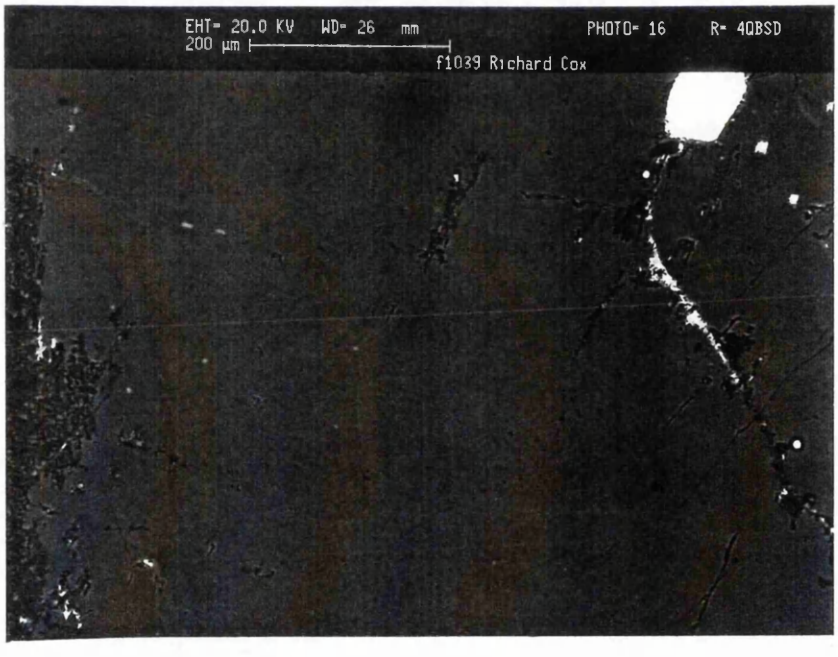

Figure 2.37(b) High-magnification, back-scattering S.E.M. image of the plagioclase crystal shown in **Figures 2.33, 2.36,** and **2.37(a)**. Note the fine high- to low-mass (dark to bright) oscillations indicating oscillatory magmatic growth.

produced the fracturing of the biotites in the granitoid matrix. This would suggest that alignment or "flow" of the minerals occurred in a near-consolidated granitoid body, rather than in a liquid magma.

John and Blundy (1993) examined near-solid granitoid emplacement in the S. Adamello Massive, Italy. They found that mafic enclaves and some matrix crystals were aligned, although lineations were not present. The core units were the least deformed and the outer units were the most xenolithic. This was due to the decreased strain of emplacement in the core of the intrusion. The Shap intrusion has andesitic xenoliths present (Harker and Marr 1891, Grantham 1926) particularly in the wall rocks and the wall-rock areas are generally the least foliated. Although the emplacement of the Shap granitoid is though to be relatively passive (Boulter and Soper 1973), increasing strain deformation caused by the later intrusion of the near-consolidated Stage II granitoid may explain some of the rotation and foliation features described.

The most significant feature of the K-feldspar megacrysts in both the granitoid and the enclave is the evidence for magmatic growth of these crystals. The twinning, large-scale core-to-rim and oscillatory zoning and euhedral, zonally aligned inclusions, are present in both the granitoid and enclave megacrysts. Simple twinning is almost unknown in metamorphic K-feldspars, (Vernon 1968; 1986). The normal core-to-rim zoning indicating a decreasing mass, as shown by back-scattering S.E.M. image (**Figure 2.12**) and the higher-mass of the oscillatory zoning is consistent with magmatic Ba-zoning in K-feldspars (Mehnert and Busch 1981), and is also consistent with the growth of oscillatory magmatic zones caused by small-scale equilibrium shifts (Allegre et al. 1981; Putnis et al. 1992). The frequency and grain-size of the inclusions in the megacrysts increases towards the rims, which along with the zonal alignment of these crystals, is clear evidence for a phenocryst origin for the megacrysts, (Kawachi and Sato 1978; Vernon 1986). Flood and Vernon (1988) concluded that microstructural evidence e.g. inclusions in phenocrysts, often recorded simultaneous crystallisation rather than orders of crystallisation, in granitoid rocks. If this is the case in the Shap granitoid then K-feldspar, plagioclase, biotite and quartz differ little in order of crystallisation, but in their growth kinetics. The increasing frequency and size of the inclusions probably reflects the change in growth rate and nucleation conditions of the mineral components of the granitoid. Whitney (1975; 1988) and Day and Fenn (1982) showed that in non-aqueous, granitic magmas (<2.8 wt. %H_2O), although plagioclase and quartz were the primary phases, K-feldspar grows with a low nucleation density and higher growth rate than

plagioclase. With increasing $\%H_2O$, the reverse becomes true, with plagioclase growing quickly with a low nucleation density. Thus, increasing growth rate of the plagioclase, and decreasing growth rate and increasing nucleation density, of the K-feldspar, may account for the change from K-feldspar megacrysts, to megacrysts with K-feldspar sub-grains near the rims, to matrix K-feldspars. The bright-birefringence rim around the sub-grain/megacryst boundaries are probably the result of either melt trapping or slight resorption of the K-feldspar, which is common in mono-mineralic glomerocryst feldspars (Hogan 1992) i.e. crystals which have formed by "sticking" together in magmatic conditions. The plagioclase having already formed as many slow-growing nuclei, early in the crystallisation history of the granitoid, would simply grow faster in the later, more H_2O-rich magma. This is reflected by the increasing size of the plagioclase inclusions towards the rim of the K-feldspar megacrysts. Again, this is a feature which is present in both the enclave and granitoid megacrysts, indicating an identical growth history for these K-feldspars.

There are however, clear differences between the K-feldspar megacrysts in the granitoid and the enclave. The presence of mafic enclaves in the Shap and many granitoids is generally regarded as indicating two magmas mixing, (Harker and Marr 1891; Grantham 1926; Didier 1973; Cantagrel et al. 1984; Bailey 1984; Castro et al 1990; Poli and Tommasini 1990; Hibbard 1991). There are textures within both the megacrysts and the matrix minerals in the granitoid to suggest hybridisation due to mixing has occurred. Similarly, there are textures within the megacrysts and other minerals in the enclave to suggest that they have been derived from the granitoid by mixing. Some of the subhedral megacrysts in the granitoid show extreme rounding which could be due to emplacement related deformation. However, the large size of the megacrysts within the granitoid (>3cm, **Table 2.1**) would mean the removal of fairly large amounts of material from the megacrysts to cause this subhedral shape. No strain shadows or rotational fractures are visible in these megacrysts, which are common features of strain deformed megacrysts (Debat et al. 1978; Paterson et al. 1989). Foliation of the matrix is also largely absent, therefore, chemical dissolution of the megacrysts to produce most of the subhedral shape, seems likely.

The detailed morphology of the large oscillatory zone, particularly using C.L. and S.E.M. techniques (**Figures 2.4, 2.10(a), 2.11(a), 2.14** and **2.15**) shows various features which point to dissolution and resorption to produce this zone, rather than small-scale changes in growth. The irregular shape to the zone certainly suggests that it has grown on a partly dissolved and therefore

irregular crystal. The presence of Ti, (as shown by the bright blue colour in C.L.), and high-mass elements shown by the bright back-scattering S.E.M. images (**Figures 2.14** and **2.15.**) within the zone indicates that elements such as Ca, Ti and Ba have been preferentially resorbed by the growing K-feldspar, after dissolution. Ca and Ba are often concentrated in feldspars as a result of resorption after mixing with high temperature magmas, (Castro et al. 1990; 1991). The zone appears somewhat wider, although with less mass, on faces which are more irregular, and therefore more dissolved. Resorption may have involved the distribution of Ba and Ca over a faster growing edge, where more dissolution had occurred. Anderson (1984) found that {001}- and {201}-faces grew faster than the other euhedral faces in feldspar phenocrysts, within basalts. Consequently, radial (i.e. sideways) growth in feldspar phenocrysts occurs. Thus, the high Ba and Ca concentration in the slow growing {010}-faces would create the high mass of the zone as seen in **Figures 2.14(a)** and **2.14(b)**, parallel to the megacryst's long axis. Faster resorption on the {001}- and {201}-faces would cause the Ba to be distributed over a larger resorption interface, which is witnessed by the lower mass, but wider zone (**Figures 2.15(a)** and **2.15(b)**). Therefore, the process of dissolution and resorption probably caused the growth of this prominent zone and chemical dissolution accounts for the high numbers of subhedral megacrysts in the granitoid.

The evidence for modification of K-feldspar megacrysts due to mixing within the enclave is quite apparent. The megacrysts have undergone much more extensive dissolution, which can be seen as extreme truncation of oscillatory zones (**Figures 2.23, 2.26** and **2.30**) and irregular embayment around the dissolved crystal edge (**Figures 2.31(a)** and **2.31(b)**).

The mantling of the K-feldspar megacrysts by plagioclase (**Figures 2.27**) is a feature often associated with xenocrysts of K-feldspar in mixed magmas (Vernon 1986; Castro et al. 1990; Hibbard 1991; Stimac and Wark 1991). Wark and Stimac (1991) experimentally investigated the development of plagioclase mantles on dissolving K-feldspars. They found that mantles often develop as inward growing plagioclase rims which cause "bladed embayments". These are very similar to the embayments seen in (**Figures 2.31(a)** and **2.31(b)**), in the Shap enclave megacrysts. The composition of the plagioclase crystals within the enclave matrix is different to that of the plagioclase in the granitoid matrix. This is shown by the Ti^{4+}-activation colour in the C.L. images (**Figure 2.32(a)**). Wark and Stimac's model involves the diffusion of Ca and Na into the growing plagioclase mantle from the surrounding mafic liquid, and K diffusion out of the dissolving rim of the megacryst. The presence of two plagioclase compositions in the plagioclase mantle is due to the differing rates

of Ca and Na diffusion. Such diffusion may well cause the resorption of Ti^{4+} into the K-feldspar and thus leading to the bright blue C.L. rim (**Figure 2.30**). The more mafic, and consequently more Ti-rich, enclave matrix has given rise to the blue plagioclase C.L. colours in the matrix of the enclave (**Figure 2.32**). The subsequent diffusion of Ca and Na from the enclave therefore imparts the growing plagioclase mantle with a similar blue C.L. colour (**Figures 2.30**). The "halo" of more mafic material around the megacrysts (**Figures 2.23** and **2.24**) is probably due to K-enrichment from the dissolving K-feldspar rim, which in turn promotes biotite growth, hence the more mafic enclave matrix observed. Therefore, the dissolution of the K-feldspar megacrysts in the enclaves of the Shap intrusion and not porphroblastic growth, has produced the differences between the Shap granitoid and enclave megacrysts.

The later crystallisation history of the K-feldspar is represented by the two perthite exsolutions. The micro-perthite appears to be present mainly in the megacrysts and is almost absent from the matrix K-feldspars. Both the matrix K-feldspars and the megacrysts have the fine crypto-perthite present. Similar coarse micro-perthites to those in the Shap megacrysts are often associated with exsolution under aqueous, magmatic conditions (Parsons 1978; Worden et al. 1989), and are called deuteric perthites. The presence of these perthites almost exclusively in the megacrysts suggests that they were exsolved prior to the formation of much of the matrix K-feldspar. The exsolution of these deuteric perthites may correspond to the increasing $\%H_2O$ conditions which also led to the change in growth rate and nucleation density. The presence of higher birefringence rims to the deuteric perthites and patchy zoning, may well be due to increased water activity at a later stage, giving rise to patch perthite growth which is often seen in K-feldspars (Worden et al. 1989). Late-stage exsolution of the crypto-perthite is probably the last of the major events in the formation of the K-feldspars in these rocks.

2.11 Conclusions

1) The petrographic evidence from the K-feldspar megacrysts in the Shap granitoid and enclaves, i.e. twinning, oscillatory zoning, zonal alignment of inclusions, suggests that they were formed as phenocrysts in magmatic conditions, and not porphyroblasts.

2) The growth kinetics of the K-feldspars have been controlled by increasing magmatic H_2O, which has caused a change in the crystallisation of K-feldspars producing firstly megacrysts, then megacrysts with sub-grains and lastly matrix crystals.

3) The presence of deuteric perthites and patch perthites, which are largely restricted to the megacrysts, also suggests an increasing H_2O content prior to the crystallisation of much of the K-feldspar in the matrix.

4) The mixing textures (e.g. dissolution) in the granitoid K-feldspar megacrysts and plagioclase crystals indicate that a mixing event(s) and thus hybridisation of the granitoid has occurred.

5) The presence of mixing textures in some of the K-feldspar megacrysts, plagioclase and quartz crystals in the quartz microdiorite enclave (i.e. dissolution and resorption, plagioclase mantles, quartz oscelli, glomerocrysts of granitoid matrix) suggests that they have been derived from the granitoid during mixing and are therefore xenocrysts in the enclave, and not porphyroblasts.

6) Small-scale, late magmatic, deformation during emplacement, caused slight rotation of megacrysts, fractured biotite in the granitoid and foliated the enclave matrix crystals.

7) Exsolution of crypto-perthites in both the K-feldspar megacrysts and matrix crystals has occurred at a late-stage in the crystallisation history of the granitoid.

Electron-microprobe investigations of textures in the Shap granitoid megacrysts: some petrological implications.

3.1 Introduction

The petrographic features of the K-feldspar megacrysts in the Shap granitoid (Chapter 2) seem to indicate that the megacrysts grew in magmatic conditions. Changes in growth kinetics, caused by cooling and increasing $\%H_2O$ in the residual melt fraction, may have brought about the change from the crystallisation of megacrysts to matrix K-feldspars. Changes in the growth rate of plagioclase may also reflect this pattern. Electron-microprobe investigations of some of the growth features of the K-feldspars and plagioclases in the Shap granitoid were carried out to determine mineral chemistry, and hopefully construct and interpret petrological models based on these measurements.

The microprobe used was a Cameca SX50 model, with an accelerating voltage of 15kV and a 20nA beam current. The detection limit for most elements is about 100ppm with a 2% error, which is based on calculated composition totals.

The technique is similar in principle to C.L. and S.E.M. imaging in that the incident beam excites the electrons in the atomic structure of the elements forming the mineral to higher energy states. Electrons subsequently emit x-rays which are then diffracted through the four crystal spectrometers to analysis equipment which calculates the elemental composition of the mineral, based on the wavelengths and the intensity of the x-rays emitted. Software within the computer attached to the microprobe can then be used to calculate mineral compositions.

The textures investigated here, were the primary growth features of the feldspars and secondary exsolution in the K-feldspars. Firstly, the oscillatory zoning and the exsolution features (perthites) of the K-feldspars, and then the general composition of the plagioclase matrix and inclusions were chemically analysed, and the petrological implications of these analyses were studied.

3.2 Chemical characteristics of oscillatory zones in the K-feldspar megacrysts

Zoning in alkali feldspars is not normally associated with fluctuations in the major-element, molecular end-member, (i.e. K-, Na-, Ca-feldspar) content. This is particularly true of K-feldspars, unless they have been quenched quickly from high temperatures, because the Ca and Na components will undergo un-mixing in the form of perthite exsolution.

This in turn will tend to disrupt and even remove any Na- and Ca-oscillations (Smith 1974).

The megacrysts in the Shap granitoid show two distinctive types of oscillatory zoning, namely fine-scale regular zones and a disrupted, large-scale oscillation. Both these oscillatory zone types have a higher mass than the normal K-feldspar (see Chapter 2). This is shown by the brightness of the zones in back-scattering S.E.M. images. This is likely to be due to a concentration of high-mass elements such as Fe^{3+} replacing Al^{3+}, and trace-elements such as Ba, Rb, Sr, Cs and Pb replacing K, (Smith 1974). Of these trace-elements, Ba is the most common in K-feldspars and Ba/K substitution is the most likely to explain the high-mass zoning in these megacrysts. Ba forms an isomorphous series with $KAlSi_3O_8$ and $BaAl_2Si_2O_8$ (celsian) end-members (Deer et al. 1992). The celsian end-member and Ba-rich feldspars are normally associated with hydrothermal activity, often accompanying magnesite in ore-bodies. However, Ba has a high distribution coefficient in granitoid melts, and will be concentrated in biotite and K-feldspar relative to plagioclase and the magma (Smith 1974; Rollinson 1993). Higher temperature growth, tends to produce the highest Ba-contents within K-feldspars (Barth 1961; Smith 1974).

Spot microprobe traverses over both large and fine oscillations were taken. The position of these and the results obtained are shown in **Figures 3.1(a), (b)** and **(c)**. Although every attempt was made to avoid impurities or perthites the very fine scale and pervasive nature of the crypto-perthites, made analysis of pure K-feldspar megacryst very difficult. This probably accounts for the random nature of some of the points shown in the diagrams.

The fine oscillatory zoning of the K-feldspar megacrysts in the Shap granitoid follows the variable fluctuations in zone frequency described by Mehnert and Busch (1981). The cores of the Shap megacrysts have oscillations which are continuous for most of the crystal, and appear to be of a similar nature throughout. The Ba-content of the fine zones (**Figure 3.1(a)**) shows a general decrease across the zone from the core to rim of the megacryst. Both the fine oscillatory zones present in the microprobe traverse (**Figure 3.1(a)**), show slight Ba-peak concentrations at the edges, with a slight decrease in the Ba-concentration at the zone centre.

The large oscillatory zone shows Ba, Na, and Ca concentration pattern differences, both from the small oscillations and in different areas of the zone itself, (**Figures 3.1(b)** and **3.1(c)**). The chemical variations across the zone correspond to the differences in back-scattering S.E.M. images observed previously (see Chapter 2), where the {010}-face of the crystal had a very

sudden mass increase across the zone. The {201}- and {001}-faces have a high mass inner area, followed by a perthite-free zone, with a gradual reoccurrence of the crypto-perthite, into the K-feldspar beyond the zone (**Figure 3.1(c)**). The morphology of this large oscillation shows nucleation and growth of the zone on an irregular crystal rim, possibly caused by dissolution of the K-feldspar megacryst prior to the growth of the zone, (see Chapter 2).

The microprobe point-scan across the {010}-face shows a very large and sharp increase in the Ba-content with a gradual reduction in Ba, towards the rim-ward edge of the zone (**Figure 3.1(b)**). This pattern is mirrored quite closely by the Ca of the {010}-zone face. Both Ba and Ca are found in high temperature K-feldspar (Barth 1961; Smith 1974; Furhman and Lindsley 1988), normally substituting for the K. Therefore, the resorption of Ba and Ca by the K-feldspar growing at a higher temperature and with a high distribution coefficient for Ba and Ca would account for the chemical distribution observed in **Figure 3.1(b)**.

A similar pattern exists for the distribution of Ba, Na and Ca in the {201}-face of the zone. The Ba-concentration shows a slightly less sudden increase, than the Ba-concentration at the zone edge on the {010}-faces. The Ba-concentrations within the zones range from 0.6wt% to 0.68wt% across the {201}-faces, in comparison with 0.9wt% to 1.05wt% across the {010}-face. Ca and Na both show a sharp increases in concentration, across the high-mass (bright S.E.M. image) rim to the zone, (**Figure 3.1(c)**). There is subsequently a steady decrease in the in Ca and Na towards the rim-ward edge of the zone, which also corresponds to a K-increase, and the reoccurrence of the crypto-perthites.

Anderson (1984) found that feldspar phenocrysts grew in a radial manner, with {201}- and {001}-faces growing faster than the {010}-faces. The resorption of Ba and Ca, and possibly Na over a faster growing interface may produce more diffuse concentrations of the elements being resorbed. This is may explain the extra width and lower Ba-content of the {201}- and {001} faces of the zone, (**Figure 3.1(c)**).

All the zones, both fine and large scale, show an increase in the Ba-content of the K-feldspar before the edge of the zone. This possibly suggests that Ba has diffused into the adjacent K-feldspar after the formation of the zone, to give the smooth profiles observed in **Figures 3.1(a), (b)** and **(c)**. This may also account for the Ba-peaks at the edges of the fine oscillatory zones (**Figure 3.1(a)**). This process must have been fairly limited as the zone would not have been preserved if extensive or long term diffusion of Ba had occurred.

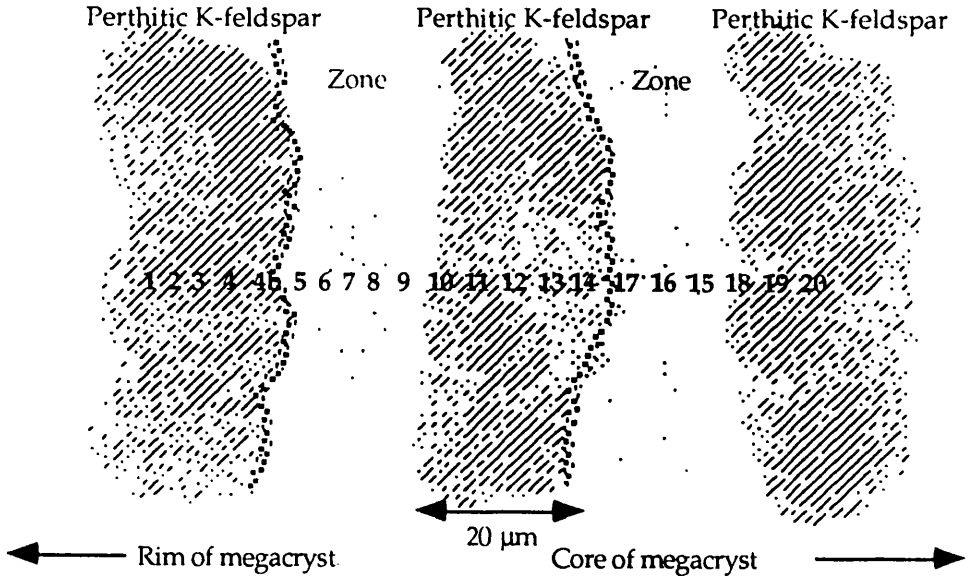

Figure 3.1(a). Sketch of fine magmatic zones with point numbers analysed.

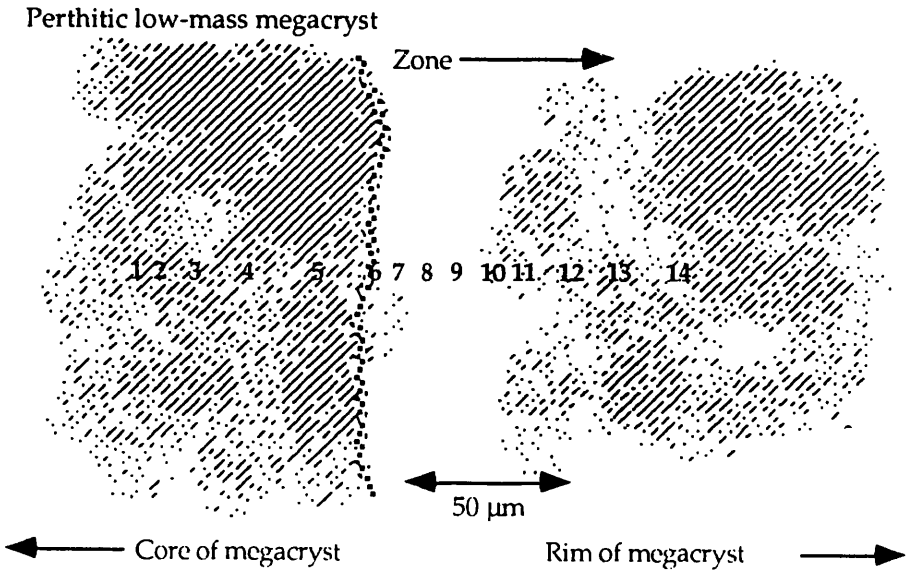

Figure 3.1(b). Sketch of {010}-face of large magmatic zones with point numbers analysed.

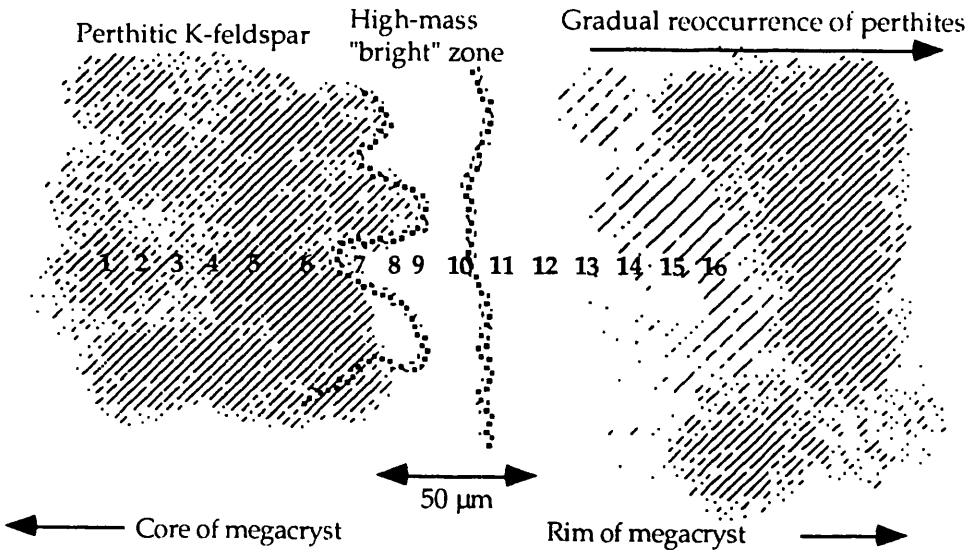

Figure 3.1(b). Sketch of {010}-face of large magmatic zones with point numbers analysed.

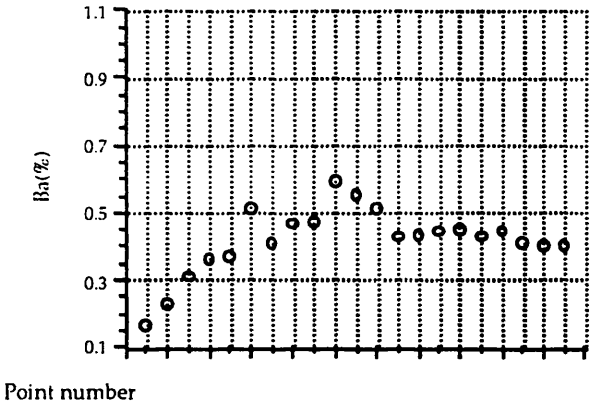

Figure 3.1(a) (cont.)

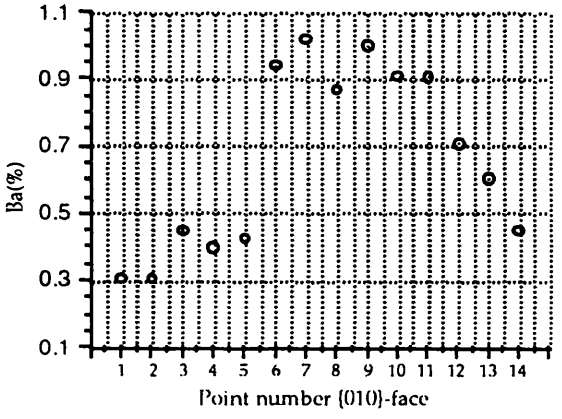

Figure 3.1(b) (cont.)

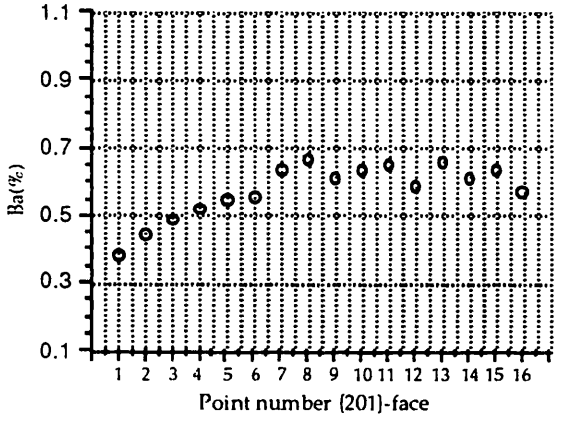

Figure 3.1(c) (cont.)

Figures 3.1(a),(b) and (c) Wt% Ba for the point analysed in the preceding sketches.

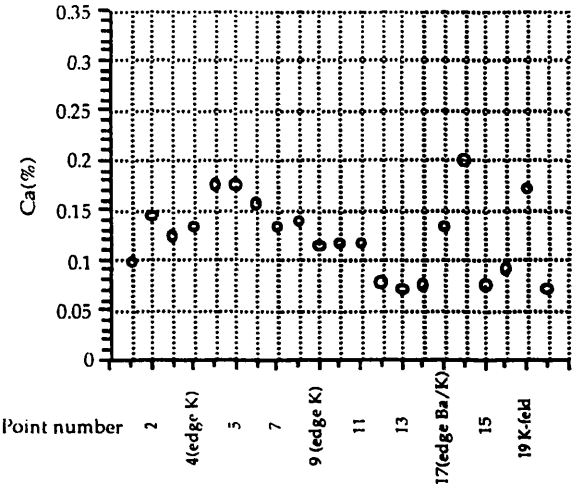

Figure 3.1(a) (cont.)

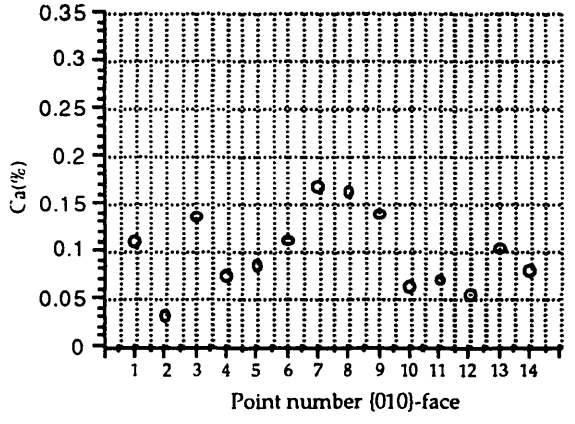

Figure 3.1(b) (cont.)

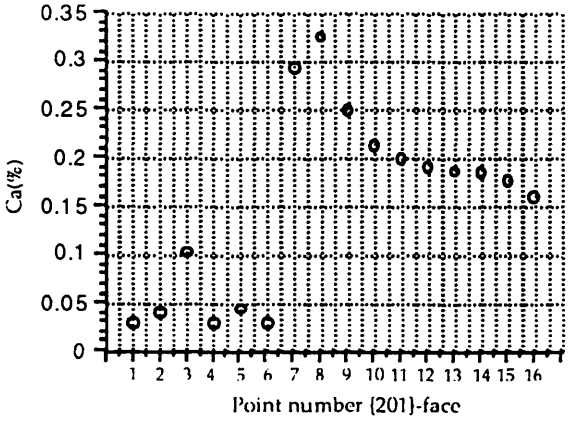

Figure 3.1(c) (cont.)

Figures 3.1(a),(b) and (c) Wt% Ca for the point analysed in the preceding sketches.

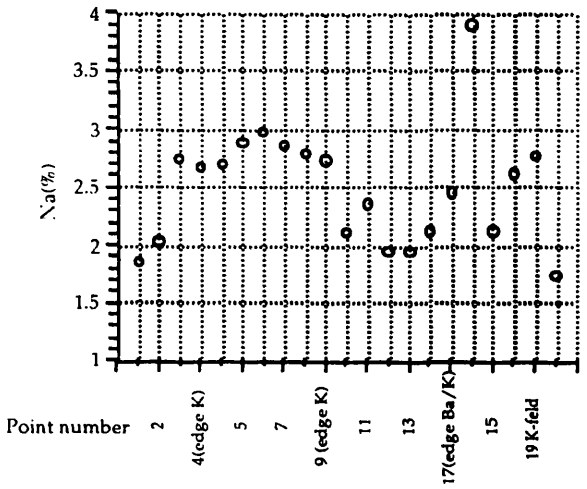

Figure 3.1(a) (cont.)

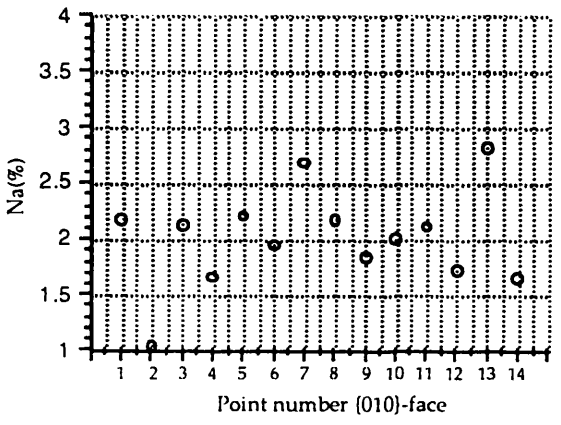

Figure 3.1(b) (cont.)

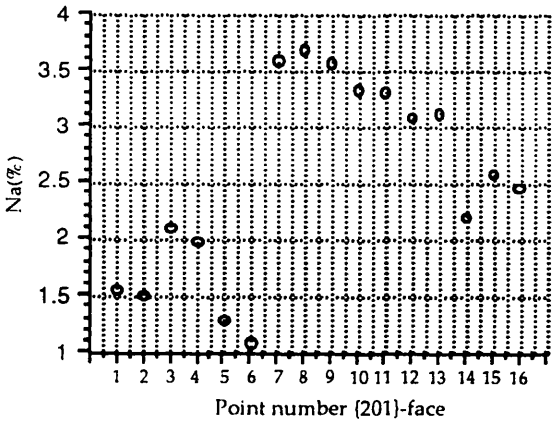

Figure 3.1(c) (cont.)

Figures 3.1(a),(b) and (c) Wt% Na for the point analysed in the preceding sketches.

3.3 Ternary growth and un-mixing of the K-feldspar megacrysts.

The K-feldspar megacrysts show two different perthite exsolutions. One is a coarse, rather irregular micro-perthite, which can be seen cutting through zones, sub-grain boundaries, but which is almost exclusively restricted to the megacrysts. The presence of a fine crypto-perthite, which is regular in occurrence and shape, but does not cut through the oscillatory zones, occurs in both the megacrysts and matrix K-feldspars. This suggests that the granitoid has undergone a sub-solvus growth history with the exsolution of the micro-perthites prior to the K-feldspar matrix growth (see Chapter 2).

The sub-solvus growth of alkali feldspars often produces a complex sequence of exsolution microtextures (Parsons 1978; Brown and Parsons 1989). These microtextures include coherent perthites (crypto-perthites) and partial deuteric un-mixing, which may be represented by irregular micro-perthites (Figure 3.2).

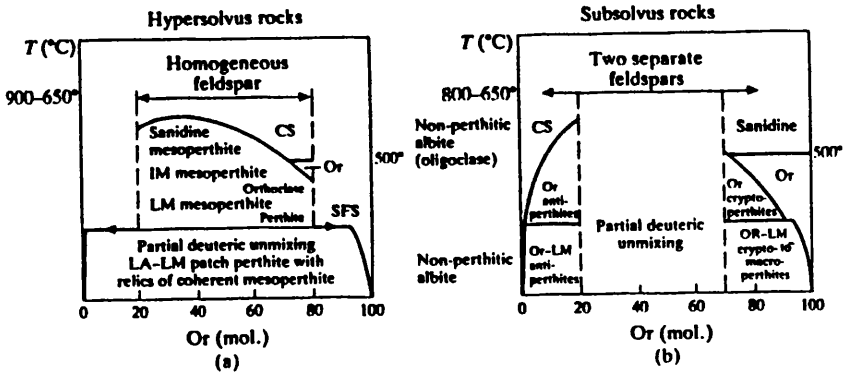

Figure 3.2. The sequence for the development of (a) hyper- and (b) sub-solvus growth textures, in alkali feldspars (from Brown and Parsons 1989).

The partial deuteric un-mixing (Figure 3.2) in the Shap granitoid, involves a move from strongly ternary (i.e. higher Ab- and An-content) composition in the alkali feldspars to a less ternary stable phase by exsolution of part of the An- and Ab- content within the crystal.

The calculation of the ternary compositions simply involves the multiplication of the micro-perthite and the K-feldspar compositions by the average micro-perthite and K-feldspar contents respectively. These figures are then added together and re-calculated to 100% to give the part un-mixed values. As there are only two crypto-perthite analyses available, the multiplied values were added to the first and the second pair of K-feldspar analyses in turn, before re-calculating to 100%. This gave the final un-mixed values shown in Table 3.1.

The compositions and relative proportions of the perthites in the K-feldspar megacrysts in the Shap granitoid were measured using electron microprobe analysis and S.E.M. image analysis respectively. The pre-exsolution (ternary) compositions of the K-feldspars can then be calculated. This is assuming the closed-system exsolution of the perthites in the megacrysts. The mineral compositions shown in **Table 3.2** are calculated by the software of the probe's computer, using stoichiometry, based on the measured element/oxide content of the sample. The measured K-feldspar mineral compositions, and calculated partly un-mixed compositions, i.e. with only the micro-perthites exsolved, and ternary compositions, i.e. with no exsolution, are shown in **Table 3.1**, along with the mineral compositions of the cores and rims of the plagioclase matrix, and measured (i.e. un-mixed) matrix K-feldspars.

Sample	Or	Ab	An	Sample	Or	Ab	An
K-feldspar	55.06	40.68	4.26	Micro-	1.12	90.75	8.12
megacryst	52.10	41.62	6.28	perthite	1.55	90.01	8.44
(ternary	59.76	35.90	4.34		1.76	88.72	9.53
i.e. both	58.54	36.85	4.61		1.47	89.24	9.29
perthites)							
K-feldspar	77.85	32.68	3.80	Crypto-	2.44	97.09	0.46
megacryst	75.20	34.46	5.68	perthite	4.03	94.83	1.14
(part	79.53	30.29	3.89				
un-mixed)	77.96	32.08	4.29	Plagioclase	1.96	72.66	25.38
				inclusions	1.66	72.05	26.29
K-feldspar	85.31	14.51	0.18	(cores)	1.85	70.85	27.31
megacryst	85.37	13.92	0.71				
(measured	82.46	17.38	0.16	Plagioclase	3.94	64.52	31.53
un-mixed)	82.90	16.85	0.25	matrix	3.98	65.47	30.55
				(cores)	3.66	68.06	28.28
K-feldspar	87.92	12.02	0.05		3.75	67.73	28.53
matrix	84.33	15.49	0.18				
(measured	88.22	11.35	0.42	Plagioclase	0.61	92.24	7.14
un-mixed)	86.01	13.90	0.09	matrix	0.77	89.35	9.88
				(rims)	0.93	91.20	7.87
					1.19	90.31	8.51
					1.26	89.00	9.75
					1.34	91.09	7.57

Micro-perthite(%)	Crypto-perthite(%)	Porosity(%)
8.8	13.4	3.8
11.8	14.9	2.8
7.2	17.4	2.6
10.2	14.3	4.3
12.6	13.1	1.5
8.7	14.9	2.5
AVE. 9.88	14.66	2.92

Table 3.2. Data showing the feldspar compositions of samples of K-feldspar megacrysts, plagioclase and perthites, and calculated ternary (pre-exsolution) compositions of the megacrysts based on the average perthite compositions (measured with microprobe) and content (measured by S.E.M. image analysis) within the megacrysts.

Furhman and Lindsley (1988) produced a geothermometer for feldspars with ternary compositions. The temperatures at which stable ternary feldspars exist, can be represented as a series of isotherms on a standard ternary feldspar diagram. The compositions of the feldspars from **Table 3.1** are plotted on such diagram, along with the isotherms determined by Furhman and Lindsley (1988), and is shown below (**Figure 3.3**).

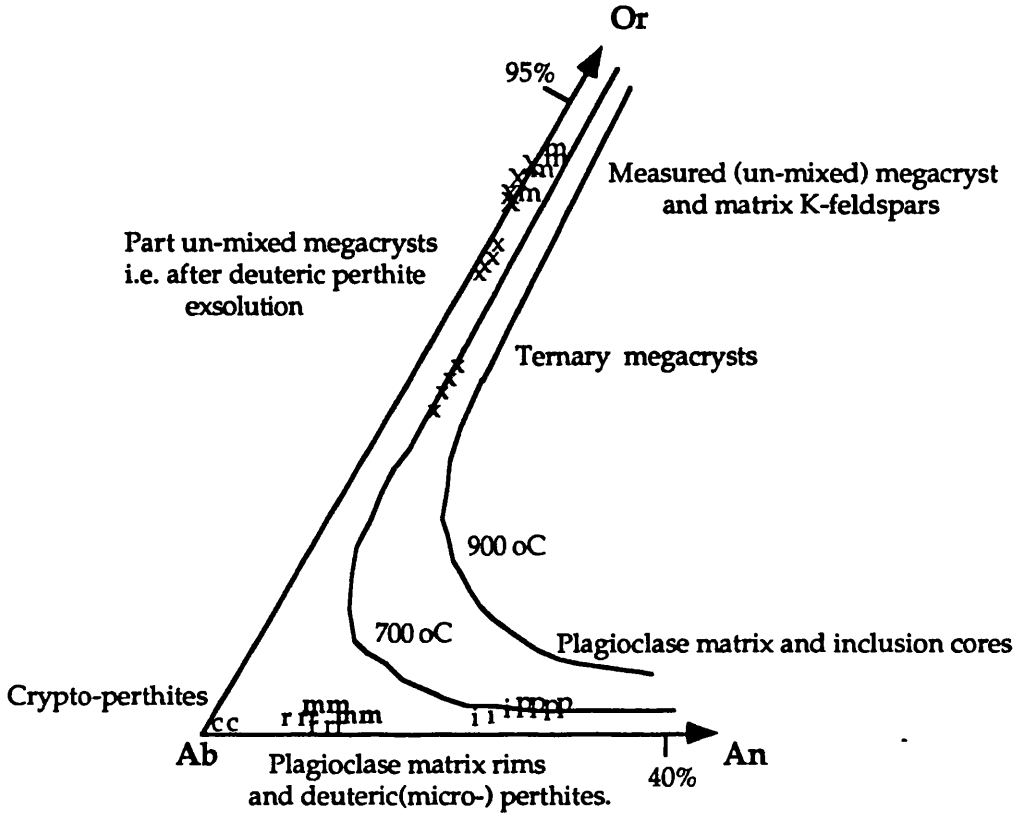

Figure 3.3. A ternary feldspar diagram with the data from **Table 3.1** plotted. The isotherms are based on the stable temperatures for ternary composition feldspars, (after Furhman and Lindsley 1988).

The inclusions within the megacrysts often have zones around them (see Chapter 2). Small amounts of Na-diffusion out of the host K-feldspar megacryst into the inclusions, may account for the slight differences in the An-content of the matrix and inclusion plagioclase crystals. This possibly accounts for the zones surrounding the inclusions (Chapter 2) and the slight variation in composition between the matrix plagioclase cores and the inclusions observed in **Figure 3.3**. Similar, high temperature redistribution of material from within K-feldspar megacrysts adjacent to plagioclase inclusions has also been reported by Dempster et al. (1994). The estimated ternary K-feldspar compositions and the plagioclase cores generally show 700°C temperatures, based on the isotherms plotted. The rims of the matrix

plagioclases show compositional ranges which are very similar to the deuteric micro-perthites. This may indicate their cogenetic formation at the same temperatures in the magma. Both the micro-perthites and the plagioclase matrix rims are below the 700°C isotherm. The crypto-perthites show almost pure albite compositions and thus, are the least ternary in nature. The distribution of the plagioclase inclusions and matrix core and the ternary K-feldspar megacryst compositions suggests that they grew as coexisting ternary crystals at >700°C temperatures. Deuteric un-mixing and the subsequent matrix plagioclase and K-feldspar growth is indicative of a change in sub-solvus conditions (Brown and Parsons 1989). Therefore, a change in the sub-solvus growth conditions of the feldspars, seems to have occurred at about 700°C in the Shap magma.

Increasing solvus temperature may be caused by a high An-content in the cooling magma (Brown and Parsons 1989). In the case of the Shap magma the ternary plagioclases have An-contents of less that 30%, which is unlikely to cause substantial increase in the temperature of the solvus. The lowering of solidus conditions in cooling granitoids has been studied by many authors (Smith 1974; Parsons; 1978; 1983; Brown and Parsons 1989; Dempster et al. 1994) and has been identified as a common process in many granitoids and the process applied to the Shap magma is illustrated in **Figure 3.4.**

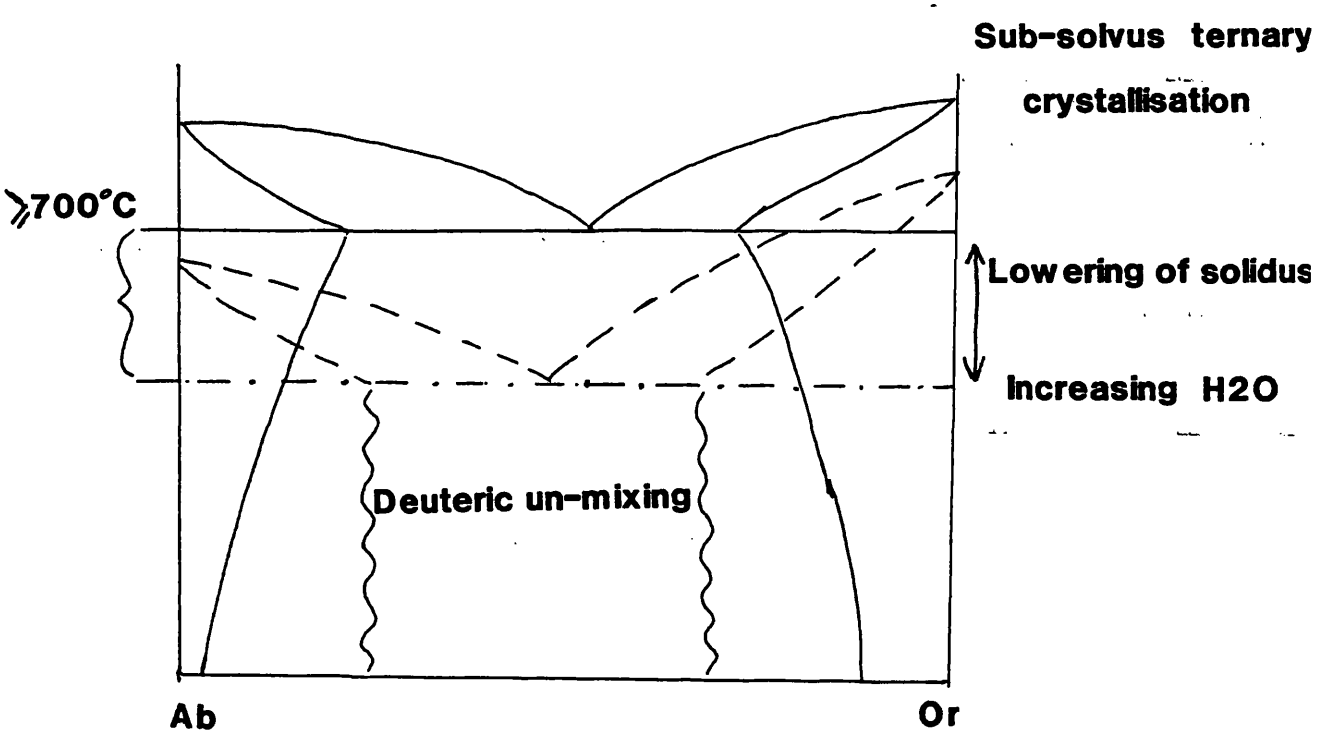

Figure 3.4. The lowering of the solidus conditions in the Shap sub-solvus magma.

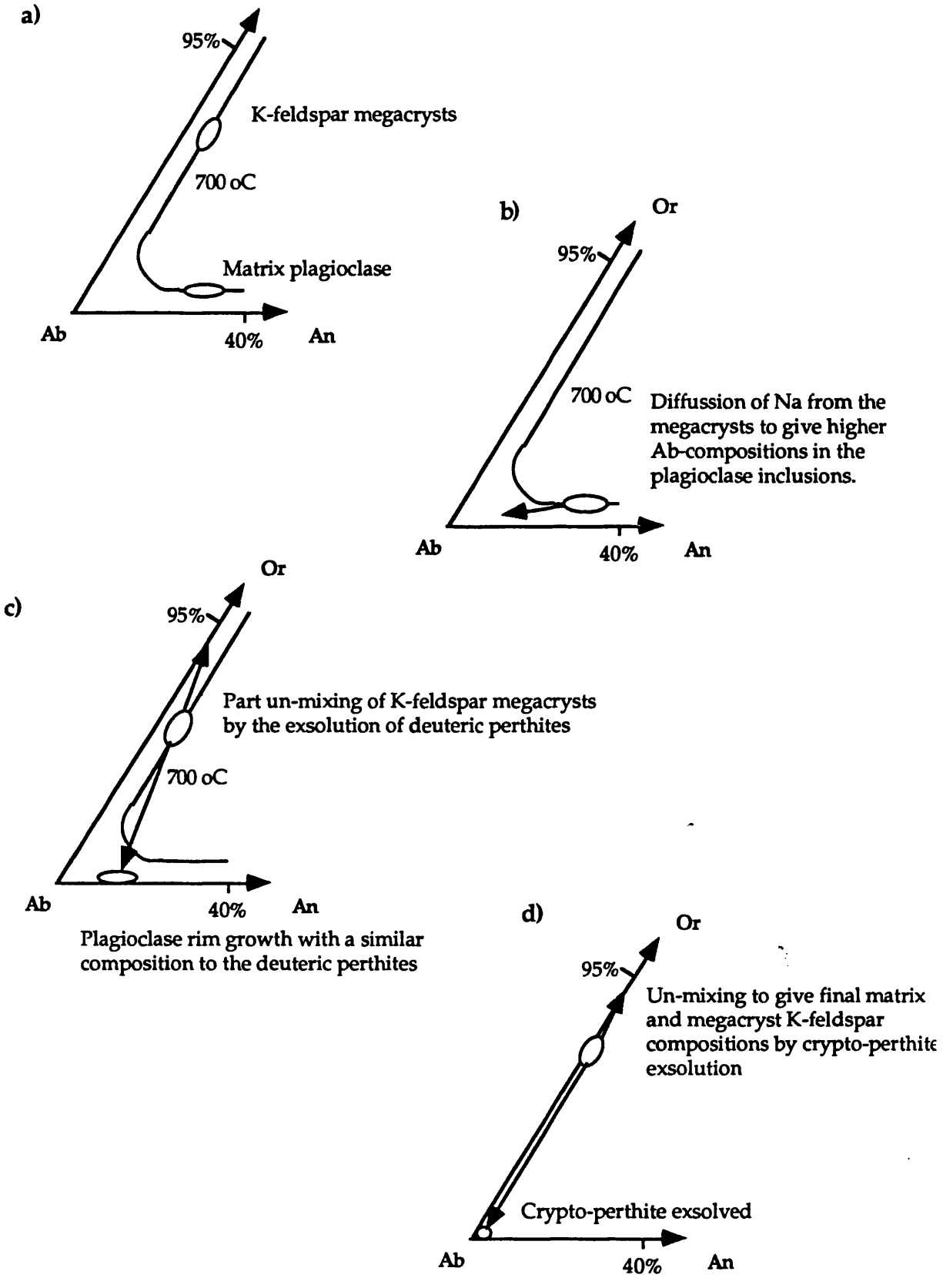

Figure 3.5. Ternary feldspar diagrams showing the crystalisation sequence of the feldspars in the Shap granitoid, a) shows ternary feldspar growth >700 oC, b) shows the diffusion of Na to alter the compositions of plagioclase inclusions within the megacrysts which would otherwise have identical compositions to the ternary plagioclase matrix crystals, c) shows the part un-mixing of the megacrysts and non-ternary growth of the plagioclase matrix below 700 oC, and d) shows the final un-mixing to produce the crypto-perhites and final K-feldspars.

The textural evidence from the Shap granitoid i.e. the change from megacrysts to matrix K-feldspar, suggests that there has been an overall H_2O increase during cooling. This would explain the both the change in growth kinetics of the K-feldspars (Fenn 1977; Day and Fenn 1982) and the reduction in the solidus of the Shap granitoid magma (Tuttle and Bowen 1958; Whitney 1975; 1988; Day and Fenn 1982). The changes in the growth conditions for the feldspars in the Shap magma are illustrated in **Figure 3.5.** based on the data in **Table 3.1** and in **Figure 3.3.**

Another feature of the perthite exsolutions in the K-feldspar megacrysts, is the way the oscillatory zones affect the un-mixing process. The deuteric micro-perthites have been exsolved in all the sub-grains and zones present (see Chapter 2).

Mason (1982) investigated by ion microprobe analysis, the distribution of trace-elements across perthites in K-feldspar megacrysts. The elements with a higher distribution coefficient for plagioclase e.g. Fe, Mg, Sr, etc., were not as concentrated in the albite perthites as might be expected. Rather, there was a build-up of these elements some distance (about 50μm) from the perthite/K-feldspar boundary, in the host megacryst. Similarly elements with a higher K_D in the K-feldspar such as Ba, Pb and Cs, showed higher than the average megacryst concentrations about 50 to 100μm from the perthite boundary. The explanation for these patterns is thought to be related to the fast Na-diffusion and slow K-diffusion during un-mixing. The diffusion rates of K and Na can show two order of magnitude difference at high temperatures i.e. >700°C (Forland 1974; Smith 1974). Thus, fast Na diffusion causes a build-up of K, which in turn inhibits the partitioning of the trace-elements into the high-temperature perthites and K-feldspars, during un-mixing.

To examine this process, an X-ray scan of a K-feldspar megacryst was carried out, using the Cameca SX50 electron microprobe. The scan was used to highlight the areas of high K within part of the crystal, which had a number of plagioclase inclusions aligned along a large oscillatory zone and a many deuteric perthites also present. An X-ray map was produced for K and this is shown in **Figure 3.6.**

It is apparent from **Figure 3.6** that K is concentrated around the edges of the deuteric perthites and the inclusions of plagioclase. The high K-content at the left edge of the scan corresponds to the rim of the Ba-rich oscillatory zone which occupies most of the centre of the images. This is in fact the large oscillatory zone which represents dissolution and resorption of the megacryst (**Figures 3.1(a)** and **3.1(b)**). The concentrations of Ba in the oscillatory zone are too low to estimate the effects of perthite exsolution on the Ba-

distibution, using this technique.

One of the K-rich edges around the deuteric perthites (shown in **Figure 3.6**) was analysed for Ba- and Fe-concentrations in a point scan. The data obtained is plotted in **Figure 3.7**.

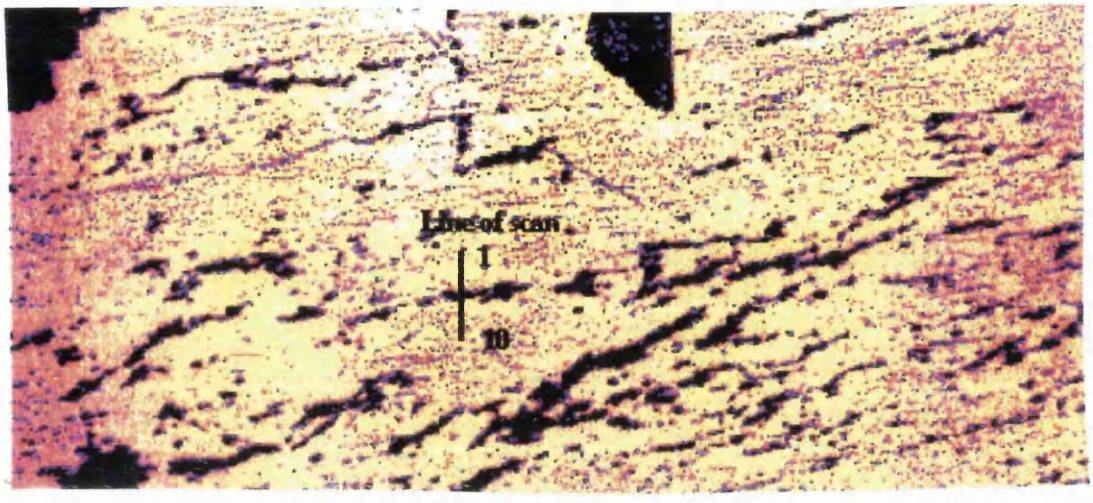

Figure 3.6. X-ray map of K-concentrations in part of a K-feldspar megacryst. Note the high concentrations at the left edge of the image and around inclusions and deuteric perthites.

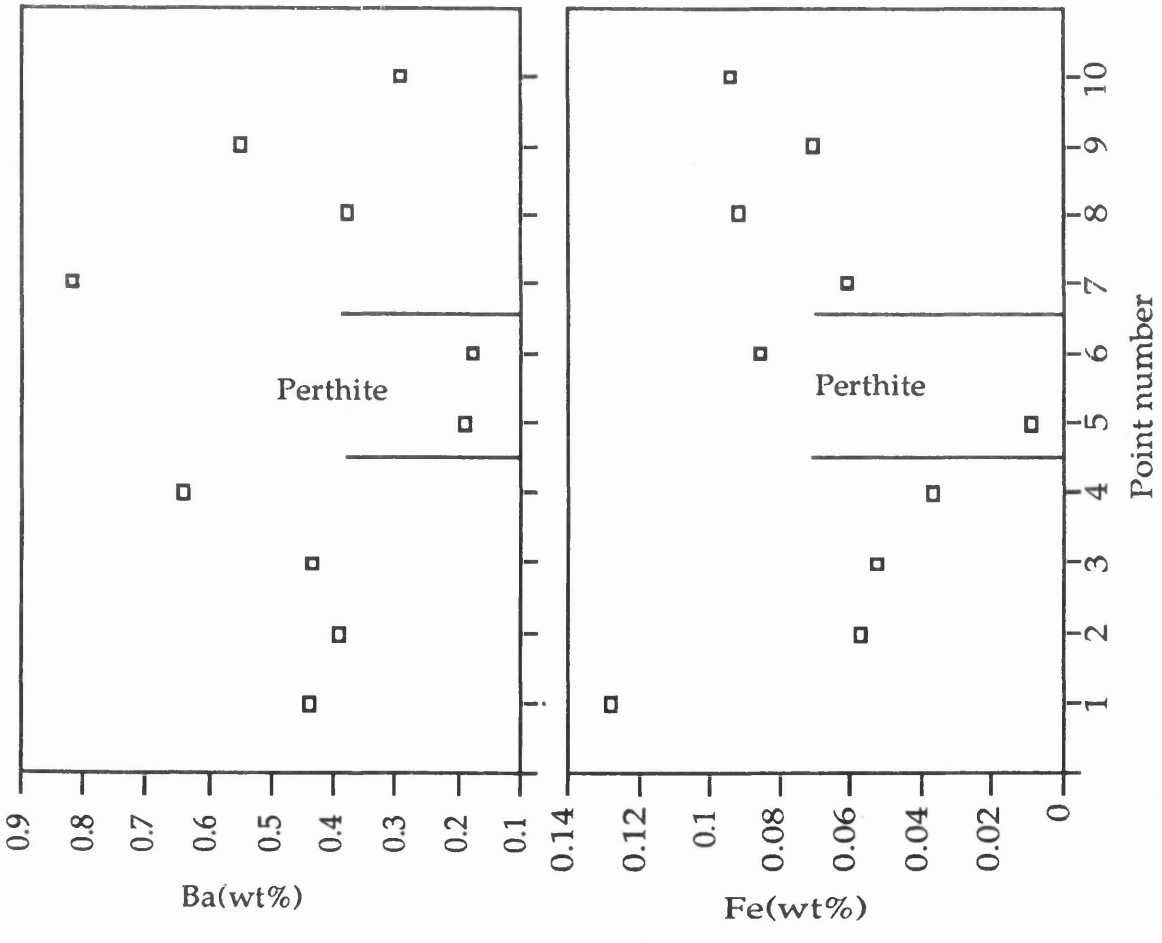

Figure 3.7. Plots of point number against wt% Ba and Fe from in a microprobe travese across one of the deuteric perthites from a K-feldspar megacryst.

The distribution of the Ba shows the same pattern as reported by Mason (1982) i.e. a build-up some distance from the boundary due to the differences in the K- and Na-diffusion rates (**Figure 3.7**). This confirms the high temperature nature of the deuteric perthites. The Fe-content shows a rather random scatter. Fe is a hydrothemally mobile element (Turner and Verhoogan 1960) and peaks will easily disrupted in a deuteric environment. Therefore the randomness of the Fe across the across the perthites may be due to the development of Fe-rich micro-inclusions and general reaction with the magmatic fluids, during the exsolution of the deuteric perthites. This process may contribute to the pink colour and turbid appearance (Chapter 2) and porosity (Worden et al. 1989; **Table 3.1**) of the megacrysts.

Back-scattering S.E.M. images (see Chapter 2) show that the crypto-perthites do not have appreciable zones of high mass around them. The formation of regular crypto-perthites is normally associated with a lack of deuteric alteration to the crystals (Parsons 1978; Brown and Parsons 1989; Worden et al. 1989). Therefore, very late-stage exsolution of these perthites, at low temperatures seems likely. This would account for the lack of heavy element diffusion and allow the megacryst to remain closed to further deuteric or hydrothermal influence, which would considerable coarsen the perthites on exsolution (Parsons 1978; Brown and Parsons 1989; Worden et al. 1989).

3.5 Discussion

The investigation of Ba-distibution in the K-feldspar megacrysts from the Shap granitoid in the previous section seems to confirm their magmatic nature. The influence of changing growth conditions and magmatic mixing can also be observed in the Ba-contents of the megacrysts in this study.

Mehnert and Busch (1981) investigated the Ba-content and zoning in K-feldspar megacrysts in the Black Forest, Germany. They summarised the growth of megacrysts, based on their petrographic and microprobe investigations as; a) formation of small primary crystals which grew together, b) formation of the megacryst by crystallisation of shells around this core, c) formation of the rim which grew into the early formed matrix, and d) local infiltration of Ba-rich K-feldspar with albite, along cracks and irregular zones of disturbance.

The K-feldspars of the Shap granitoid have some similarities but also a great many differences. A major criticism of Mehnert and Busch's conclusions on megacryst growth involves their sampling of the crystals for sectioning. They assume that they have sampled the core of a megacryst and

their scans are along the {001}-axis. This leads to the conclusion that small crystals of K-feldspar have amalgamated to from this core region based on the Ba-zoning and petrographic evidence, such as thin septa of quartz, which surround these "core-grains". Similar grains are seen in the Shap megacrysts but these are exclusively restricted to the rims of the crystals.

To ensure proper sampling of core and rim regions of the megacrysts in this study, sequential slices of the megacrysts were taken, for all section in this study, (see Appendix A). **Figures 3.8(a), (b),** and **(c)** show a sequence of slices through a K-feldspar megacryst sampled in this way.

The sequence shows the core region of the crystal in **(a)**, with a 0.5cm slice thickness before **(b)**. The presence of the prominent oscillatory zone can be seen in both the slices but a large sub-grain, also with a bright zone can be seen in **(b)**. Slice **(c)** shows the complete disappearance of the megacryst only a saw-width (<10mm) from slice **(b)**. Therefore, slice **(b)**, despite having the appearance of being at the core of a megacryst, is in fact very near the rim. The presence of small sub-grains of K-feldspar as described by Mehnert and Busch are likely to be similar sub-grains near the rim, and not the core, of the megacrysts sampled.

The presence of the fine-scale, fairly regular, oscillatory zones may be explained by small-scale changes in equilibrium, during the growth of the megacryst. It is apparent that most inclusions, including biotite, generally increase in size and frequency from core to rim in the megacrysts. Biotite has a very high distribution coefficient for Ba in granitoid magmas, up to five times that of K-feldspar (Rollinson 1993). Thus, anything other than minor amounts of biotite crystallisation within the granitoid would cause Ba-partitioning into the biotite, and rapid depletion of the Ba in the magma. This in turn would lead to relatively Ba-poor K-feldspars. In comparison with other studies reporting the Ba-content of K-feldspars (Smith 1974; Deer et al. 1992), the Shap granitoid megacrysts are quite Ba- (celsian) rich. Therefore, the amount of biotite crystallisation in the granitoid was limited until late in the cooling history of the intrusion. However, small fluctuations in biotite growth and subsequently in the Ba-concentrations may have induced small-scale depletion in the Ba and thus Ba-poor zones. Similarly less biotite growth would mean slight increases in the H_2O-content of the magma. This in turn would lead to a slight reduction in the solidus of the granitoid for K-feldspar (Whitney 1975; 1988) and thus the higher K_D-element, namely the Ba, would enter into the growing K-feldspar to create a Ba-rich oscillatory zone.

A complex model for the formation of oscillatory zones was presented by Allegre et al. (1981). This basically involved small-scale

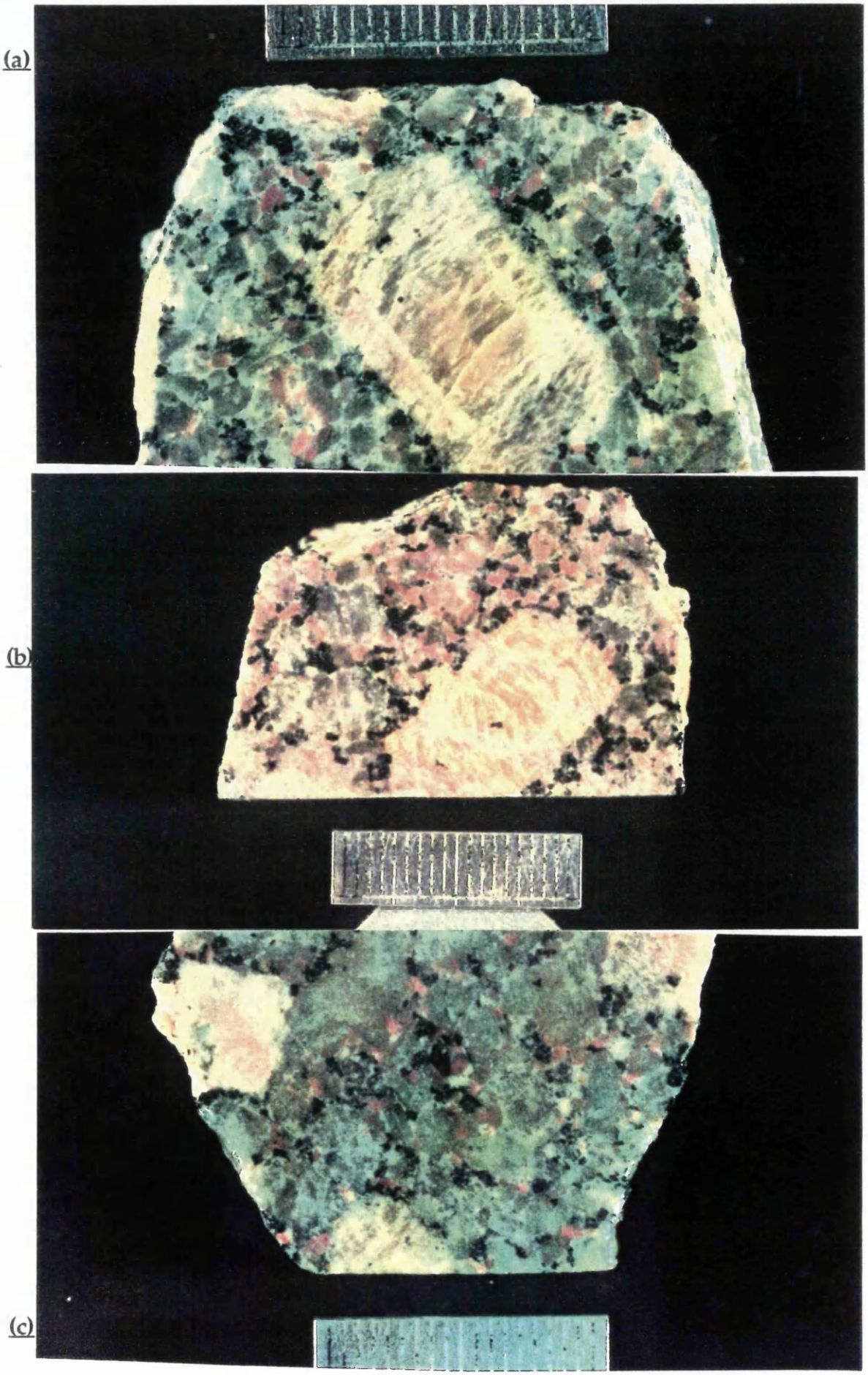

Figure 3.8(a), (b) and (c) Photographs showing sequential slices through a megacryst from **(a)** core to **(b)** rim with slice **(c)** showing the disappearance of the megacryst.

depletion of the higher K_D-element at the crystal/liquid interface. In this case i.e. the of the growth of K-feldspar megacrysts, this depletion may be due to biotite growth, or the megacryst itself depleting the local magma in Ba. Another possibility may be that the crystal was moved into a different pocket of magma by convection or by tectonic movement, etc. The equilibrium conditions may be sufficiently different in this new position to cause either resorption into the magma of K from the crystal, or nucleation of a Ba-rich zone into the growing crystal. The explanation of the growth of the fine-scale oscillations may involve a number of factors but, in general, small-scale growth condition changes during the megacryst's formation are likely.

The formation of the large, disrupted, oscillatory zone involves a much longer and potentially larger change in the growth equilibrium of the megacryst. Dissolution of the megacryst may be due to a number of factors. The textural evidence from the K-feldspars and other minerals (Chapter 2) seems to suggest a state of disequilibrium during the growth of the crystals in the granitoid, caused by mixing with a more mafic magma. As Ba, Ca and to some extent Na, are higher temperature phases of the K-feldspar crystal (Barth 1961; Smith 1974; Furhman and Lindsley 1988) then these would be expected to be concentrated in the highest temperature phases of K-feldspar megacryst growth. The mixing of the granitoid with a higher temperature, more mafic magma would clearly cause large scale disequilibrium and therefore dissolution of the K-feldspar crystals. This would continue until the highest temperature phases (i.e. Ba, Ca, and Na) re-establish equilibrium and form the next zone of the crystal. The fastest growing faces of the megacrysts, i.e. {201}- and {001}-faces (Anderson 1984) are often the faces where most dissolution has occurred. Thus, the dissolution and subsequent resorption of the Ba, Ca, and Na along the fastest growing faces of the crystal may account for the lower, and more diffuse Ba-concentrations of the zone.

In all cases the larger, deuteric micro-perthite cut the magmatic zones. The crypto-perthites however, transect all but the highest-mass areas of the {010}-face of the resorption zone, and do not seem to occur in the {201}- and {001}-faces or the normal fine-scale oscillations at all. Smith (1974) pointed out that, in general, Na- and Ca-rich oscillatory zoning is unusual in K-feldspars. This is due to perthite exsolution which will often overprint and obscure such zones, in all but the most rapidly quenched K-feldspar crystals. All the perthites were avoided during the point-scan across these zones. This however is extremely difficult as the crypto-perthites are highly pervasive and may lie undetected just below the K-feldspar surface being analysed. The formation of the highly pervasive crypto-perthite, which

occurs in the normal composition (i.e. orthoclase-rich) areas of the K-feldspar megacrysts, may well account for the Na and to some extent the Ca-fluctuations of some of the points analysed. However, the crypto-perthite exsolution is clearly restricted by the higher Ba-contents of the zones, where high Ca- and Na-concentrations are preserved.

In the {010}-face of the crystal, the resorption zone is much less wide than the {201}- and {001}-faces. Na can diffuse up to 2 orders of magnitude faster than K, Ca, and Ba in the K-feldspar lattice, (Forland 1972; Smith 1974; Mason 1982). Therefore, Na-diffusion at high temperatures, across the growing crystal/melt interface has probably disrupted the Na-zone profile on the slow growing and narrow {010}-face of the resorption oscillatory zone **(Figure 3.1(a))**.

The exsolution of the perthites in the K-feldspar megacrysts appears to be closely associated with an increase in the $\%H_2O$ of the magma. Textural changes involve the increase in nucleation density and the decrease in growth rate of the K-feldspar which causes a change from the small numbers of fast growing megacrysts to the slow growing, multi-nuclei matrix K-feldspars. The opposite effect in found in plagioclase (Day and Fenn 1982). The microprobe evidence supports this view. The megacrysts and the plagioclase crystals have ternary compositions which indicate hyper-solvus growth (Tuttle and Bowen 1958; Brown and Parsons 1989). The compositions of the ternary feldspars in the Shap magma must have been above 700°C, based on the geothermometer of Furhman and Lindsley (1988) which is shown in **Figure 3.3**. A lowering of the solidus while the feldspars were growing would not only account for the kinetic changes in growth but would also cause the deuteric un-mixing of the K-feldspar megacrysts. An increase in the $\%H_2O$ to lower solidus temperatures is favoured over an increase in the solvus temperature in the Shap magma. This is partly due to the low An-content of the Shap generally, and the textural evidence, which points to an increase in the H_2O-content. Feldspars in granite systems may undergo dissolution with lower temperature solidus conditions. Johannes (1980) showed that this process is very slow with feldspars remaining metastable despite a temperature reduction of the solidus conditions. Therefore, deuteric un-mixing, with the megacryst reacting with the magmatic fluids at high temperatures (700°C) seems the most likely explanation for both their chemical properties and their textures. The diffusion of Na to create the build-up of slower diffusing elements as described by Mason (1982) is present in these megacrysts also and this supports the evidence for high temperature exsolution of these deuteric perthites. The minor changes to the plagioclase inclusion compositions,

which would otherwise have identical compositions to the matrix plagioclase cores, probably occurred at a similar stage, although no attempt to calculate the amount of diffusion involved, was made.

The crypto-perthites must have been exsolved at a much later stage when the megacrysts and matrix crystals were closed to deuteric fluids. This would account for their fine scale and the lack of diffusion zones around them. The presence of deuteric fluids has been shown to coarsen perthites considerable after exsolution even at temperatures below 400°C (Parsons 1978; Brown and Parsons 1989; Worden et al. 1989). Therefore, late, low-temperature exsolution of the crypto-perthites in both the megacrysts and the matrix K-feldspars was probably the last event in the cooling history of the K-feldspars, in the Shap granitoid.

3.6 Conclusions

1) The fine oscillatory zoning in the megacrysts has been formed by small changes in equilibrium during the growth of the megacrysts, to give the higher Ba-content of these zones.

2) The large, disrupted oscillatory zone has higher Ba-contents and this along with the textural evidence suggests a major dissolution/resorption event during the growth of the megacrysts. This may have been due to the introduction of a higher temperature magma which subsequently mixed with the granitoid.

3) The megacryst has resorbed Ba at the same rate on face with different growth rates i.e. slow {010}-faces and fast {201}- and {001} faces. This accounts for the different Ba-, Ca- and Na-contents along the resorption interface, and also the different textures of these crystal faces.

4) Ternary growth followed by deuteric un-mixing caused by a lowering of solidus conditions during sub-solvus growth of the feldspars probably followed in the wake of an increase in the H_2O-content of the magma.

5) Much lower temperature exsolution of the crypto-perthites after the closure of the megacrysts to deuteric fluids gave the final composition of the un-mixed megacrysts.

Major-element, trace-element and Rb/ Sr isotope studies of the Shap granitoid to investigate K-feldspar megacryst distributions

4.1 Introduction

The presence of micro-diorite enclaves within the Shap granitoid is considered to be the result of magma-mixing (Harker and Marr 1891; Grantham 1926). The textural characteristics of the K-feldspar megacrysts (twinning, zoning, inclusions, resorption, etc., see Chapter 2), plagioclase (zoning, resorption) and quartz (large euhedral crystals) within the enclaves, suggests that they may represent xenocrysts within the enclave, most likely trapped within a liquid globule of mafic material upon mixing with the host granitoid, (Vernon 1986; Hibbard 1991). The distribution of major- and trace-elements and Rb/Sr isotopes was investigated to determine the nature of the relationship between the diorite and granite magmas, and the K-feldspar megacrysts therein.

4.2 Shap Granitoid: A review of petrogenetic models.

The magmatic activity, represented by the igneous rocks in the NW. of England, is thought to have been the result of two Palaeozoic events, related to the Caledonian Orogeny. The first of these events, possibly subduction-related volcanic activity (Moseley 1983; O'Brien 1985) produced the Eycott and Borrowdale Volcanic Groups and the Ordovician intrusions associated with them, namely the Carrock Fell, Threlkeld, Eskdale and Ennerdale intrusions. This view is supported by the relative ages of these intrusions and volcanic rocks. The Borrowdale Volcanics are reported to be 457+/-9Ma (Thirlwall and Fitton 1983) to 430+/-7Ma (Compston et al. 1987) and the ages of intrusions range from 460+/-10Ma to 420 +/-4Ma (Rundle 1979). Chondrite-normalised REE patterns, also indicate a cogenetic relationship for these magmas (Millward et al. 1978; O'Brien 1985). For example Eu-anomalies and light REE-enrichment is common to all the Ordovician intrusions and volcanic rocks (O'Brien 1985).

The second of the magmatic events resulted in the generation of the Devonian Shap and Skiddaw granitoids. This event is dated at by radiogenic isotopes and by indirect structural evidence at, 394+/-3Ma (Brown et al. 1963; Boulter and Soper 1973; Shepard et al. 1976; Wadge et al. 1978). The emplacement of these granitoids is thought to be facilitated by the relaxation of the end-Silurian stress field which caused the folding in the country-rocks surrounding the Shap intrusion (Clarke 1964; Boulter and Soper 1973; Branney and Soper 1988).

O'Brien (1985) showed that relatively small amounts of fractional crystallisation of the Shap magma had occurred. This was based upon the relatively low $^{87}Sr/^{86}Sr$ initial ratios, light REE enrichment and LIL element variations, which show Nb-anomalies, suggesting a similar source for the Ordovician and Devonian magmas. Moseley (1983) and O'Brien (1985) have suggested that the Devonian Shap and Skiddaw granitoids were generated by deep, sub-crustal, partial-melting of similar source mantle rocks as the Ordovician igneous complexes. This view is supported by the structural information (Clarke 1964; Boulter and Soper 1973; Soper and Moseley 1978; Branney and Soper 1988) which shows crustal thickening in the Silurian, prior to granitoid emplacement. This in turn inhibited magma escape and hence promoted sufficient partial mantle-melting to produce the granitoid magma. This partial melting model is strengthened by geophysical evidence (Bott 1974, 1978; Lee 1984) which indicates that the area lacks any high gravitational anomalies which would suggest a basic rock pluton beneath the main granite mass. Rather, the area is underlain by an extensive low gravity-producing body, indicating that a granite mass forms the basement to the area and crops out as the Shap and Skiddaw intrusions.

The rapid emplacement of the Shap granitoid, as deduced by O'Brien (1985) may have been partially facilitated by pre-existing zones of weakness in the heavily folded overlying slates and by stoping through the Borrowdale Volcanics, as indicated by the presence of andesite xenoliths in the main body of the intrusion (Harker and Marr 1891; Grantham 1926).

Thus, most of the evidence points to the Shap granitoid representing a mantle partial melt, which has been rapidly intruded to a fairly high crustal level, with little fractionation.

4.3 Crystallisation, mixing and hybrid granitoid production

The process of magma-mixing to account for the presence of the diorite xenoliths within the Shap intrusion was suggested by Harker and Marr (1893) and Grantham (1926), and is commonly suggested for mafic schlieren and enclaves within other granitoid intrusions, (e.g. Vernon 1983; Cantagrel et al. 1984; Castro et al. 1990; Pitcher 1991). Castro et al. (1991) suggested that hybridisation of granitic bodies in the Hercynian belt of Spain is represented by enclaves within the granites. This mixing of a synplutonic dyke magma which is basic in composition, and a granitoid, results in a homogenous, hybrid granitic rock with tonalite enclaves, (**Figure 4.1**).

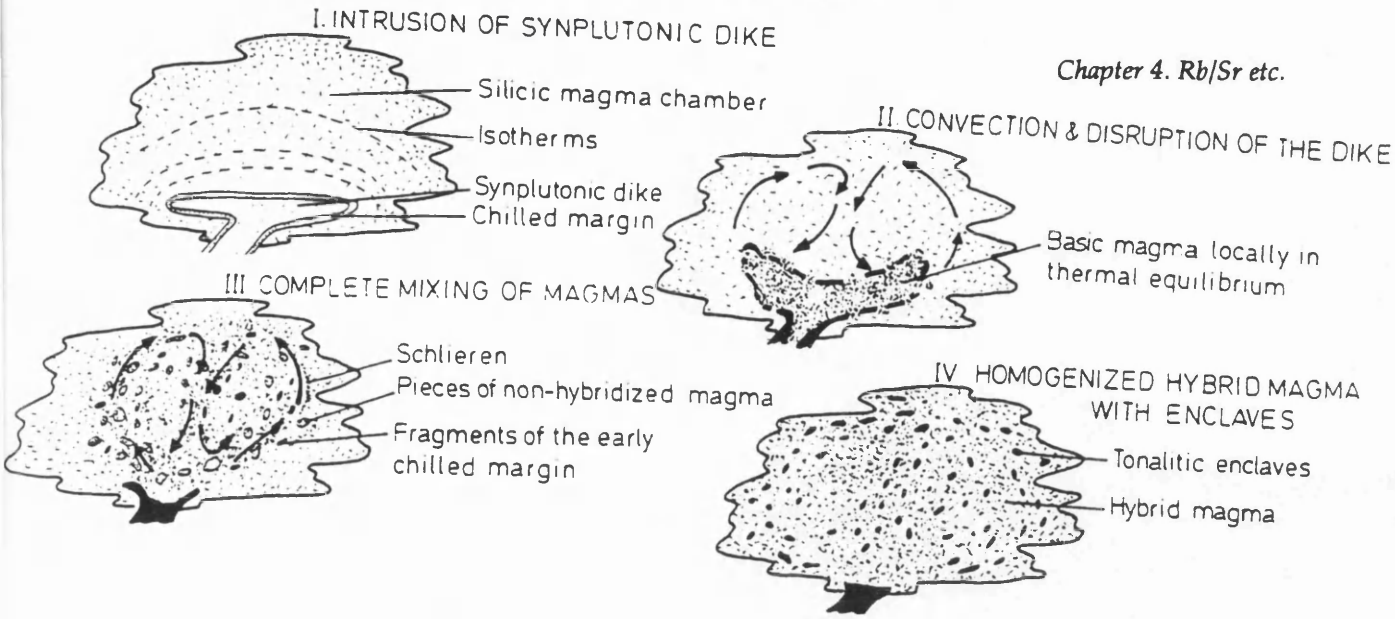

Figure 4.1. Model of magma-mixing and hybrid granitoid formation (after Castro et al. 1990).

The Shap granitoid, while showing clear evidence of magma-mixing, is not homogeneous, in that there are three separate stages (Grantham 1926), and different xenolith types and schlieren present, (Harker and Marr 1891; Grantham 1926). Therefore, the main difficulty in testing a mixing model is the identification of basic and acidic end-members. Firman (1978) showed that the Shap Stages (I,II,III) plotted on a linear trend, using major-element data from Grantham (1926). By plotting major-elements (mol Na_2O/K_2O against mol $Al_2O_3/CaO+Na_2O+K_2O$) Castro et al. (1990) were able to identify the end-member magmas in hybrid granitoids from Spain, based on their peraluminous nature. The same method is employed here, using data from, Grantham (1926), O'Brien (1985), and major-element concentrations which were determined by XRF analysis of a number of samples, of the Stage II Shap granitoid, and enclaves. All the data are presented below, (**Table 4.1**).

Sample	Mol Na_2O	Mol K_2O	Mol CaO	Mol Al_2O_3
(Enclaves)				
Grantham(1926)i	0.3501	0.0619	0.0087	0.1198
Grantham(1926)ii	0.0286	0.0411	0.1191	0.1483
Diorite(present)	0.0321	0.0330	0.0541	0.1440
(Granitoids)				
Grantham(1926)e.basic	0.0658	0.0440	0.0428	0.1589
" stage I	0.0683	0.0472	0.0354	0.1552
" stage II	0.0569	0.0422	0.0563	0.1442
" stage III	0.0542	0.0495	0.0456	0.1434
O'Brien(1985)	0.0532	0.0594	0.0321	0.1461
Stage II (present)i	0.0632	0.0511	0.0330	0.1541
" " ii	0.0641	0.0521	0.0311	0.1592

Table 4.1. Table of molecular proportions of some major elements from the Shap intrusion enclaves and granitoids.

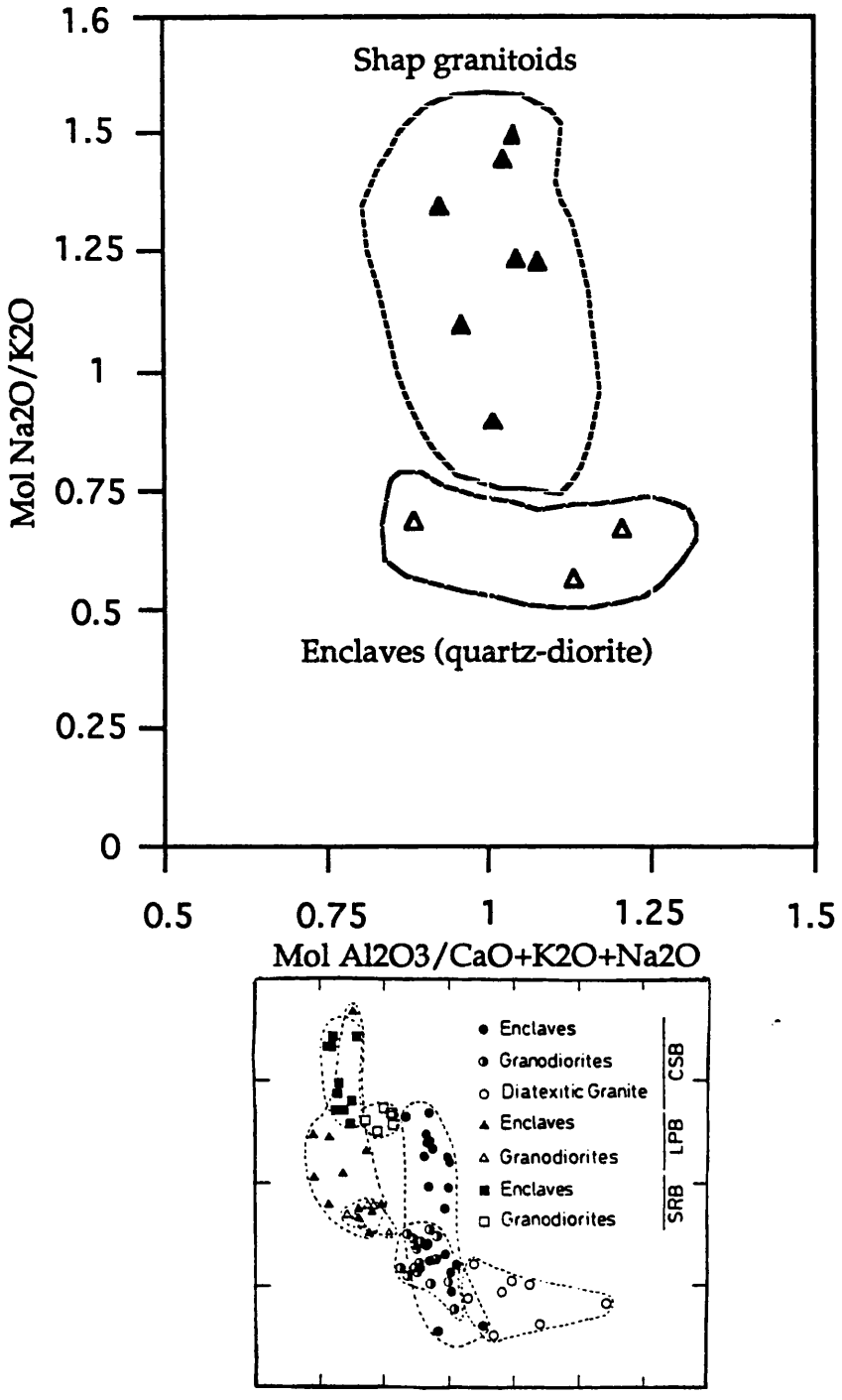

Figure 4.2. Graph of mol Na_2O/K_2O against mol $Al_2O_3/CaO+Na_2O+K_2O$ showing mixing pattern between the magma groups, with possible end-members of enclaves and granitoids (granitoids=black triangles, enclaves=clear triangles). The theoretical mixing line shown by Castro et al. (1990) using the same plot is shown for comparison.

The plot (**Figure 4.2**) shows that the enclaves and granitoids have a negative exponential relationship, with the Shap stages lying on a mixing trend with peraluminous enclave, and peralkaline granitoid end-members. Therefore, mixing between the granitoid magma and the enclave (essentially quartz-diorite) magma may have produced the increasing peraluminous nature of the

rocks within the Shap granitoid stages. Another way of determining end-members in a mixing series is to look at the variation in elements capable of undergoing fractionation in the two magma groups, on Harker plots. In this case, the granitoids should plot with higher SiO_2 contents but lower in the elements enriched in the enclave magma. The Shap enclaves are richer in biotite and Ca-plagioclase than the granitoids by about 20% (see Chapter 2), and therefore elements such as Fe, Mg, Ca, etc. should be of higher concentration in the enclaves. Harker plots often show similarities or differences between magma groups. This technique has been used by a number of authors e.g. Bailey (1984), Flood et al. (1988), in studying magma mixing in acid magma systems.

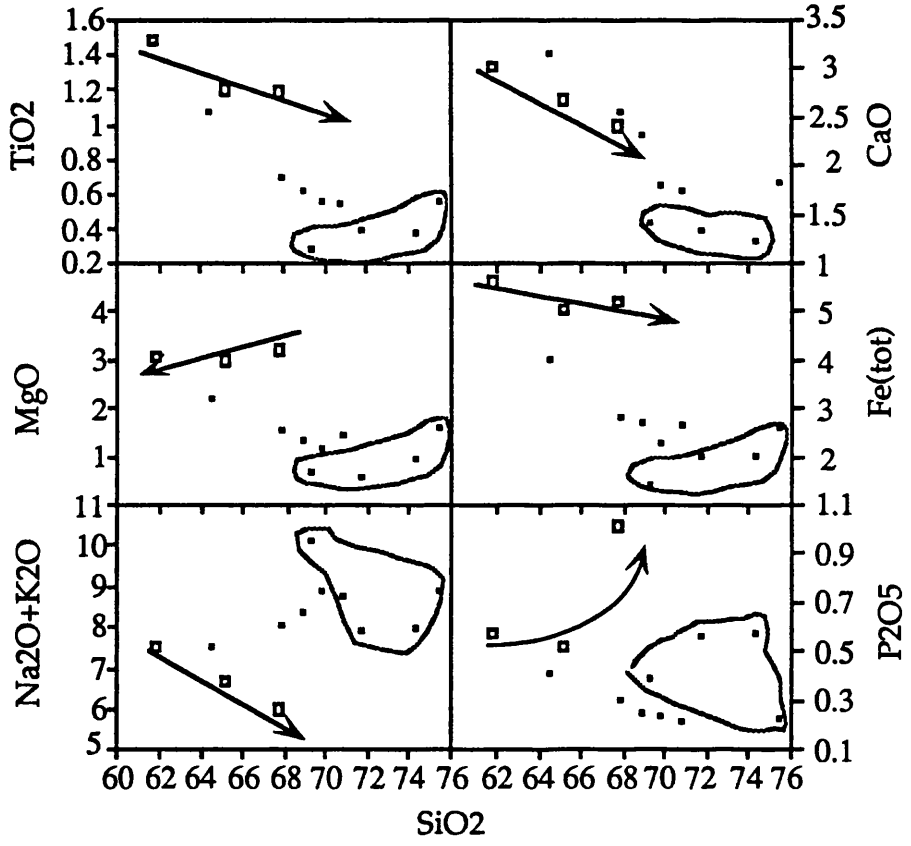

Figure 4.3. Selected Harker plots showing end-members of enclave (squares) and granitoid (black dots) magmas, with possible hybrid granitoid types lying on a mixing line in between. Note; the arrowed lines show likely fraction trends in the enclave magma. The likely non-hybrid granitoids are circled.

Harker plots (Figure 4.3) clearly show that the enclaves have independent linear trends which form end-member components of the granitoid series which also have higher SiO_2 end-members. The trends between the granitoid and enclave end-members is possibly an exponential one which is consistent

with a mixing curve (Flood et al. 1988; Castro et al. 1990). Thus a mixing test would use the SiO_2-rich granitoids and the peraluminous enclave magmas as the end-members, with the main granitoid mass types (early basic, and Stages I,II & III) showing the mixing trend.

To test this mixing hypothesis, average trace element concentrations from the main granitoid (O'Brien 1985) were used in conjunction with trace element data obtained on the Shap (Stage II), non-peraluminous granitoid and diorite enclaves, again using XRF analysis. Mixing of two magmas can be examined using the formula;

$$C^i_m - C^i_B = x(C^i_A - C^i_B).$$

where:

C^i_m=concentration of element i in mixture,
C^i_A=concentration of element i in component A,
C^i_B=concentration of element i in component B,
and,
x= weight proportion of component A.

Such a mixing test has been used by Langmuir (1978) and Forcade and Allegre (1981). In the case of the Shap magma-mixing hypothesis, component A is the granitoid end-member, component B is the dioritic enclave, with the Shap granitoid (Stage III) the mixture. The data used, along with the mixing line obtained is shown below, (**Table 4.2** and **Figure 4.4**).

Element	Granitoid (A)	H.Granite (m)	Diorite (B)	$C^i_A-C^i_B$	$C^i_m-C^i_B$
Cr	46	6	94	-48	-88
Ni	12	14	42	-30	-28
Rb	256	408	274	-18	134
Sr	424	408	432	-8	-24
Y	12	12	22	-10	-10
Zr	174	169	411	-237	-242
Ba	645	801	360	285	441
La	42	52	86	-44	-34
Pb	41	41	34	7	7
Th	32	25	40	-8	-15
U	13	9	8	5	1
Ga	22	23	24	-2	-1
Zn	34	26	32	2	-6
Cu	20	31	10	10	21
Ce	84	95	209	-125	-114
Co	6	6	12	-6	-6

Table 4.2. Table of trace element concentrations and calculated mixing components for the non-peraluminous granitoids and enclave end-members with a hybrid granite representing the mixture as identified using mol alkali vs. aluminium plots, and Harker plots (**Figures 4.2 & 4.3**).

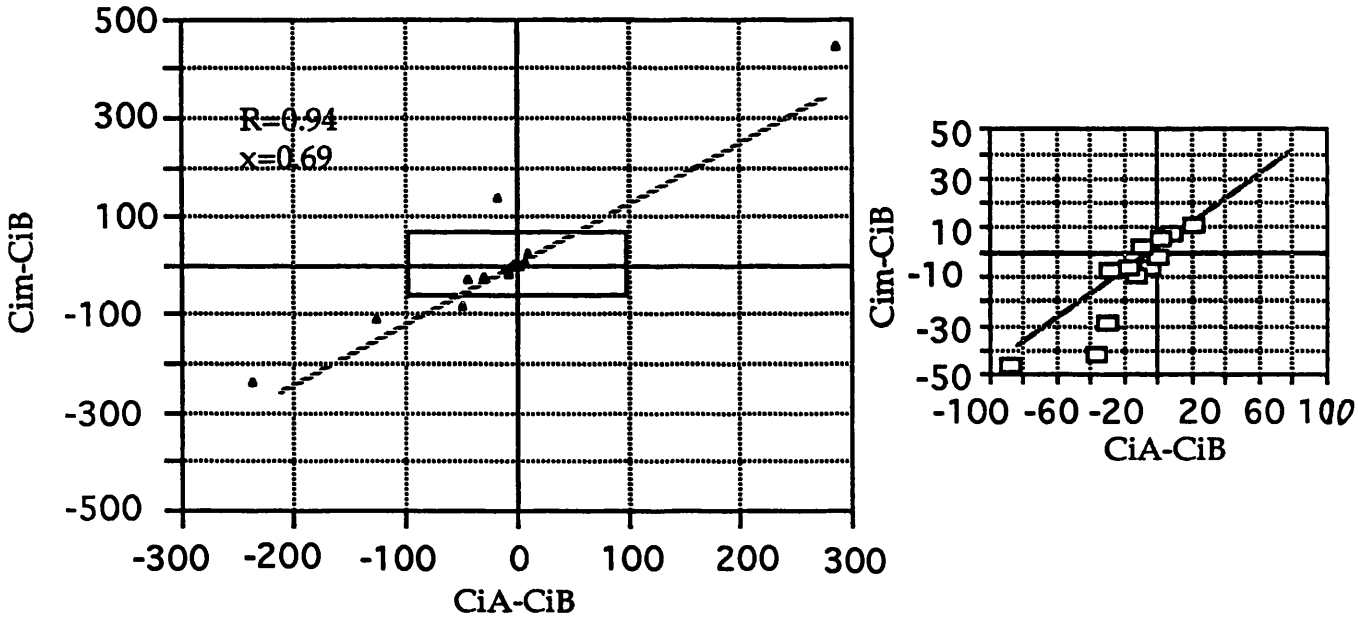

Figure 4.4. Plot of mixing line obtained using data in Table 4.2.

A strong linear trend is shown in the graph (Figure 4.4) with a proportion of 0.69 of component A i.e. the granitoid (non-peraluminous) magma. This in turn suggests that at most a 0.31 proportion of the Shap magma is hybrid in nature. Therefore only a relatively small mafic intrusion of enclave (quartz-diorite) magma could account for the trace element variation in the main intrusion as displayed in the above data.

The linear trend of the major element data (Figure 4.2 &Figure 4.3) along with the textural observations such as increasing grain size, etc. (Grantham 1926, and Chapter 2), indicate that some crystallisation differences have taken place in the main Shap intrusion i.e. a change in composition from early basic types to the Stage III end-member. The REE element patterns described by O'Brien (1985) suggest that little open system fractionation has taken place during the emplacement of the Shap granitoid. By plotting the CIPW-norm values of quartz, albite and orthoclase, which are recalculated to 100%, the

crystallisation of a "granite system" can be examined, (Tuttle and Bowen 1958, Luth et al. 1964). In this case the data in **Table 4.3**, the CIPW-norms of various Shap granitoid analyses, was plotted for the granite system and is shown below in **Figure 4.5(a)**.

Element	StgII(A)	StgII(B)	StgII(AS)	StgII(BS)	e.b.	Stagei
SIO2	65.14	64.33	68.10	66.91	61.34	64.10
TIO2	0.36	0.38	0.26	0.27	0.77	0.50
AL2O3	16.47	16.79	15.25	16.62	16.48	16.25
FE2O3	0.60	0.64	0.48	0.49	1.01	0.71
FEO	1.37	1.47	1.11	1.13	2.31	1.62
MNO	0.04	0.04	0.03	0.04	0.06	0.02
MGO	2.07	1.98	1.30	0.85	3.15	2.23
CAO	1.69	1.71	1.22	1.35	3.22	2.59
NA2O	6.70	6.88	7.32	7.20	6.51	6.14
K2O	5.39	5.61	4.48	4.69	4.83	5.61
P2O5	0.17	0.17	0.44	0.44	0.33	0.25
TOTAL	100.00	100.00	100.00	100.00	100.00	100.00
Ap	1	1	1	1	1	1
Il	1	1	1	1	2	1
Mt	1	1	1	1	2	1
Or	29	29	23	23	23	27
Ab	34	33	35	34	30	28
An	8	7	2	3	12	11
Di	0	0	0	0	0	0
Hy	6	6	4	3	8	6
C	2	1	2	3	0	0
Q	27	23	33	31	19	23
Total	107	102	102	100	98	99

Element	StgII	StgIII	General	Enclave1	Enclave2	Enclave3
SIO2	65.00	65.17	65.06	59.18	62.41	61.13
TIO2	0.44	0.21	0.39	1.07	0.82	0.06
AL2O3	15.76	16.56	16.37	16.59	15.51	16.71
FE2O3	0.68	0.36	0.56	1.41	1.26	0.26
FEO	1.56	0.82	1.30	3.23	2.89	0.59
MNO	0.02	0.03	0.04	0.11	0.10	0.07
MGO	1.87	0.97	1.67	4.37	4.38	4.15
CAO	2.35	1.43	1.80	4.78	2.38	3.70
NA2O	6.04	5.84	5.96	5.59	7.11	8.67
K2O	6.09	8.32	6.66	3.47	2.36	4.65
P2O5	0.20	0.31	0.19	0.19	0.79	0.02
TOTAL	100.00	100.00	100.00	100.00	100.00	100.00
Ap	1	1	1	1	2	0
Il	1	1	1	3	2	0
Mt	1	1	1	3	3	1
Or	30	41	33	17	12	23
Ab	28	27	28	25	34	40
An	9	4	7	18	5	8
Di	1	0	0	3	0	8
Hy	5	3	5	10	12	5
C	0	1	1	0	4	0
Q	23	21	23	54	57	53
Total	99	99	100	98	101	97

Table 4.3. Table showing the CIPW-norms for major element concentrations in the main phases of the Shap granitoid. Note: StageII(A-BS) is present study, e.b. to Stage III and Enclave 3 is from Grantham (1926) and General is from O'Brien (1985).

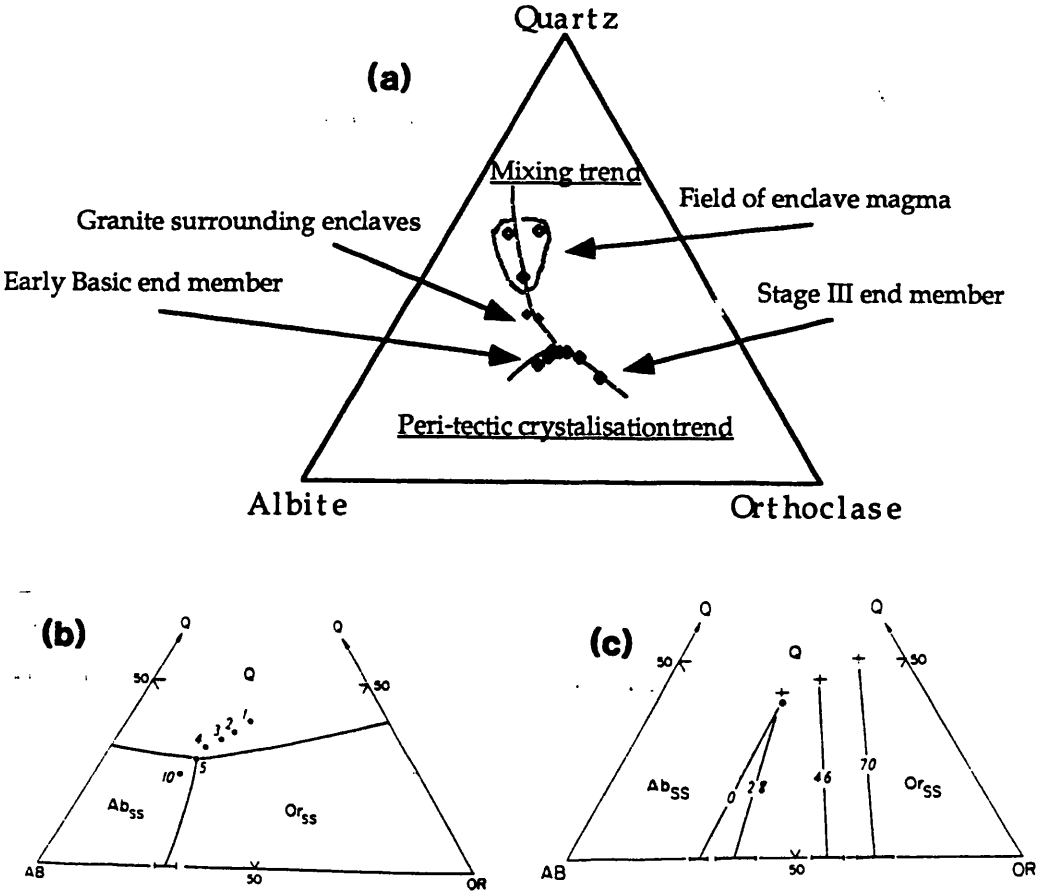

Figure 4.5(a, b & c). Granite system plot for the Shap granitoids and enclaves, and crystallisation trends for the granite system with changing pressure and %H_2O content, from Day and Fenn (1981).

The trend shown by the main Shap granitoid phases appears to be very similar to peritecic crystallisation controlled by changing pressure and %H_2O content from the early basic types to the Stage II granitoids (Day and Fenn 1982) as shown in **Figure 4.5 (b & c)**. The general composition granitoid (O'Brien 1985), the Stage III (Grantham 1926) and granitoids which surround the enclaves as well as the enclave magmas themselves lie on a trend which is independent of the %H_2O and pressure changes which are apparent in the other parts of the intrusion. The best explanation for this is the mixing of the enclave magma at a relatively late stage in the crystallisation history of the granitoid.

4.4 Rb/Sr isotope analyses

Four K-feldspar megacrysts, two from the granitoid and two from a micro-diorite enclave, were thin-sliced and had a number of small pieces of K-feldspar removed, (see Appendix I for full method of sample preparation). These samples, along with small samples of matrix material from both the granitoid and the enclave were analysed by thermal ionisation mass-spectrometry to determine the concentration and isotopic composition of the Rb

and Sr in each case. The exact location from which the samples were removed from the rock thin-slice is shown in **Figure 4.6** and the results obtained are listed in **Table 4.4.**

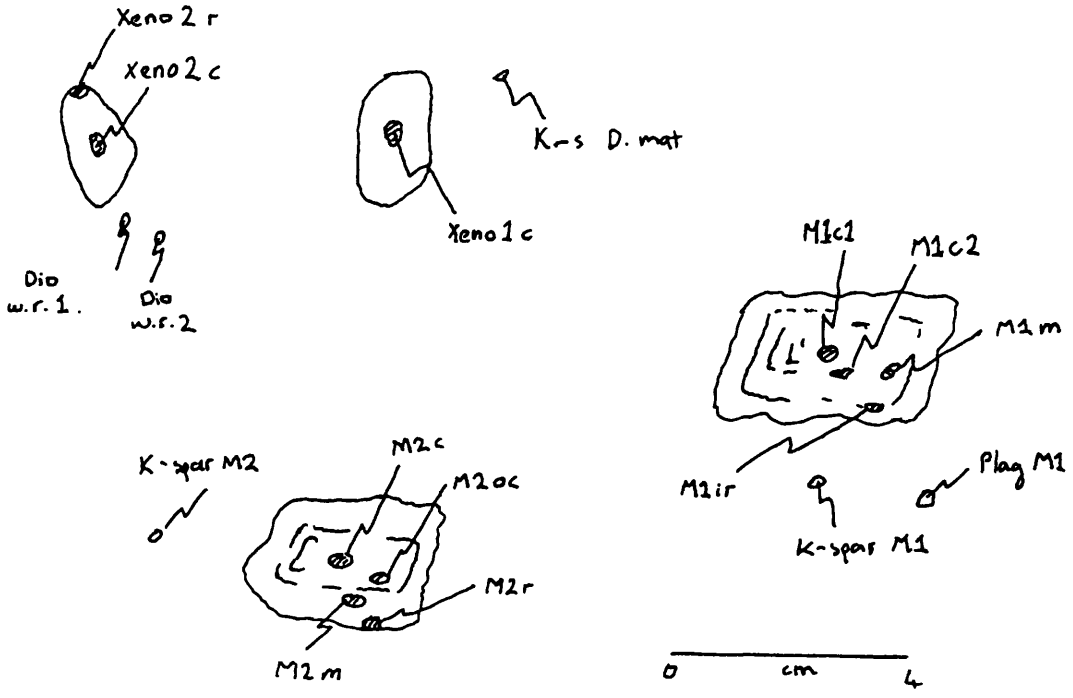

Figure 4.6. Sketch of thin-sliced rock samples and location of separates obtained for Rb/Sr isotope analyses.

Sample	Sr(ppm)	Rb(ppm)	$^{87}Rb/^{86}Sr$	$^{87}Sr/^{86}Sr$	Sr(i.r)
Xeno1c	974	451	1.342	0.7149	0.7074
Xeno2c	896	322	1.041	0.7130	0.7072
Xeno2r	949	326	0.995	0.7129	0.7073
Dio w.r.1	480	313	1.891	0.7181	0.7076
Dio w.r.2	646	343	1.535	0.7167	0.7082
K-s D.mat.	844	357	1.225	0.7149	0.7081
M1c1	599	496	2.401	0.7207	0.7074
M1c2	805	369	1.329	0.7147	0.7074
M1m	801	362	1.309	0.7147	0.7074
M1ir	821	361	1.273	0.7147	0.7074
M2c	849	325	1.070	0.7133	0.7071
M2oc	915	417	1.321	0.7146	0.7073
M2m	782	372	1.376	0.7151	0.7075
M2r	809	318	1.137	0.7151	0.7088
K-sparM1	844	68	0.232	0.7083	0.7070
K-sparM2	696	140	0.583	0.7103	0.7071
PlagM1	1179	34	0.083	0.7076	0.7076

Table 4.6. Rb/Sr data obtained on separates indicated in **Figure 4.6.** Note: errors for Rb are all +/-0.7%. Errors for Sr are all less than 0.0001 of the given values.

The initial ratios were calculated using York's method (1969), where the age of the Shap intrusion used was 393Ma. This age is based on the structural considerations presented by Boulter and Soper (1973) and K/Ar and Rb/Sr dates determined by Brown et al. (1963) and Wadge et al. (1978).

The first general point to note is the decreasing Rb/Sr (ppm) ratio from core to rim to matrix material (**Figure 4.7**) in the granitoid.

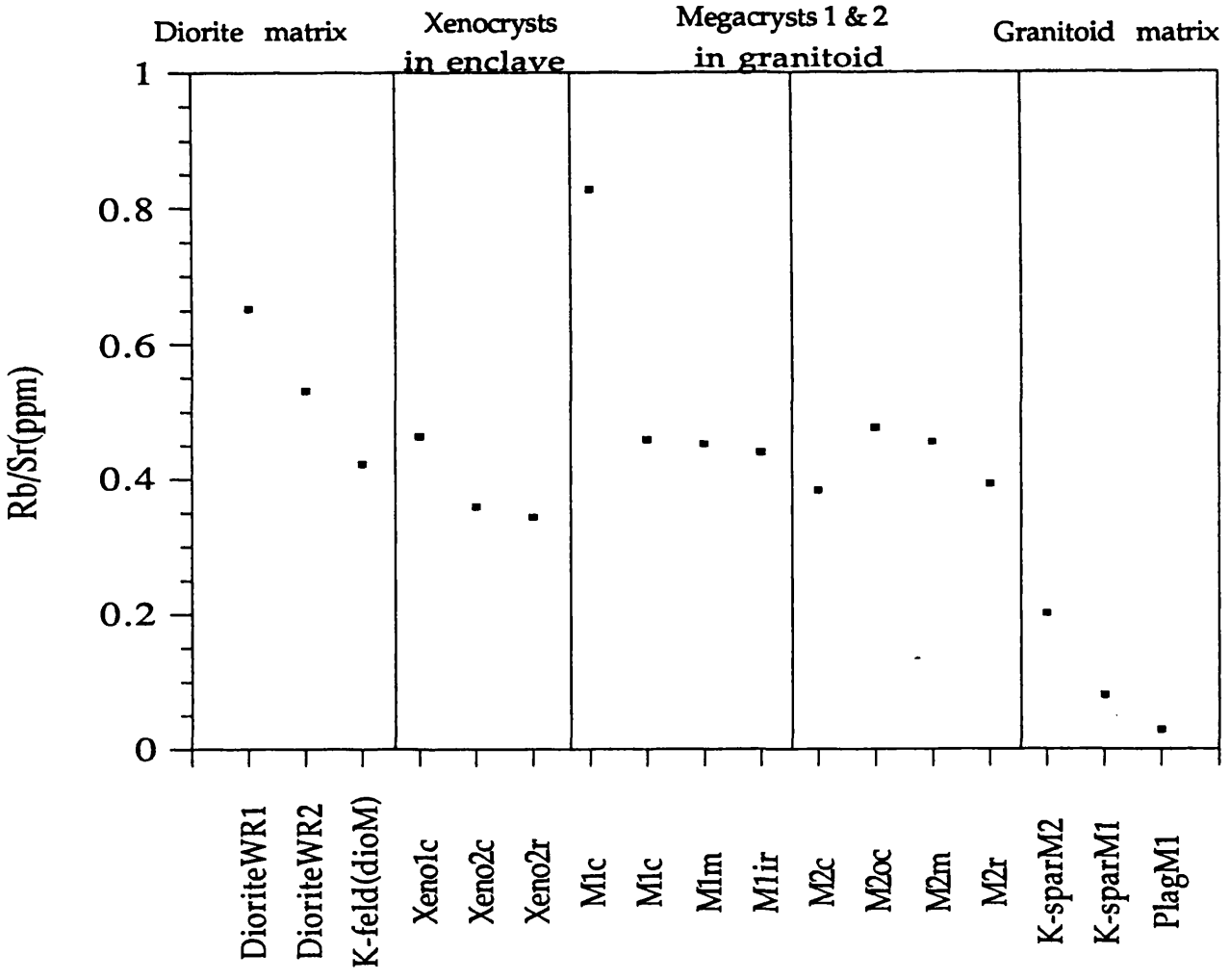

Figure 4.7. Diagram showing decreasing Rb/Sr concentration ratios from megacryst and xenocryst cores to rims in the samples shown in **Figure 4.6**. Note: the granitoid matrix also follows this decreasing Rb/Sr trend.

The second point to note is the increase in $^{87}Sr/^{86}Sr$ initial ratios from the cores to rims to the diorite matrix, with the granitoid matrix showing lower initial ratios for the K-feldspars than the plagioclase crystals, (**Figure 4.8**).

One of the main difficulties in interpreting the Rb/Sr isotopic data and any subsequent analysis of results obtained on the data in this study, is the potential for isotopic re-equilibration. The process of Rb/Sr isotopic re-equilibration between host granitoids and enclaves has been documented by Holden et al. (1987,1991) and was pointed out by Dr. G. Rogers (pers. comm.).

Cherniak and Watson (1991) determined the rate at which feldspar crystals lost their initial ratios, (**Figure 4.9**).

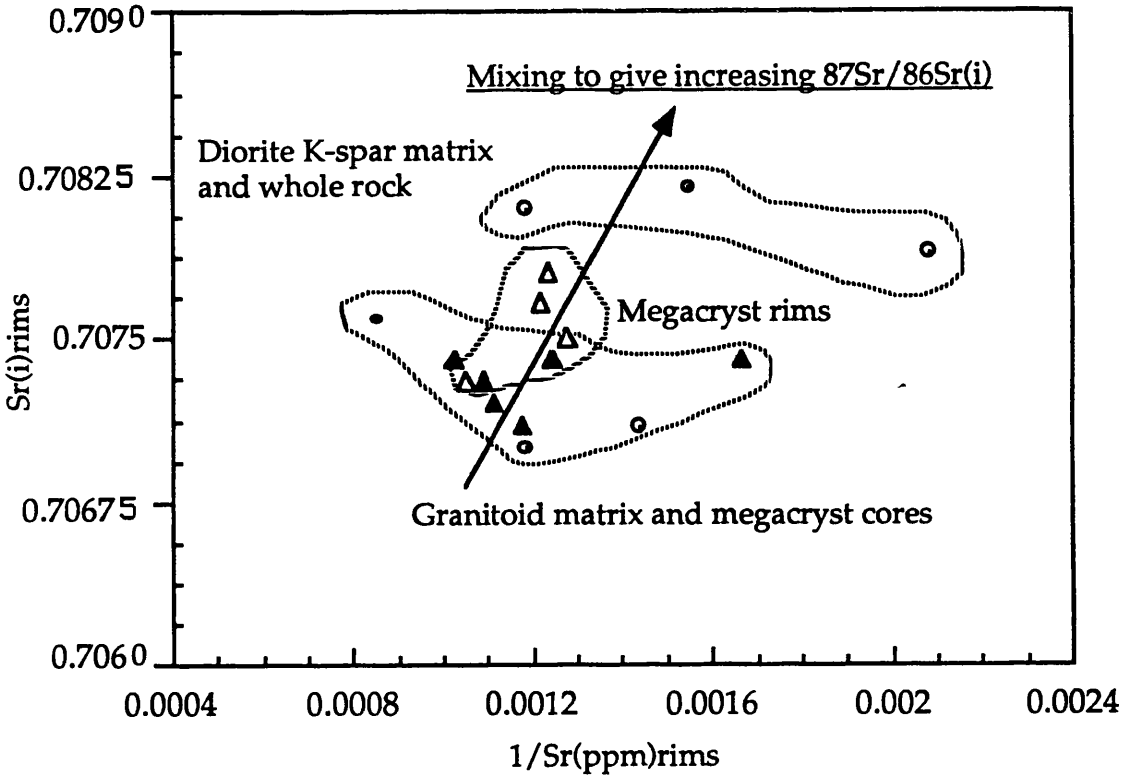

Figure 4.8. Initial ratios plotted against 1/Sr(ppm) from the samples in **Table 4.6.** Note: the increase in initial ratios from cores (black triangles) to rims (clear triangles) in the megacrysts which are from both the diorite enclaves and the granitoid.

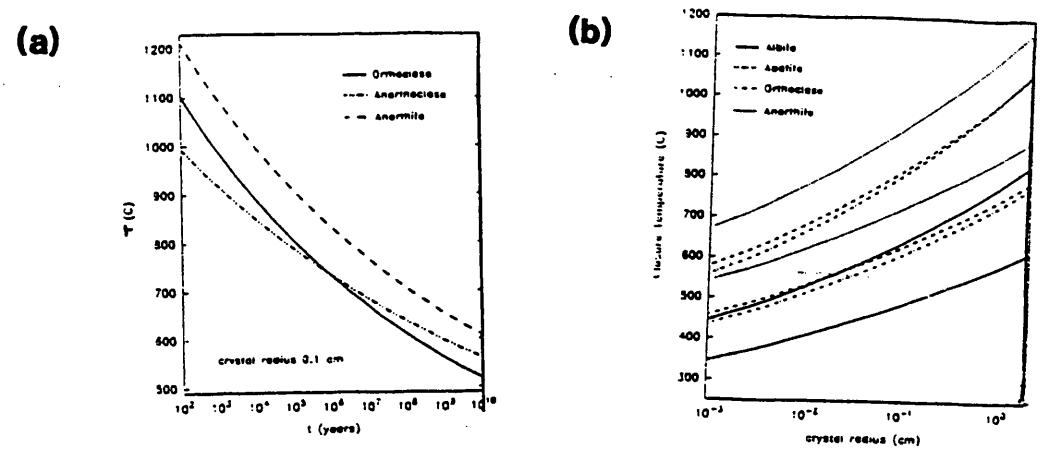

Figure 4.9. Graphs showing the temperature and rate at which minerals loose their Rb/Sr initial ratios, (after Cherniak and Watson 1991), a) for a fixed crystal radius and different temperatures and b) the temperatures at which different sizes of crystal become closed.

The very large size of both the megacrysts and the xenocrysts of K-feldspar, and indeed, the matrix feldspars analysed, should enable retention of the Rb/Sr initial ratios within these crystals. However, Gilletti (1991) and Cherniak and Watson (1991) pointed out that the development of twinning or perthitic texture could reduce the effective diffusion radius in the crystal. In the case of the Shap megacrysts, the very fine perthites were exsolved at low temperatures and will not cause isotopic resetting. The coarse deuteric perthites were exsolved at much higher temperatures (see Chapter 3) and thus, could enhance the rate of Rb/Sr isotopic re-equilibration. The conclusions of Mason (1982), that slow diffusion of K and fast diffusion of Na during perthite exsolution in K-feldspars creates a large K concentration gradient around perthite edges are supported by the data in Chapter 3, which clearly shows this K-rich rim around the high temperature perthites in the Shap megacrysts. This in turn greatly reduces the rate at which other elements will equilibrate with the Na-rich perthite. This is demonstrated by the Ba in the Shap megacrysts (Chapter 3), but will also affect diffusion of most other elements, including Rb and Sr, (Mason 1982). Cherniak and Watson (1991), found that in orthoclase the exchange reaction,

$$Sr^{2+} + Al^{3+} \rightarrow K^{+} + Si^{4+}$$

was the main cause of Sr-diffusion. Given the high K-concentration gradients around the deuteric perthites in the Shap megacrysts, it is almost certain that

Sr-diffusion in the Shap megacrysts would be too slow to reset the initial ratios. Therefore by avoiding the edges of these larger perthites during sample removal the original Sr-initial ratios should have been measured. The matrix K-feldspars seem to have lower initial ratios than the megacrysts. Fractionation of Rb and Sr in magmas has been shown to cause changes in the initial ratios of magmas over fairly short periods of time i.e. <10Ma (MaCarthy and Cawthorn 1980). The fractionation of Rb by the megacrysts in the Shap magma may have in turn produced low Rb/Sr ratios. Subsequent recalculation of the initial ratios using a fixed age would then lead to high and low initial ratios for the megacrysts and matrix K-feldspars respectively. This may explain the lower initial ratios for the matrix K-feldspars.

By plotting the evolved $^{87}Sr/^{86}Sr$ ratios against the $^{87}Rb/^{86}Sr$ ratios in a standard isochron plot (York 1968), a determination of the radiogenic ^{87}Rb evolution differences can be made between the megacrysts in the granitoid and enclaves.

In **Figure 4.10**, the megacrysts lie on the same isochron as the xenocrysts. The initial ratios represented by this trend have an almost identical pattern as shown in **Figure 4.8** with cores having lower initial ratios to the rims and thus, the evolved ratios of $^{87}Sr/^{86}Sr$ due to radioactive decay of the ^{87}Rb are also higher. Thus, it is likely that the megacrysts represent crystals grown from the same magma. The lower $^{87}Rb/^{86}Sr$ ratios in the xenocrysts suggest that they were formed at an early stage in the magma prior to mixing. This is consitant with their smaller size when compared to the megacrysts within the granitoid, (see Chapter 2).

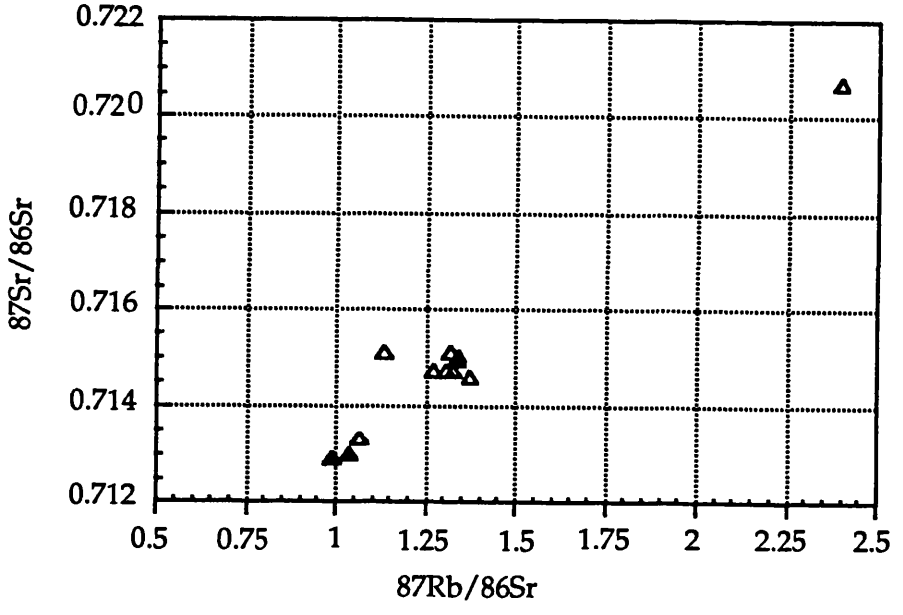

Figure 4.10. $^{87}Sr/^{86}Sr$ ratios against $^{87}Rb/^{86}Sr$ ratios for the megacrysts and xenocrysts in the Shap granitoid and enclave respectively, with open triangles = granitoid megacrysts and black triangles= xenocrysts.

4.5 Discussion

The mixing test shown in **Figure 4.4** indicates that the distribution of trace elements within the Shap granitoid is due to mixing of an enclave (quartz-diorite) magma and a granitoid magma, with a maximum of 31% of the mixture consisting of the enclave melt. Field evidence from, Harker and Marr (1891) and Grantham (1926) and chemical evidence from Firman (1978) and data plotted in **Figures 4.2, 4.3 & 4.5,** suggests that the Shap granitoid has a basic parent which was less evolved than the dominant (Stage II) composition of the intrusion. This however has an independent in composition, and is probably unrelated to, the diorite-enclave magma. The trend of fractionation (**Figure 4.5**) as previously mentioned appears to show a simple pressure and/or $\%H_2O$ increase, apart from the latter stages and in the granitoids which surround the enclave. Such changes in overall pressure to cause the observed peritectic crystallisation trend in the granite system diagram may be simply related to uplift of the magma through the crust. The shift in the eutectic due to pressure and/or $\%H_2O$, as shown in Tuttle and Bowen (1958), Luth et al. (1964), and Day and Fenn (1982), (**Figure 5b & c**), has a very similar pattern to the majority of the Shap granitoid data. As the REE patterns and other geochemical evidence presented in O'Brien (1985) suggest a closed system crystallisation of the intrusion it would seem likely that pressure decrease would indeed cause the observed crystallisation trend in the Shap granitoid magmas. An increase in the $\%H_2O$ may also have occurred but this is not conclusively shown in **Figure 4.5.**

The exchange of elements between enclaves and host granitoids in the Shap granitoid has been shown to have taken place with the granitoid surrounding the enclaves being generally enriched in K_2O, and the enclave margins being enriched in Ca, Rb, Ba, Ti, and other hydrothermally mobile elements, (Grantham 1926; Farrand 1960; Eberz and Nicholls 1990). This is probably the best explanation for the chemical distribution of the granitoids surrounding the enclaves, particularly in **Figure 4.5.** The mixing of the granitoid with the enclave magma must have had a more profound effect than simple exchange on a local scale to produce the mixing trend shown in **Figure 4.4.** and the deviation from the peritectic crystallisation trend observed by the main granitoid types. The term hybridisation (Castro et al. 1990) may be applied in this case, to the latter stages of the Shap granitoid. As these were the latest to be emplaced (Grantham 1926), they would presumably have had longer to mix with the enclave magma to become homogenised. It seems likely that extensive, peritectic, closed system crystallisation, followed by mixing may be used to account for the major- and trace-element, and Rb/Sr isotopic distribution in the Shap granitoids and enclaves.

The megacrysts have many textures which suggest they have been involved in the mixing of these two magmas, (see Chapter 2). The Rb/Sr isotope data seems to confirm this. In particular, the trend of increasing initial ratios from core to rim, can be observed. The highest initial ratios in the Shap system belong to the enclaves. This may be due to a higher crustal component in the enclave magma, which is partly shown by the peraluminous nature of the enclaves (**Figure 4.2**). The increasing initial ratios of the megacrysts is consitant with a phenocryst of K-feldspar growing in a magma with a slightly increasing $^{87}Sr/^{86}Sr$ isotopic due to mixing with the enclaves magma. As isotopic mobility and re-equilibration is a faster process than chemical re-equilibration (Holden et al. 1987, 1991), this could occur without wholesale changes to the chemistry of the magma in which the megacrysts were growing. The xenocrysts show not only the same initial ratio pattern, but the measured $^{87}Sr/^{86}Sr$ ratios indicate that a very similar post-crystallisation history has occurred. If the megacrysts in the enclave had grown in this liquid or subsequently in a solid-state environment then they would have initial ratios that were greater that or equal to those of the enclave material. This is common in all crystals growing in metamorphic environments (Rollinson 1993). Therefore the megacrysts in both the granitoids and the enclaves grew from the same magma and the resulting occurrence of megacrysts in the enclaves is the result of magma mixing.

4.6 Conclusions

1) The enclaves and the granitoids are chemically different and have different $^{87}Sr/^{86}Sr$ initial ratios, and therefore most likely have independent origins.

2) Mixing of the enclave and granitoid magmas is represented by a correlated linear mixing line based on trace-element distributions in the granitoids and enclaves, where the latter granitoids represent a hybrid magma and the enclaves account for a maximum of 31% of the mixture.

3) The megacrysts show Rb/Sr isotopic patterns which are consitant with phenocrysts growing in a magma with a changing $^{87}Sr/^{86}Sr$ initial ratio due to mixing with the enclave magma. This pattern is common to both the megacrysts in both the enclave and the granitoid and is best explained by latter incorporation of the K-feldspar megacrysts into the enclave by mixing, i.e. that they are in fact xenocrysts in the enclave derived from the granitoid.

4) The Shap granitoids originated from the same parent melt. This is shown by; a) the peritectic fraction pattern for the majority of the phases of the intrusion, b) the low $^{87}Sr/^{86}Sr$ initial ratios for the Shap granitoids which indicate rapid emplacement with little crustal contamination, and, c) the REE

patterns which show the lack of fractionation of the magma in Shap intrusion (O'Brien 1985).

The distribution of Li in the main minerals of the Shap granitoid and it's use as an indicator of water influence on mineral growth.

5.1 Introduction.

The hypothesis of Vernon (1986) is that low water content during early K-feldspar growth produces the large megacrysts observed in many granitic rocks. This is based on petrological evidence from Swanson (1977) and Fenn (1977), and indicates that H_2O/melt interaction is one of the major controlling factors influencing the growth of megacrysts in granites.

The textural evidence presented previously in this study, e.g. deuteric perthites, chloritisation, etc. (see Chapter 2) points to prolonged water interaction with the crystallising magma. The findings of Firman (1957) point to fissure metasomatism associated with late stage fluid activity in the granitoid. Spears (1961) noted that radioactivity is concentrated in the late stage minerals, and this would seem to support the view that prolonged aqueous, hot fluid activity, which has concentrated U and Th in these phases, has occurred during the history of the Shap granitoid.

Li is one of the elements which is often concentrated in high temperature aqueous conditions (Turner and Verhoogan 1960) and thus, an investigation of it's distribution may reveal something of the fluid/magma interaction in the Shap intrusion.

5.2 H_2O in granitic melts: some general considerations.

H_2O in granitic magmas has been shown by Tuttle and Bowen (1958) and Day and Fenn (1982) to have profound kinetic and geochemical influences on the crystals forming in its presence. In the case of alkali feldspars, the reduction of nucleation density, and the increase in growth rate have been noted (Fenn 1977).

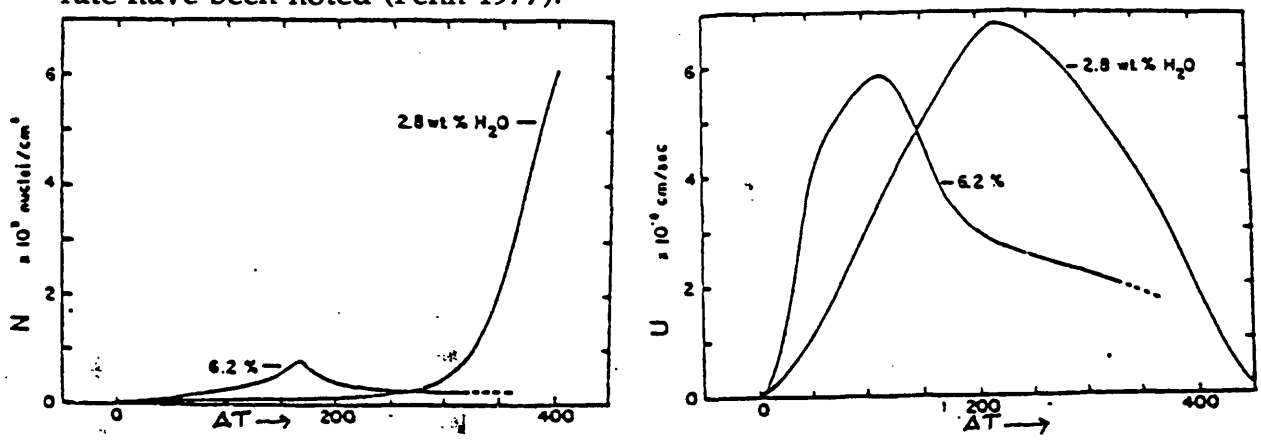

Figure 5.1. Graphs of nucleation density, (N) and growth rate, (U) for $Na_{0.5}K_{0.5}AlSi_3O_8$ plus the indicated H_2O contents, plotted against system undercooling,(ΔT), after Fenn (1977).

The graphs presented in Figure 5.1 show that higher nucleation density with less undercooling occurs, if the H_2Owt% of the magma is higher. The growth rates for alkali feldspars are quite similar to one another, for both the water contents shown. The growth rate reduces, with nucleation density increase, at lower temperatures. Swanson (1977) found that at the time of greatest alkali feldspar growth, plagioclase growth was almost at its slowest. In granitic rocks this would mean that K-feldspar megacryst growth would correspond approximately with lowest amount of plagioclase crystal formation.

Mysen (1992) observed that in Al-bearing melts, low H_2O content caused melt polymerisation. This view was supported in an earlier work by Stolper (1982) who showed that higher water content caused melt de-polymerisation. Thus, with increasing H_2O in a granitic magma, a change from larger to finer grains of K-feldspar would result. Stolper (1982) also suggested that the process of oxygen reacting with molecular H_2O would produce OH ions in the magma at high temperatures, regardless of the composition of the melt. Therefore a high initial H_2O content in the melt would produce a high OH content in the melt. De-polymerisation was found to be related to the formation of Na-OH bonds in the experiments carried out by Mysen (1992). The speciation of alkalis (Na,K,Cs,Li,etc), will greatly influence their crystal/melt partitioning. In other words at higher temperatures, the greater the H_2O (melt) content, the greater the OH (melt) content, and thus Na,K,Cs,Li etc., will form large numbers of OH-bonds in the fluid-bearing melt. This will produce the nucleation of small-sized, but large numbers of alkali-bearing crystals, such as K-feldspars. The growth rate of these crystals will be slow, due to the necessity for OH-bond breakdown, before the alkali cation is incorporated into the crystal lattice. This process largely accounts for the findings of Swanson (1977) and Fenn (1977).

5.3 The geochemical behaviour of Li.

The geochemical behaviour of Li is thought to be strongly influenced by it's affinity with water (Hall, 1987). In magmatic environments, Li is enriched in high temperature, aqueous fluids (Turner and Verhoogan 1960). This results in the high concentrations of Li often observed in pegmatites and aplites (Cameron et al. 1949; Jans and Tuttle 1963; Dujon et al. 1991).

The range of temperatures over which Li is most enriched in granitic environments, is from pegmatites to early pneumatolysis, i.e. the last crystallisation phase of most siliceous magmas (Turner and Verhoogan 1960; Dujon et al. 1991).

Stage	Temperature range (^{0}C)	Phases present	Main active elements
Magmatic	>800	Crystals,melt	----------
Pegmatitic	800-600	Crystals,melt,gas	Th,Y,Ta,Nb,Ti,U, etc.
Pneumatolysis	600-400	Crystals,gas	B,F,Be,Na,Li,Fe, Mn,Pb.
Hydrothermal	400-100	Crystals,gas and aqueous solution.	Al,F,Ca,Fe,Mn,Cu, Zn.

Table 5.1. The evolution of granite to quartz vein (Turner and Verhoogan 1960).

In the Shap granitoid the process of speciating H_2O into the magma may be used to account for nucleation density and growth changes of K-feldspar with lowering temperatures. This may result in the change from megacrysts to matrix K-feldspars. Consequently, Li may show an affinity with the most aqueous phase of the melt. The major control on Li enrichment in the melt would seem to be the presence of OH ions (Mysen 1992). Clearly, the T-conditions and thus the ionic state of the water, during mineral growth, will greatly influence the partitioning of the Li between melt and growing crystals. If the magma is water rich at higher temperatures then the Li-OH bonding will cause melt partitioning of the Li and crystals relatively poor in Li will grow. Clearly, the melt will remain Li-rich until at lower temperatures the latest stage minerals will become Li-enriched as more H_2O exists in the melt.

5.4 Li in minerals.

Ahrens and Liebenberg (1945) found that Li contents increased with increasing Rb contents in micas and feldspars, but in general, low Li concentrations are present even in Rb-rich micas and feldspars. The process controlling Li substitution is clearly different from most alkalis, with Li rarely substituting directly with the other alkalis, unlike Rb for K and Sr for Ca.

Li is thought to substitute for Fe and Mg in minerals, particularly micas, alkali amphiboles and pyroxenes and feldspars. This is usually in a coupled exchange with Al (Dutrow 1986):

$$Li^{+}+Al^{3+} = 2Fe^{2+},(2Mg^{2+})$$

Dutrow (1991) found that the main control on Li distribution was the

coupled exchange with Al, rather than Fe and Mg content of the host mineral.

In quartz, the presence of Li is also linked closely with the amount of Al substitution for Si, and also the amount of Fe^{3+} for Si, (rose quartz) (Deer et al. 1992):

$$Li^{+}+Al^{3+},(Fe^{3+}) = Si^{4+}$$

Keith and Tuttle (1952) found that the quartz structure was capable of containing far more Li+Al at high temperatures than at low temperatures. Ono (1982) concluded that for given P/T conditions the Al content of quartz was reduced in a H_2O-rich magmatic environment, and that Al+Li-bearing quartz crystals were normally metastable, thus reflected the water activity of the magma at the time of crystal formation. Thus, Li is concentrated in Al-bearing phases of minerals and is enriched in the melt by OH ions.

5.5 The mobility of Li at lower temperatures.

Li movement at lower temperatures during sub-solidus reactions potentially could cause resetting of the magmatic Li contents of the minerals. Ellis and Mahon (1964) modelled hydrothermal reactions and found that below 350^0C almost no increase in the Li content of the hot fluid which was used to represent water/rock reactions was observed. As previously mentioned, Ono (1982) stated that Al+Li-rich quartz was metastable and compositions are not easily changed at low temperatures. The exchange of O-isotopes is greatly enhanced by high temperatures, the grain size of a mineral and the exchanging medium, e.g. a fluid, (Valley and O'Neil 1984). For K-feldspar megacrysts, quartz, plagioclase and even matrix K-feldspars, the amount of O-isotope exchange is expected to be enhanced along fractures and to perthitic boundaries and fractures in alkali feldspars (Worden et al. 1989). A similar pattern is predicted for Li-exchange. Deubener et al. (1991) produced Li-feldspar by ion exchange at only 300^0C, although this was in a highly disordered sanidine and points towards an extremely open lattice for Li-diffusion to have taken place. Textural evidence, such as relatively undisturbed oscillatory zoning, indicates that an open structure does not exist in the Shap crystals, (see Chapter 2). Ba movement for instance is restricted to the deuteric perthite edges, (see Chapter 3), and therefore by avoiding obviously altered patches such as extremely turbid areas and areas of visible inclusions during sampling, the problems associated with the resetting of magmatic Li-contents of the Shap

should have been avoided.

The **Table 5.2** summarises the Li data obtained on the main minerals of the Stage II Shap granitoid.

Sample	Li(ppm)	% ^{6}Li	Al(ppm)	Be(ppm)
Biotite 1	927	28.4	----	100.0
Biotite 2	968	28.4	----	102.5
Chloritised Biotite	564	4.6	----	16.0
K-feldspar(matrix)	50	31.3	----	11.6
K-feldspar megacryst (Core)	15	17.3	----	1.8
K-feldspar megacryst (Rim)	17	13.0	----	2.5
Quartz 1	34	17.8	943	trace
Quartz 2	32	19.6	993	trace
Plagioclase(matrix)	20	18.0	----	5.1

Minerals	Li(ppm)
K-feldspars	0-13
Plagioclase	0-10
Biotite	198(Diorite)-1,960(Granite)
Quartz(non-vein)	0-19

Table 5.2. Tables of Li data obtained on Shap mineral separates by atomic emission, and average Li contents of minerals from various granitoids (from Wedephol 1978). The Be concentrations and quartz Al contents were measured by atomic absorption. (See Appendix II for detailed description of the methods.) The chloritised biotite contained 40% chlorite and the separates were over 99% pure, as determined by XRD analysis. The error for Li concentrations is +/- 0.5ppm and for ^{6}Li% is +/- 5% ^{6}Li. The errors for Be are +/- 0.1ppm and for Al +/- 18ppm.

5.6 Discussion of data.

By comparing the Li data with average figures of Li concentrations in granitic minerals from the data in Wedephol (1978), the general pattern of Li-distribution in the Shap samples can be assessed more meaningfully.

The general pattern of Li concentrations in the Shap granitoid shows that the feldspars and quartz samples are Li-rich and that the biotites (and chloritised biotites), are Li-rich when compared to more basic granitoid rock-types, but Li-poor compared with acidic granites. Within the pattern of Li-contents in the Shap minerals, there is a general increase from the megacryst to the matrix K-feldspars. The plagioclase contains marginally more Li than the megacryst samples. This pattern is often found in coexisting feldspars (Smith 1974). The Shap granitoid biotites have lower Li-contents than might be expected, (only 50% of the Li), when compared with the reported Li-concentrations in acidic granitoids (Wedephol 1978).

It is apparent that the chlorite-rich sample of biotite is depleted in Li and that the presence of chlorite in the biotite corresponds to a reduction in the Li-content of the biotite. The retrograde formation of chlorite from biotite often results from the reaction (from Yardley 1991):

Biotite+Quartz+Water->Chlorite+Muscovite+K-feldspar.

In such a reaction, which would usually occur below 400^{0}C, the breakdown of the quartz and the liberation of the K from the biotite to form the muscovite and K-feldspar would probably cause a reduction in both the Al and Li content of the quartz as Al is mobile in hydrothermal environments (Turner and Verhoogan 1960; see **Table 5.1**). The findings of Keith and Tuttle (1952) and Ono (1982) that Al+Li-rich quartz is metastable at these temperatures would rule out Al+Li exchange into low temperature quartz. The quartz in the Shap granitoid is generally unaltered, euhedral to subhedral, and ranges from 0.5mm to 2.0mm in size, along with smaller interstitial grains and glass on early plagioclase and other matrix crystals, (**Figure 5.2**). Quartz is also present in the megacrysts as primary inclusions. The quartz must have grown during a prolonged magmatic history, with rather limited late-stage, interstitial growth.

The presence of muscovite has been recorded by Harker and Marr (1891) and Grantham (1926) but is generally absent from the hand specimens from which the samples were obtained. This suggests that considerable movement of reactants may have taken place in the Shap intrusion, indicating an open system in which the reactions have taken place.

The presence of adularia, as determined by XRD analysis of the matrix K-feldspar suggests that retrogression reactions to produce the chlorite, have occurred, as outlined in the reaction above. Adularia is a low temperature, K-feldspar often found in hydrothermal veins and some pegmatites (Cerny and Chapman 1984). The structure of adularia can range from semi-ordered sanidine/orthoclase to sub-ordered microcline (Smith and Brown 1988). Progressive ordering of the crystal structure of K-feldspars, on cooling, will produce a change from sanidine/orthoclase to microcline (Kroll and Knitter 1991). Laves (1952) suggested that the interaction of water and K-feldspars, at low temperatures, could cause disordering in cooling crystals, giving rise to metastable adularia, which is unable to re-order the Al/Si structure. Texturally the matrix K-feldspars are generally perthitic and are often twinned (see **Figure 5.2**), which is inconsitant with low temperature crystals of adularia (Cerny and Chapman 1984). Thus, the adularia present in the matrix of the Shap samples is not due to the retrogression of the biotite to

chlorite but is formed by water reacting with the cooling K-feldspars. Both the matrix K-feldspar and the quartz can be treated as magmatic in origin although the interstitial quartz represents a late stage.

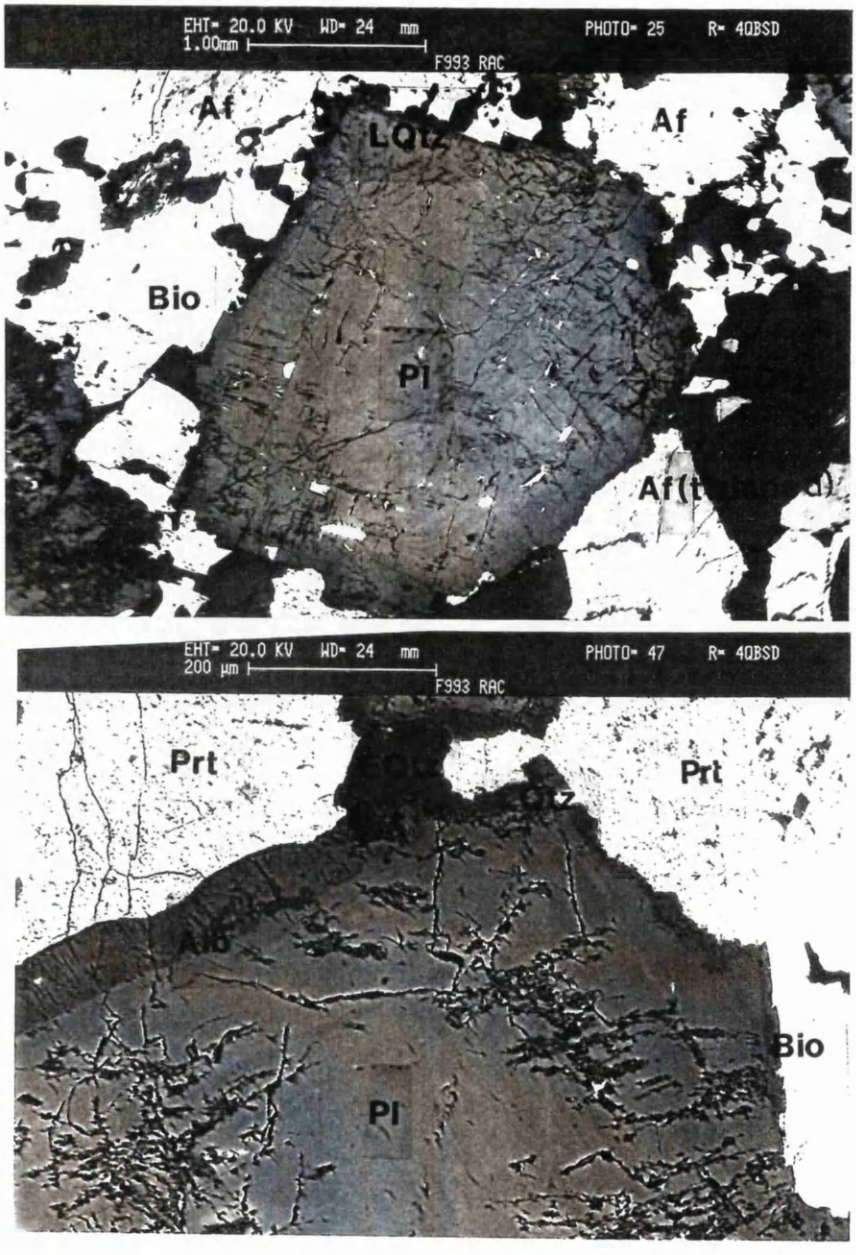

Figure 5.2. Back-scattering SEM images of matrix crystals in the Shap granitoid. Pl=plagioclase, Alb=albitized rim, LQtz=late interstitial quartz, EQtz=euheadral to subhedral grain quartz, Af=matrix alkali(K)feldspar, Prt=perthite, Bio=biotite. Note the interstitial glass and albitized rims of the plagioclase. The K-feldspar shows perthitic texture and twinning despite it's adularian crystal structure.

A late stage fluid transporting the liberated products from the biotite breakdown in an open system is probably the best explanation for the formation of the chlorite and transportation of the reaction products to joints, fissures, etc. (Grantham 1926). Firman (1957) surmised that potash metasomatism and silicification, along with epidote and garnet formation in

fissures and at the intrusion contact, resulted from percolating fluids, rich in Si,K,Ca,Fe and CO_2, derived from the granitoid. This explains the concentration of muscovite along the joint and fissures, (Harker and Marr 1891; Grantham 1926) without wholesale changes to, and extensive mineralisation of, the granitic body.

We can thus conclude that the fresh biotite, matrix K-feldspar and quartz, megacrysts and plagioclase have magmatic Li-contents. The biotite must have crystallised from an effectively Li-poor magma. This can be seen by the comparison with the late stage granite from the data in **Table 5.1.**

The high temperature crystallisation of the quartz, as represented by the high Al+Li concentrations, and its textural characteristics (**Figure 5.2**) along with the high temperature growth of the plagioclase and K-feldspar megacrysts indicated by the textures, (grain size, zoning, etc., see Chapter 2) and chemistry of these crystals, (Ba, Rb and Sr content, etc., see Chapter 3) must point to prolonged cogenetic growth of the quartz, plagioclase and K-feldspar megacrysts in the Shap magma at high temperatures, (>800°C). The cogenetic growth of these minerals in granites has been discussed by many authors (Tuttle and Bowen 1958, Luth et al. 1964, Whitney 1975, Day and Fenn 1982). The pressure of 8kb presented in the following diagram represents a depth of about 24km. This is likely to be an over-estimation for the final depth of emplacement of the granitoid. However, the main controls on the stability fields in this system are temperature and wt%H_2O and pressure only causes small differences in the size of the stability fields in this system (Whitney 1975; Day and Fenn 1982). Therefore, the overall pattern of **Figure 5.3** can be used to represent the fields of stability of the Shap minerals with varying H_2O contents.

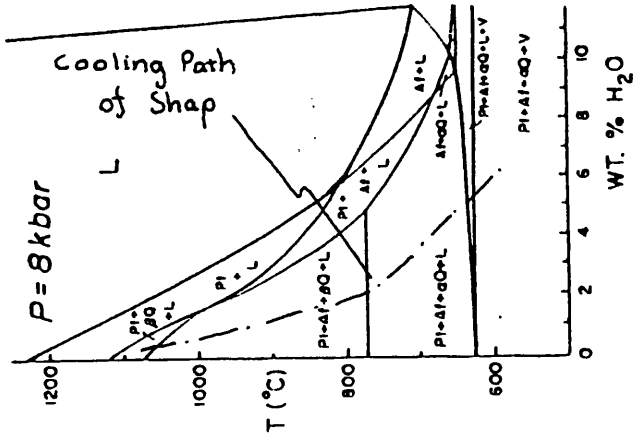

Figure 5.3. Solidus, liquidus and vapour saturation surfaces of granite at 8kb, (Day and Fenn 1982, after Whitney 1975). Symbols: Af=alkali feldspar, Pl=plagioclase, aQ=alpha quartz, bQ=beta quartz, L=liquid, V=aqueous vapour.

If the order of crystallisation, as shown in **Figure 5.3** (i.e. that quartz, plagioclase and K-feldspar were coexisting), then the initial Shap magma must have been dry, with a H_2O-content of less than 3wt%. This explains the high Li contents of the initial phases, and high Al content of the quartz (Ono 1984). The increasing water content at lower temperatures could be caused by speciation of H_2O into the melt, (i.e. fractionation). This in turn would produce a high nucleation density of K-feldspar, and general de-polymerisation of the melt (Fenn 1977; Mysen 1992). Slow growing crystals of K-feldspar resulting from this process will generally incorporate the Li,Na,K,etc. as the water content of the magma moves from ionic to molecular, (Stolper 1982), causing the observed growth changes but only temporarily reducing the Li partition coefficient. This will result in a Li-rich environment for the matrix K-feldspar growth, hence their high Li contents. The high Al+Li content of the quartz will reduce it's inversion temperature to nearer the 600^0C mark (Keith and Tuttle 1952), effectively extending the Pl+Af+bQ+L field (**Figure 5.3**). At lower temperatures even a very low H_2O-content of 3wt% will cause melt de-polymerisation (Fenn 1977; Stolper 1982; Mysen 1992), but only small amounts of Li-OH bonds will be formed. The effect of these bonds is shown by the many times greater numbers of K-feldspars forming and the enrichment of the matrix K-feldspars in Li, as is represented by the measured Li-contents of the matrix K-feldspars (**Table 5.2**).

5.7 The isotopic composition and distribution of Li.

The natural abundance of Li isotopes, of which there are two stable forms ^{7}Li and ^{6}Li, has been investigated by several authors. The ranges in geological materials both terrestrial and meteorites are generally from 11.5% ^{6}Li to 14% ^{6}Li (Svec and Anderson 1965; Balsiger et al. 1968). 5% ^{6}Li-variations due to anhydrous, magmatic, fractionation processes and 25% ^{6}Li-variations in high temperature, hydrothermal systems, have been recorded by Morozova and Alferofsky (1974). Taylor and Urey (1938) found that extreme fractionation of ^{6}Li and ^{7}Li was possible in experiments using zeolite exchange columns, with up to 35% increase in ^{6}Li initial compositions, being recorded. In other stable isotopic systems e.g. $^{18}O/^{16}O$ in granites, fractionation of the O-isotopes is found to be controlled by temperature (Faure 1986; Taylor and Sheppard 1986), with low temperature exchange resulting in the most extreme fractionation of ^{18}O and ^{16}O. A similar pattern is expected for the distribution of Li isotopes in this study.

The isotopic compositions of the Li in the Shap samples is shown below (**Figure 5.4**).

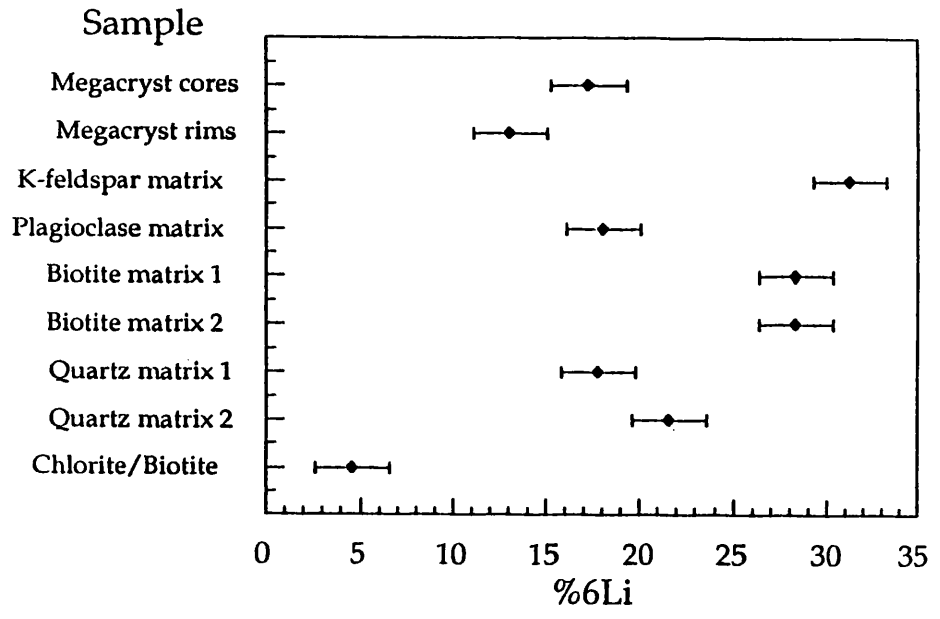

Figure 5.4. Graph showing the distribution of the Li isotopes between the samples in the Shap granitoid, with the field of measured abundances and the errors based on +/- 2.5% experimental variation.

Isotopic compositions are detectable for only a few elements by atomic emission but the shifts in concentrations detected for these samples was in excess of experimental error and must be due to changes in the isotopic ratios of the Li (see Appendix II for a description of the method). ^{6}Li has a higher emission spectrum than ^{7}Li (Zadiel and Korrenoi 1961; Manning and Slavin 1962). Assuming that a plus or minus 5% ^{6}Li variation in the recorded isotopic values is due to anhydrous magmatic processes (Morozova and Alferofsky 1974) the Li isotopic composition of the K-feldspar matrix and biotite samples from the Shap granitoid are almost certainly representative of a fractionation process controlled by high temperature H_2O-influence. The plagioclase, quartz and K-feldspar show a ^{6}Li-isotopic distribution within the range of previously reported anhydrous, magmatic fractionation, i.e. within 5% of each other (Morozova and Alferofsky 1974) .

The biotite and the K-feldspar matrix show very much higher ^{6}Li%'s. If the order of crystallisation of these minerals is as discussed previously, then they may have grown from the magma at significantly lower temperatures

along with higher magmatic H_2O-contents, than the other main minerals. This variation i.e. the fractionation of "heavy" and "light" isotopes is common in other stable isotopic systems as previously mentioned (Faure 1986; Taylor and Sheppard 1986). This seems the most likely explanation for the variations recorded here.

The chloritised biotite shows a very low $^6Li\%$ content. At the low temperature of the chlorite formation (400°C or less), the preferential exchange of ^6Li into the fluid would cause the increase of residual ^7Li in the crystal, and would account for the high $^7Li\%$ observed. The amount of O-isotope exchange between minerals and fluids is greatly dependant on the diffusion rates in a mineral, (Valley and O'Neil 1984). Thus, biotite will have a high rate of ^{16}O and presumably ^6Li, exchange in the chloritised sample. Again, this is a common process in stable isotopic systems in metamorphic environments (Taylor and Epstein 1962; Taylor 1968; Truesdell 1974; Faure 1986).

Be behaves in a very similar manner geochemically to Li, in that Be is enriched in the same high-temperature, aqueous conditions, and the same relative proportions are found although in lower concentrations in the same minerals (Turner and Verhoogan 1960; Wedepohl 1978; Deer et al 1992). The pattern of Be-distribution in the Shap granitoid samples analysed (**Table 5.2**) shows an identical pattern and therefore seems to confirm the pattern of crystal growth and increasing H_2O influence shown by the Li-contents and Li-isotopic variations.

5.8 Conclusions.

1) The Li concentrations and isotopic variations are consistent with a model of a magma undersaturated in H_2O at high temperatures, resulting in a low OH-ionic content in the melt. This consequently produced a slightly polymerised melt, high Al+Li in the quartz and relatively high Li contents in the plagioclase and K-feldspar megacrysts.

2) The speciation and build-up of H_2O at lower temperatures caused the change from megacrysts to matrix K-feldspars due to the de-polymerisation of the melt. The much lower temperatures, as indicated by the Li isotopic variation, produced a high molecular to ionic water ratio preventing Li from being melt partitioned and thus is concentrated in the matrix K-feldspars.

3) The majority of the matrix biotite probably formed at a slightly later stage in a Li-poor melt. This results in the low Li-concentrations for the matrix biotites in the Shap granitoid when compared to similar biotites from

acidic granitioids.

4) The interaction of water at low temperatures is shown with ^{6}Li preferential exchange taking place during chlorite formation, giving a high range of ^{7}Li values.

5) The pattern of Li-concentrations and isotopic variations is consistent with the change from megacrysts to matrix K-feldspars due to water fractionation into the melt at lower temperatures. The measured Be-contents of the samples analysed confirm this pattern.

Interpretation of evidence

6.1 Discussion and summary of conclusions

The petrographic study of the K-feldspar megacrysts in the Shap granitoid and mafic enclaves, shows strong evidence that the megacrysts were formed almost entirely by magmatic processes. The megacrysts in both the granitoid and the enclave studied all showed one or more of the features identified by Vernon (1986) as being characteristic of magmatic K-feldspars. The features most likely to represent magmatic growth such as twinned crystals, magmatic oscillatory zoning and zonally aligned inclusions are present in most of the megacrysts in the granitoid and the enclaves. The megacrysts which occur in the enclave show clear petrographic evidence of mixing. Many of the megacrysts from the enclave have dissolved edges which truncate the magmatic oscillatory zoning, as well as having developed plagioclase mantles. This, along with the occurrence of granitoid matrix glomerocrysts, resorbed plagioclase crystals and quartz ocelli, suggest that the Shap granitoid has undergone a mixing event(s) with the quartz microdiorite enclave magma. Thus, the Shap intrusion represents a hybrid-type granitoid.

Microprobe investigations confirm a Ba-rich composition and the magmatic nature of the oscillatory zones. Both petrographic and microprobe evidence suggests that the K-feldspar in the Shap granitoid magma probably grew in increasing H_2O conditions. This caused the change from megacryst to matrix K-feldspar growth and the deuteric un-mixing which produced the micro-perthites in the megacrysts. This theory is consistent with models for K-feldspar growth and un-mixing in granitoid magmas (Fenn 1977; Parsons 1978; Day and Fenn 1982; Whitney 1975; 1988; Brown and Parsons 1989).

Major- and trace-element concentrations show probable end-members in the mixing of the enclave and granitoid magmas. This along with the Rb/Sr patterns confirm the magmatic nature of the megacrysts and also the hybrid nature of the rock.

The distribution of the hydrophile element Li in the main minerals of the granitoid and the composition of the Li-isoptopes in these minerals, confirm the view that the Shap intrusion crystallised with an increasing H_2O-content. The Li distribution also seems to support the view that increasing H_2O-content in the magma caused the change from megacryst to matrix K-feldspar growth.

There remains a few points which were not fully discussed in the preceeding chapters. Firstly, the presence of subhedral megacrysts in the granitoid seems to be the result of dissolution after magma mixing. But, why should nearly half the megacrysts in the granitoid remain subhedral after the

dissolution caused by mixing while half re-grew to give euhedral shapes? A clue to this may lie with the growth patterns of the large oscillatory zone which was analysed by microprobe in Chapter 3. The zone shows evidence of growth by Ba-resorption after dissolution of the megacryst, caused by mixing. The re-growth of the megacryst appears to be slow on the {010}-face and faster on the {001}- and {201}-faces. Similar growth trends have been reported in feldspar phenocrysts by Anderson (1984). If after dissolution the megacryst lost its primary euhedral shape, and the {001}- and {201}-faces in particular, then nucleation difficulties and slow re-growth of the crystal may account for the subhedral shapes. Ba-diffusion also seems to have taken place to partly disrupt the Ba-profiles of the oscillatory zones in the megacrysts. This appears to have affected the {201}-face more than the {010}-face of the crystal. Therefore, not only is growth faster but possibly diffusion is also faster on the {001}- and {201}- faces of the megacryst. Thus, diffusion disruption of the re-growing {001}- and {201}-faces may also inhibit re-growth of partly dissolved megacrysts and consequently contribute to their final subhedral nature. Euhedral megacrysts may represent crystals which have seen less original dissolution, thereby preserving the euhedral shape upon re-growth

A second point not fully discussed, is the classification and source of the granitoid, based on the major- and trace-element composition and the Rb/Sr initial ratios. The low $^{87}Sr/^{86}Sr$ initial ratios suggest a mantle or basic crustal origin and the REE-patterns (O'Brien 1985) indicate that there has been little fractionation. However, high concentrations of Li, Ba and Rb suggest a large crustal input to the Shap granitoid (Hall et al. 1993), and the equally high concentrations of Sr, Ce, and La also suggest a large mantle content. The best explanation for the above trace-element patterns and equal K- and Ca-contents of the intrusion, along with the low $^{87}Sr/^{86}Sr$ initial ratios, is a mixed source, metaluminous granitoid in a post-Caledonian tectonic setting, i.e. a H_{LO}-class granitoid (Barbarin 1993). Using the classification of hybrid granitoids by Castro et al. (1991) the Shap granitoid can be further grouped as a H_{SS}-type, based on the types of the enclaves present, and the mixing textures within. The more mafic nature of the enclaves and their trace-element characteristics (i.e. low Rb, Ba, U, Pb etc. and high Sr, Ce, La etc.) point to a more basic source for the enclave magma, than the granitoid. However, the enclave have the higher of the two $^{87}Sr/^{86}Sr$ initial ratios. The two most likely explanations are that the enclaves have come from an enriched mantle source or that they have been contaminated by crustal rocks with a higher $^{87}Sr/^{86}Sr$ initial ratio than the parent melt. What ever the origin of the enclave magma it is evident that the Shap intrusion represents a hybrid- (H_{SS}-) type granitoid and that the apparent mantle source for the granitoid is probably a false impression caused by the hybridisation of the intrusion.

6.2 A model for K-feldspar megacryst growth in the Shap granitoid magma

The growth of the K-feldspar megacrysts in the Shap granitoid can be divided into four main phases;

1) Primary, (ternary) sub-solvus, crystallisation dominated by small fluctuations in growth conditions in the granitic magma to produce megacrysts with small Ba-rich oscillatory zones.

2) Part, deuteric, un-mixing and subsequent non-ternary growth of the megacrysts due to a lowering of the solidus, probably caused by a increase in H_2O-content of the residual melt fraction. Prior to this the gradual increase in the H_2O-content of the melt may have caused nucleation density decrease to give the presence of sub-grains on the megacryst rims. The increase in H_2O eventually caused the change from megacrysts to matrix K-feldspars.

3) Magma mixing to cause dissolution and Ba-resorption during re-growth in the megacrysts. This probably occurred at some intermediate point in the cooling history of the intrusion, prior to the final increase in H_2O-content.

4) Low-temperature exsolution of the crypto-perthites and small amounts of emplacement related deformation produced the final compositions and shapes of the megacrysts.

These processes are summarised in Figure 6.1, below.

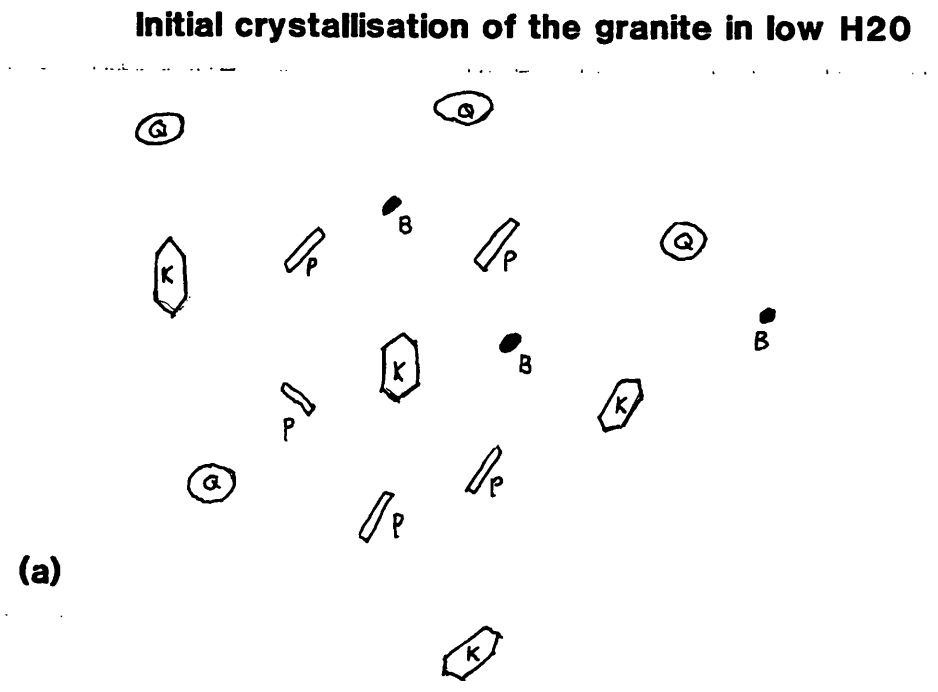

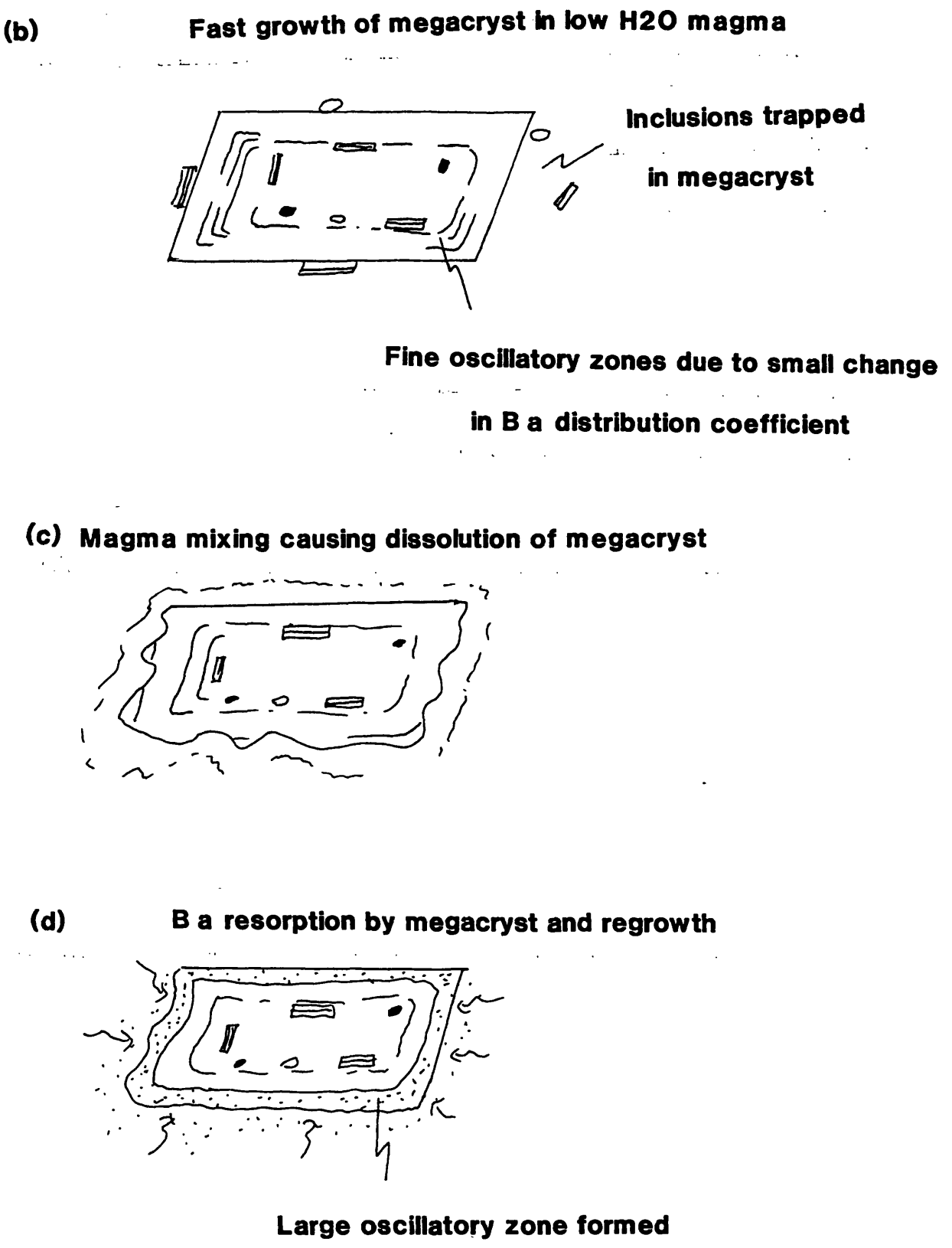

Figure 6.1. The main processes involved in the formation and distribution of the megacrysts in the Shap granitoid.

(e) Inreasing H2O causing increasing nucleation density of K-spar

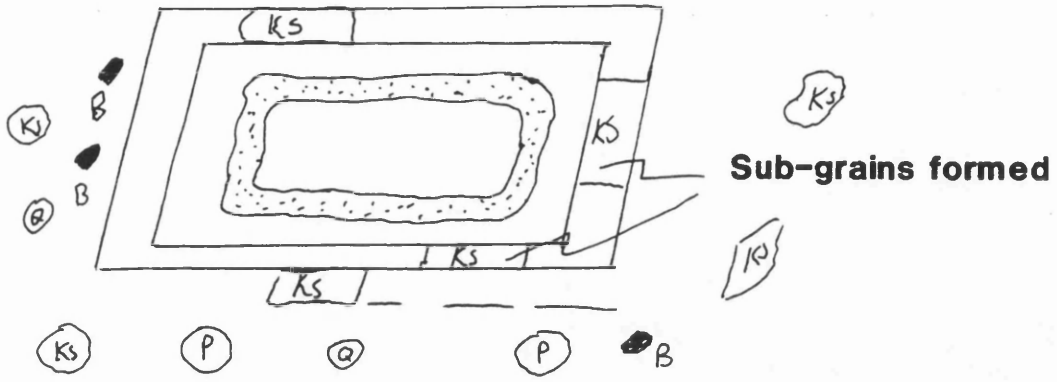

Sub-grains formed

(f) Lowering of solidus and deuteric un-mixing (less than 700°C)

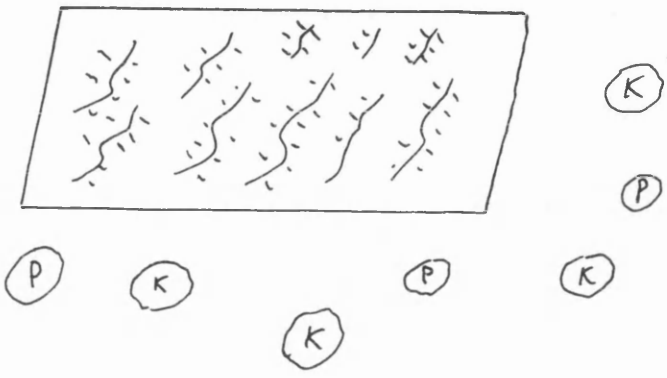

Non-ternary feldspar growth of matrix K-spar and plagioclase

(g) Final low temperature exsolution of perthtie

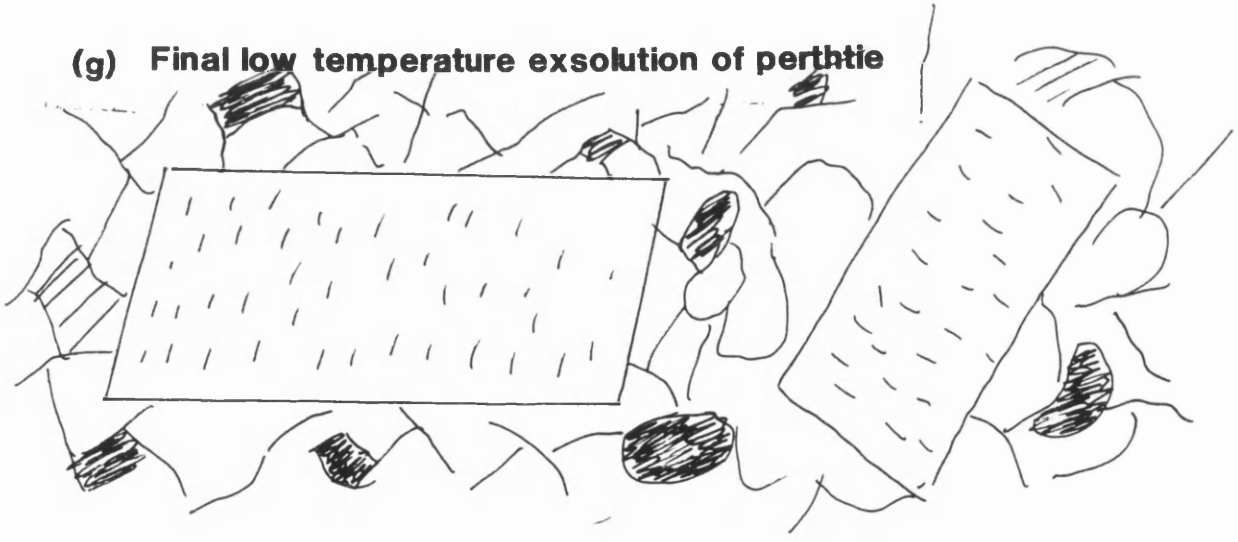

Complete solidification of matrix

Figure 6.1. (cont.)

6.3 Concluding statements

1) The evidence from the Shap granitoid suggests that the K-feldspar megacrysts have grown as phenocrysts.

2) The change from megacrysts to matrix K-feldspars has been caused by the increasing in H_2O-content of the residual melt.

3) The crystals have been incorporated into the enclaves by mixing.

4) The granitoid represents an H_{SS}-type intrusion.

Appendix I

Preliminary petrological techniques

(i) Sample selection and preparation

Two large, hand specimens, one of the Stage II Shap granitoid and one of the Stage II Shap granitoid surrounding a quartz microdiorite enclave were first sliced into 3cm thick slabs. This facilitated the selection of fresh {001}-parallel sliced megacrysts for polishing. Before samples were selected for polished section preparation the crystals were removed as small cubes from the large slabs. A series of thin sequential slices were taken using an ISOMET low-speed saw. The slices were taken parallel to the {001}-face of the crystal in the cube to enable accurate location of the core and rim regions of the megacryst. One of the slices was then sent to be made into a 30μm thick polished section which was used in microscope, C.L., S.E.M. and microprobe studies. Some of the remaining thin slices were re-cut to provide 100μm-thick sections and were subsequently micro-sampled for Rb/Sr analysis. Micro-sample removal involved sticking the thin-slice to strong tape. The slice was then broken-up, but the pieces remained attached to the tape. The tape and broken slices were then soaked with a small quantity of acetone in petri dish, which caused the adhesive on the tape to dissolve. Very small pieces of the thin slices could then be removed and their location recorded on a photograph or sketch of the slice.

For XRF analysis larger sections of the hand specimens were selected before crushing to a fine powder. The sections were chosen on the grounds that they represented average megacrysts to groundmass ratios, which was easy to determine using the thick-sliced specimens.

(ii) Mineral separations

To enable the Li, Al, and Be A.A. and A.E. analyses to be carried out a number of very pure mineral separates were obtained. To separate K-feldspar megacryst material for A.A./A.E. analysis the same method as above was employed, i.e. pieces were removed from the thin slices. However, as far bigger samples were required the thin slices were divided more coarsely into core and rim separates and had viable mica removed by hand picking and then were placed into heavy liquid with a S.G. of 2.9. This allowed the heavy micas, etc. to sink leaving only the pure feldspar powder. Similarly, matrix feldspars were purified, partly by magnetic separation of the biotites and ore minerals and then by heavy liquid to remove quartz. The K-feldspar and plagioclase matrix feldspars were then separated from each other by very fine adjustment of the density of the heavy liquid to concentrate the lightest K-feldspar and heaviest plagioclase, which produced the pure separates required. The biotite was purified by magnetic separation to concentrate the mica fraction and then by grinding under acetone to remove the remaining non-sheet silicate minerals. As the micas

purified by magnetic separation to concentrate the mica fraction and then by grinding under acetone to remove the remaining non-sheet silicate minerals. As the micas (and chlorite) tend to lie in a preferred orientation in the acetone they are more resistant to abrasion. Thus, by grinding and then sieving through a 90μm mesh the biotite separates were purified. The chlorite was removed by a process of grinding to fracture the mica grains and then by magnetically removing the portion with the highest magnetic susceptibility. This tends to concentrate the chlorite and purify the less magnetically susceptible biotite, after many repetitions. Quartz was separated by dissolving felsic fractions of matrix in flourosilicic acid for over a month which destroys all but the quartz crystals.

The purity of each separate was checked several times by XRD analyses until absolute purity (greater than 99%) was reached, except in the case of the chlorite/biotite sample which was about 40% chlorite and 60% biotite. The sample of matrix K-feldspar gave an interesting XRD pattern (**Figure AI.1**).

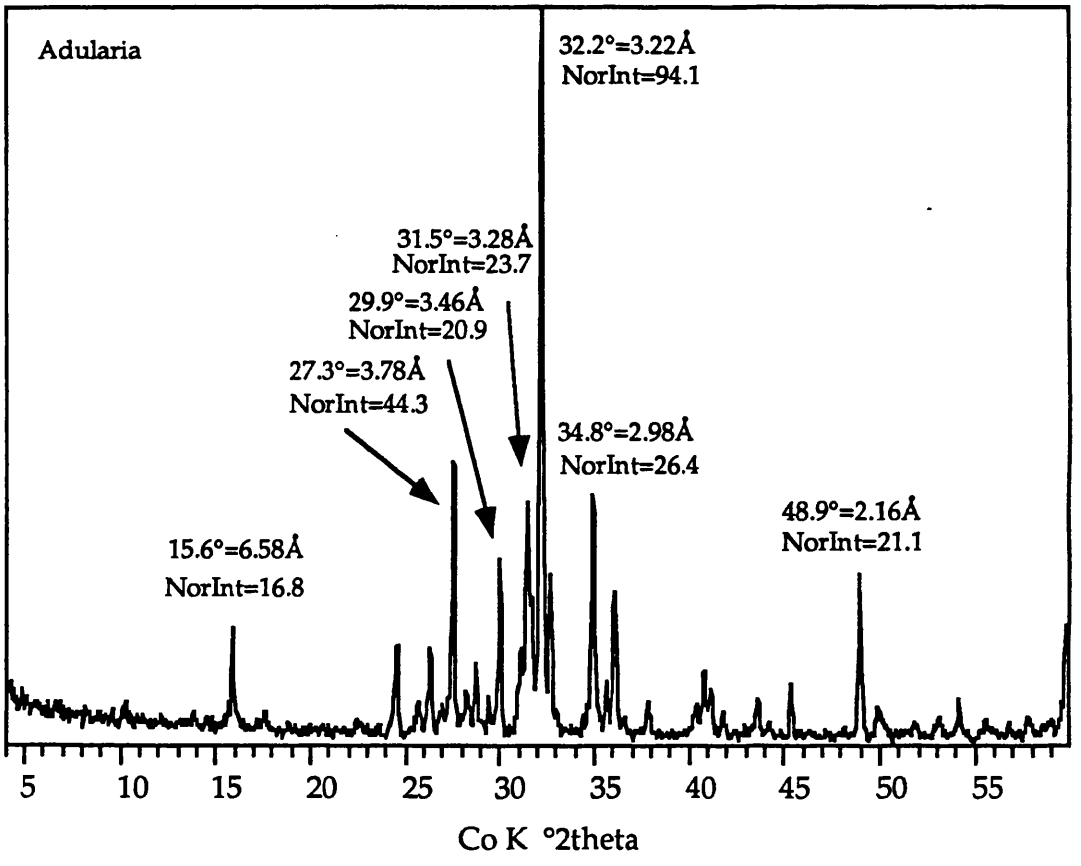

Figure AI.1. XRD pattern of the matrix K-feldspar with the main peak positions and their intensities (normalised to 100) shown.

The pattern is very similar to that of most K-feldspars with the main peaks and intensities corresponding to those reported by the J.C.P.D.S. (1980). However, the size of the peaks at 6.58Å and 3.28Å are almost always found exclusively in adularian feldspar standards (Hall and Macleod pers. comms. 1993). Thus, a large part of the crystal structure of the matrix K-feldspar is probably adularian in nature. The reasons for this are explained in Chapter 5.

(iii) Petrographic examinations

30μm polished sections were first examined using transmitted and reflected light microscopy, at various magnifications up to x50. C.L. microscopy was carried out on the sections at either x6 or x20 magnification with an accelerating voltage of up to 15kV and incident beam current of about 1 to 5μamps. S.E.M. images were studied using the optimum conditions for enhancing the zones, etc. and the general S.E.M. conditions are on the photomicrographs (see Chapter 2). All sections were carbon coated prior to S.E.M. investigation.

After C.L. and S.E.M. imaging sections of enclave megacrysts were either etched for 1 to 3 minutes in flouroboric acid or reserved for staining. The etching of the K-feldspars tends to remove K and Na in preference to Ca and Ba and thus enhances the oscillatory zones. Staining involves first etching the section for 25 to 35 seconds over HF fumes, and then dipped into Na-cobaltinitrate for 45 seconds. The slide is then rinsed in tap water, dried and then dipped in 2 to 5 percent BaCl solution for 2 seconds. The slide is then rinsed again in tap water and distilled water. The surface is allowed to remain wet and the slide and two drops of rhodizonate agent are placed on to, and spread over the surface. This technique produces yellow K-feldspars (or unstained) and red plagioclases which can be easily seen with a binocular microscope. This technique was useful in identifying the K-feldspar and plagioclase in the rather fine-grained enclave matrix and for showing the nature and extent of the plagioclase mantles around many of the K-feldspar megacrysts in the enclave.

Appendix II

Analytical Methods

(i) Microprobe analysis

Carbon coated 30μm polished sections were analysed using a Cameca SX50 electron microprobe, with a 15kV accelerating voltage and a beam current of 20nA for all analyses. The reported detection limit with these conditions is 100ppm, with an accuracy of better 2% based on the formula totals for the feldspars analysed. The full analyses of the feldspars from **Table 3.1**, Chapter 3 are presented in **Table AII.1.** The Ba-wt% were analysed separately and the same conditions, detection limits and errors should apply.

(ii) Rb/Sr isotope determinations

All preparations and analyses of Rb/Sr isotopes were carried out at the Scottish Universities Research Reactor Centre (S.U.R.R.C.) between February and July 1993. The micro-samples removed from thin slices of rock (Appendix I) were first cleaned with acetone in an ultra-sonic basin and Rb/Sr isotopic "spike" solutions were added. The samples were then reduced to insoluble salts by acid digestion and separated into pure Sr-and Rb-salts through cation exchange columns. These salts were then loaded into thermal-ionisation mass spectrometers (a V.G. isomass 54 for the Rb and a V.G. sector for the Sr) and the isotopic abundances and Rb/Sr contents determined. An isochron based on the measured ages gave a date of 412 +/- 12Ma, which is close to the range reported by Wadge et al. (1978) i.e. 393 +/- 4Ma. A more complete table of these results of the data presented in Chapter 4 is shown in **Table AII.2.**

Note; the errors for 87Rb/86Sr are x10-3 and for 87Sr/86Sr are x10-5.

Sample	Rb(ppm)	Sr(ppm)	87Rb/86Sr	87Sr/86Sr	IR(393Ma)	IR(412Ma)
Se1a	451	974	1.3416+/-9	0.71488+/-2	0.70743	0.70700
SeK	357	844	1.2246+/-9	0.71493+/-1	0.70812	0.70773
Se5a	313	480	1.8908+/-13	0.71810+/-2	0.70760	0.70700
b	343	646	1.5351+/-11	0.71672+/-2	0.70820	0.70771
c	322	896	1.0412+/-3	0.71299+/-2	0.70721	0.70688
d	326	949	0.9954+/-7	0.71287+/-2	0.70734	0.70702
Sg4a	496	599	2.3999+/-7	0.72070+/-2	0.70738	0.70661
b	390	531	2.1262+/-17	0.71598+/-2	0.70417	0.70349
c	362	801	1.3087+/-15	0.71472+/-2	0.70745	0.70703
d	1682	771	6.3192+/-9	0.71514+/-2	0.68004	0.67802
e	369	805	1.3293+/-44	0.71473+/-2	0.70735	0.70692
f	361	821	1.2726+/-9	0.71473+/-2	0.70766	0.70725
g	68	844	0.2324+/-8	0.71329+/-2	0.70714	0.70696
Sg3a	325	849	1.0700+/-1	0.71329+/-2	0.70714	0.70700
b			NOT RUN			
c	417	915	1.3214+/-7	0.71464+/-2	0.70730	0.70688
d	318	809	1.1365+/-9	0.71514+/-2	0.70883	0.70847
e	372	782	1.3761+/-7	0.71514+/-2	0.70750	0.70706
f	323	335	2.7870+/-2	0.71030+/-2	0.69482	0.69393
g	140	696	0.5829+/-4	0.71030+/-2	0.70706	0.70688
h	34	1179	0.0834+/-1	0.70762+/-2	0.70758	0.70713
SgM			NOT RUN			

Table AII.2. Rb/Sr-isotope results obtained for samples removed from four thin slices.

	Mega1	Mega2	Mega3	Mega4	Crypt1	Crypt2	Micro1	Micro2	Micro3	Micro4	MatxK1	MatxK2	MatxK3	MatxK4
SiO_2	64.16	64.24	64.35	63.77	67.48	67.39	68.77	68.50	65.33	65.69	64.585	63.82	63.14	64.50
TiO_2	0.003	0.028	0.030	0.005	0.015	0.014	0.009	0.011	0.001	0.009	0.023	0.017	0.040	0.007
Al_2O_3	18.75	18.85	18.60	18.67	19.39	19.25	18.64	19.55	21.56	21.19	18.79	18.67	18.09	18.60
FeO	0.108	0.069	0.073	0.104	0.069	0.064	0.091	0.067	0.102	0.017	0.067	0.097	0.110	0.062
CaO	0.032	0.051	0.037	0.145	0.100	0.244	0.622	0.727	2.030	1.972	0.018	0.011	0.087	0.037
Na_2O	1.965	1.890	1.646	1.571	11.603	11.026	10.531	11.094	10.450	10.472	1.593	1.365	1.292	1.727
K_2O	14.17	14.13	14.71	14.64	0.444	0.719	0.188	0.275	0.314	0.263	14.97	15.17	15.26	14.294
Σ	99.19	99.28	99.45	98.92	99.11	98.71	98.86	100.22	99.80	99.60	100.06	99.18	98.07	99.22
Si	2.9749	2.9739	2.9807	2.9717	2.9833	2.9741	3.0296	2.9889	2.8814	2.8988	2.9761	2.9719	2.9793	2.9865
Ti	0.0001	0.0010	0.0010	0.0002	0.0005	0.0005	0.0003	0.0004	0.0001	0.0001	0.0008	0.0006	0.0014	0.0003
Al	1.0247	1.0286	1.0155	1.0255	1.0103	1.0094	0.9681	1.0054	1.1205	1.1019	1.0207	1.0247	1.0062	1.0151
Fe	0.0042	0.0027	0.0028	0.0040	0.0047	0.0042	0.0034	0.0024	0.0038	0.0006	0.0026	0.0038	0.0044	0.0018
Ca	0.1766	0.0025	0.0018	0.0072	0.0026	0.0052	0.0294	0.0340	0.0960	0.0933	0.0009	0.0005	0.0043	0.0024
Na	0.1766	0.1696	0.1478	0.1419	0.9945	0.9822	0.8995	0.9385	0.8933	0.8960	0.1423	0.1232	0.1182	0.1551
K	0.8380	0.8346	0.8693	0.8703	0.0250	0.0493	0.0105	0.0153	0.0177	0.0148	0.8801	0.9010	0.9184	0.8443
Σ	5.0200	5.0129	5.0191	5.0215	5.0209	5.0149	4.9411	4.9850	5.0138	5.0055	5.0239	5.0273	5.0345	5.0054
An	0.16	0.25	0.18	0.71	0.46	1.14	8.12	8.44	9.53	9.29	0.09	0.05	0.42	0.18
Ab	17.38	16.85	14.51	13.92	97.09	94.83	90.75	90.01	88.72	89.24	13.90	12.02	11.35	15.49
Or	82.46	82.90	85.31	85.37	2.44	4.03	1.12	1.55	1.76	1.47	86.01	87.92	88.22	84.33

Table AII.1. Table of compositions of feldspars obtained by microprobe analysis, with formula weights based on 8 oxygens.

	MplaR1	MplaR2	MplaR3	MplaR4	MplaR5	MplaR6	MplaC1	MplaC2	MPlaC3	MplaC4	Ipla1	Ipla2	Ipla3
SiO_2	69.42	66.26	68.62	67.92	68.01	68.23	60.24	60.91	61.21	60.63	61.10	61.09	61.28
TiO_2	0.014	0.001	0.023	0.002	0.013	0.001	0.001	0.030	0.028	0.005	0.018	0.006	0.013
Al_2O_3	18.66	21.32	19.09	19.91	19.73	20.15	24.99	24.42	24.63	25.05	24.482	24.16	24.12
FeO	0.093	0.067	0.080	0.065	0.071	0.048	0.236	0.162	0.147	0.205	0.193	0.170	0.150
CaO	1.893	1.680	1.396	1.745	1.811	1.561	6.361	5.819	6.042	6.638	5.756	5.704	5.413
Na_2O	9.458	10.754	9.959	10.112	9.943	10.231	7.533	7.737	7.927	7.506	8.252	8.637	8.563
K_2O	0.123	0.167	0.101	0.199	0.231	0.165	0.696	0.633	0.667	0.697	0.327	0.302	0.351
Σ	99.66	100.25	99.31	99.23	99.81	100.38	100.05	99.711	100.65	100.73	100.13	100.07	99.890
Si	3.0314	2.9030	3.0105	3.0010	3.0092	3.0041	2.6856	2.7177	2.7096	2.6863	2.7148	2.7194	2.7285
Ti	0.0005	0.0001	0.0007	0.0006	0.0005	0.0001	0.0001	0.0010	0.0009	0.0002	0.0006	0.0002	0.0004
Al	0.9602	1.1008	0.9873	0.9891	0.9564	1.0026	1.3135	1.2838	1.2852	1.3079	1.2820	1.2674	1.2656
Fe	0.0034	0.0025	0.0030	0.0021	0.0025	0.0021	0.0088	0.0060	0.0055	0.0076	0.0072	0.0063	0.0056
Ca	0.0886	0.0789	0.0656	0.0801	0.0842	0.0798	0.3038	0.2782	0.2866	0.3151	0.2740	0.2720	0.2582
Na	0.8008	0.9135	0.8472	0.9012	0.8092	0.9054	0.6512	0.6693	0.6804	0.6448	0.7109	0.7455	0.7392
K	0.0069	0.0093	0.0056	0.0101	0.0105	0.0097	0.0396	0.0360	0.0376	0.0394	0.0185	0.0172	0.0199
Σ	4.8919	5.0080	4.9216	4.9842	4.8725	5.0038	5.0026	4.9920	5.0058	5.0013	5.0080	5.0280	5.0174
An	7.14	9.88	7.87	8.51	9.75	7.57	30.55	28.28	28.53	31.53	27.31	26.29	25.38
Ab	92.24	89.35	91.20	90.31	89.00	91.09	65.47	68.06	67.73	64.52	70.85	72.05	72.66
Or	0.77	0.61	0.93	1.19	1.26	1.34	3.98	3.66	3.75	3.94	1.85	1.66	1.96

Table AII.1. (cont.)

The data presented in the text (Chapter 3) may include some rounding errors but these were taken into considerations when the relevant plots were constructed.

(iii) XRF analysis

The XRF major and trace element analyses were carried out using a Phillips PW140 XRF spectrometer. Powders of the granitoid and enclave material analysed (see Chapter 4) were made into either pressed pellets or glass beads for trace- and major-element analysis respectively. The reported error for the machine during the time the samples were run was 1.23% for trace-elements and 94.67% for major-elements. Any trace-elements which were below the detection limit of the machine were ignores and not incorporated into the final interpretation.

(iv) A.A. and A.E. analysis

The pure mineral separates were weighed and dissolved into HF and HNO_3. They were then taken to dryness and made into solutions for analysis with dilute HNO_3. These were then run through the Thermo-Jarrel Ash flame spectrophotometer and compared against standard solutions to give the concentrations of Be and Al which were both run on absorption mode (A.A.). The determination of the Li-isotopic ratios and concentrations required a more complex method and were run on emission mode (A.E.).

A series of standard solutions of different isotopic mixtures and ppm concentrations were first run to calibrate the A.E. machine. Although drift will cause the change in emission values over time, the ratio of the emission shifts for the different isotopic solutions will remain constant. The fact that ^{6}Li has a higher emission spectrum than ^{7}Li (Zadiel and Korrenoi 1961; Manning and Slavin 1962) enables the detection of isotopic differences in the sample. Once the isotopic emission shift ratios are known for the machine, only one isotopic standard, in this case 90% ^{7}Li (or a 0.1111 $^{6}Li/^{7}Li$ ratio solution) need be used. Other isotopic ratios can be calculated based on the emission shift ratios. **Table AII.3** shows the emission values for the different standards and **Figure AII.1** shows the linear calibration lines for these standards.

Li (ppm)	100%7Li	90%7Li	80%7Li	50%7Li	100%6Li
0.5	1.423	1.460	1.488	1.558	1.692
1.0	2.768	2.881	2.917	3.126	3.290
1.5	3.986	4.152	4.228	4.510	4.650
2.0	5.010	5.243	5.408	5.740	5.816
2.5	5.926	6.205	6.412	6.794	6.822
Li (ppm) conversion	90:100%7Li 1.0404	90:90%7Li 1.0000	80:90%7Li 0.97761		50:90%7Li 0.92121

Table AII.3. Table showing the emission values for the standard solutions used to calibrate the A.E. spectrophotometer for Li-isotope analysis and the ratios which are used to construct new calibration graphs as required.

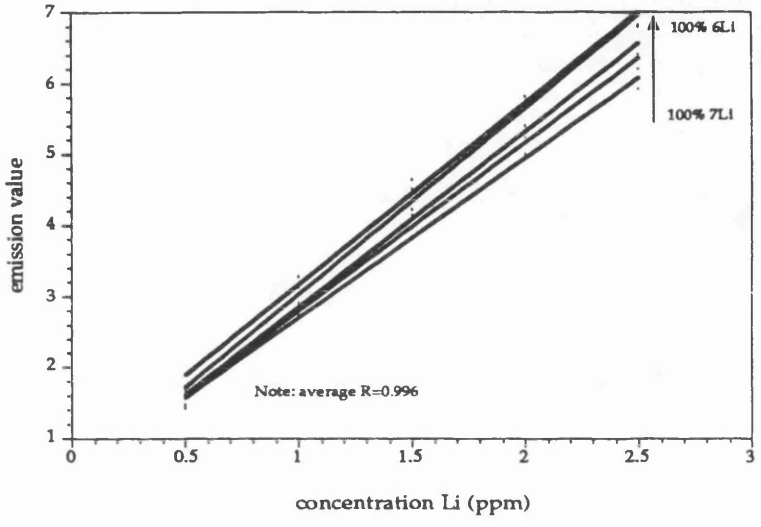

Figure AII.1. Li-concentrations against emission values for the different isotopic standards.

The graph above shows that with increasing ^{6}Li% in the standards a correspondingly higher gradient to the calibration line occurs. At >50% ^{6}Li% the gradients of the calibration lines become too close to accurately determine. Thus, this method cannot resolve the isotopic compositions of samples which contain >50% ^{6}Li. The gradients of the calibration lines are plotted on a graph against isotopic ratio and a polynomial curve is then fitted (**Figure AII.2**). The formula for this curve can then be used to calculate the gradient for every isotopic composition from 100% ^{7}Li (or a $^{6}Li/^{7}Li$ ratio of 0) to 50% ^{6}Li(or a $^{6}Li/^{7}Li$ ratio of 1). These can then be plotted on to a suitable calibration standard graph. The emission value for the samples then measured along with a second emission value for the same samples but at 50% dilution. The two emission values can then be plotted any of the calibration lines. If the two values give ppm concentrations which are exactly 50% of each other then the sample must have the isotopic composition of the chosen calibration line. More

likely however, the sample will have a shift in concentration which is caused by the samples having a different isotopic mixture and thus, a different emission value. Thus, by trail and error the isotopic composition of the sample can be determined.

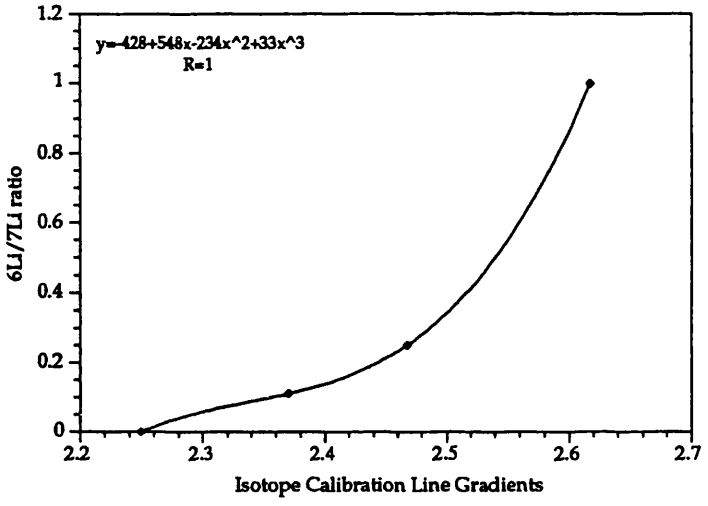

Figure AII.2. Li-isotopic ratios against calibration line gradients from **Figure AII.1**, with a fitted polynomial curve.

The emission values for the mineral separates are shown in **Table AII.4** along with the isotopic compositions and Li-concentrations. The 90% Li calibration lines are also shown. These were used in conjunction with the conversion ratios shown in **Table AII.3** to construct new calibration graphs to compensate for natural shift in the emission reading of the machine. The emissions shown are averages of at least three readings.

Sample	Ist reading	2nd reading (x0.5)	Error%	%^{6}Li	ppm
Biotite1	6.522+/-0.08	3.873	1.227	28.5	927
Biotite2	6.537+/-0.09	4.003	1.377	28.0	968
K-matrix	7.061+/-0.102	4.368	1.444	4.5	50
Mega-core	2.126+/-0.03	1.192	1.411	31.0	15
Mega-rim	2.272+/-0.03	1.270	1.320	17.0	17
Qtz1	4.608+/-0.04	2.505	0.868	14.0	34
Qtz2	4.397+/-0.05	2.457	1.371	19.5	32
Plag	2.872+/-0.03	1.648	1.044	18.5	20

Li(ppm)	Calibration 1	Calibration 2	Calibration 3
0.5	1.628	1.609	1.590
1.0	3.284	3.292	3.233
1.5	4.723	4.695	4.611
2.0	5.977	5.914	5.814
2.5	7.031	6.988	6.854

Table AII.4. Emission values for the samples measured and the 90%7Li calibrations.

The errors show a maximum of 1.444% of the emission values but in reality the isotopic compositions of the samples could only be accurately matched to an isotopic value with a plus or minus 2.5% ^{6}Li error as the two emission values gave a 5% range of possible ^{6}Li%-compositions on any of the calibration graphs constructed. Therefore, the technique showed only the variation in the ^{6}Li-compositions in the minerals which were caused by fractionation as a result of an increase in the H_2O-content of the magma, which can be up to 25% (Morozova and Alferofsky 1974).

References

Ahrens, L. H.; Liebenberg, W. R. (1945): Lithium in mica and feldspar. Trans. Geol. Soc. S. A. 68, 75-83.

Allegre, J. C.; Provost, A.; Jaupart, C. (1981): Oscillatory zoning: a pathological case of crystal growth. Nature, 294, 223-228.

Anderson, A. T. Jnr. (1984): Probable relations between zoning and magma dynamics, Fuego Volcano, Guatemala. Amer. Min., 69, 660-676.

Balducci, S.; Leoni, L. (1981): Sanidine megacrysts from M. Amiata trachytes and Roccastrada rhyolites. Neus Jarbh. Mineral. Abh., 143, 15-36.

Bailey, J.C. (1984): Geochemistry and origin of hornblende-bearing xenoliths in the I-type Petford Granite, north-east Queensland. Aust. J. Earth. Sci., 31, 7-23.

Balsiger, H.; Geiss J.; Groegler, N. (1968): Distribution and abundance of lithium in stone meteorites. Earth. Planet. Sci. Lett. 5, 17-22.

Barbarin, B. (1990): Granitoids: main petrogenetic classifications in relation to origin and tectonic setting. Geol. Jour., 25, 227-238.

Barth (1961): reported in, **Smith, J.V. (1974):** Feldspar Minerals, Vol. 2. Chemical and Textural Properties. Springer-Verlag, Berlin.

Boettcher, A.L; Pinwinskii, A.J.; Knowles, C.R. (1967): Zoned potash feldspars from the Rainy Creek complex near Libby, Montana. Earth Planet. Sci. Lett., 3, 8-10.

Booth, B. (1968): Petrogenetic significance of alkali feldspar megacrysts and their inclusions in Cornubian granites. Nature, 217, 1036-1038.

Bott, M. H. P. (1974): The geological interpretation of a gravity survey of the English Lake District and Vale of Eden. J. Geol Soc. Lond. 130, 309-331.

Bott, M. H. P. (1978): Deep structure: in, The Geology of the Lake District. Yorks. Geol. Soc. Occasional Pub. No. 3.

Boulter, C. A.; Soper, N. J. (1973): Structural relationships of the Shap granite. Proc. Yorks. Geol Soc. 34, 331-342.

Branney, M. J.; Soper, N. J. (1988): Ordovician volcano-tectonics in the English Lake District. J. Geol. Soc. Lond., 145, 367-376.

Bringham, R.H., (1984): K feldspar genesis and stable isotope relations of the Papoose Flat Pluton, Inyo Mountains, California. Unpubl. Ph. D. thesis, Stanford Univ.

Brown, P. E.; Miller, J. A.; Soper, N. J. (1964): Age of the principal intrusions of the Lake District. Proc. Yorks. Geol. Soc., 34, 331-342.

Brown, W. L.; Parsons, I. (1988): Zoned ternary feldspars in the Klokken intrusion: exsolution microtextures and mechanisms. Contrib. Min. Pet., 98, 444-454.

Brown, W. L.; Parsons, I. (1989): Alkali feldspars: ordering rates, phase transformations and behaviour diagrams for igneous rocks. Min. Mag., 53, 25-42.

Cameron, E. N.; Jahns, R. H.; McNair, A. H.; Page, L. R. (1949): Internal structure of granitic pegmatites. Econ. Geol. Monograph., 2, 115.

Cannon, R.T. (1962): The genesis of the Bartica assemblage, British Guiana. Geol. Mag., 99, 164-172.

Cantagrel, J. M.; Didier, J.; Gourgaud, A. (1984): Magma mixing: origin of intermediate rocks and enclaves from volcanism to plutonism. Phys. Earth. Planet. Intern., 35, 63-76.

Castro, A.; Moreno Ventas, I.; De la Rosa, J.D. (1990): Microgranular enclaves as indicators of hybridisation processes in granitoid rocks, Hercynian belt, Spain. Geological Journal, 25, 391-404.

Castro, A.; Moreno Ventas, I.; De la Rosa, J.D. (1991): H(Hybrid)- type granitoids: a proposed revision of the granite type classification and nomenclature. Earth Sci. Reviews, 31, 1-17.

Cerny, P.; Chapman, R. (1984): Paragenesis, chemistry and structural state of adularia from granitic pegmatites. Bull. de Mineralogic, 107, 369-384.

Cherniak, D.J.; Watson, E.B. (1992): A study of strontium diffusion in K feldspar, Na K feldspar and anorthite using Rutherford Backscattering Spectroscopy. Earth Planet. Sci. Lett., 113, 411-425.

Clark, A. H.; Pearce, T. H.; Roeder, P. L.; Wolfson, I. (1986): Oscillatory zoning and other microstructures in magmatic olivine and augite: Normarski interference contrast observations on etched polished surfaces. Amer. Mineral., 71, 734-741.

Clark, L (1964): The Borrowdale Volcanic Series between Buttermere and Wasdale, Cumberland. Proc. Yorks. Geol. Soc., 34, 343-356.

Compston, W.; McDougall, I.; Wyborn D. (1982): Possible two stage ^{87}Sr evolution in the Stockdale Rhyolite. Earth. Planet. Sci. Lett., 61, 297-302.

Day, H. W.; Fenn P. W. (1982): Estimating the P-T-X_{H_2O} conditions during crystallisation of low calcium granites. Jour. Geol., 90, 485-508.

Debat, P.; Soula, J.-C.; Kubin, L.; Vidal, J.-L. (1978): Optical studies of natural deformation microstructures in feldspars (gneiss and pegmatites from Occitania, southern France). Lithos, 11, 133-145.

Deer, W.A.; Howie, R.A.; Zussman, J. (1992): Rock forming minerals. Longman, London, pp. 1-919.

Dempster, T. J.; Jenkin, G. R. T.; Rogers, G. (1994): The origin of Rapakivi Texture. (in press).

Deubner, J.; Sternitzke, M.; Muller, G. (1991): Feldspars Malsi308 (M=H, Li, Ag) synthesis by low-temperature ion-exchange. Amer. Min., 76, 1620-1627.

Didier, J. (1973): Granites and their enclaves. Elsevier, Amsterdam.

Didier, J. (1987): Contribution of enclave studies to the understanding of origin and evolution of granitic magmas. Geologische Rundschau, 76(1), 41-50.

Dujon, S.; Lagache, M.; Sebastian, A. (1991): Experimental study of Li-rich granitic pegmatites. 3: Thermodynamic implications of the experiments in the Na-Li-Cs system: Consequences for the properties of solutes. Amer. Min., 76, 1614-1619.

Dutrow, B,; Holdaway, M. J.; Hinton, R. W. (1986): Li in staurolite and its petrologic significance. Contrib. Min. Pet., 94, 496-506.

Dutrow, B. (1991): The effects of Al and vacancies on Li substitution in Iron staurolite: A synthesis approach. Amer. Min., 76, 42-48.

Eberz, G.W.; Nicholls, I.A. (1990): Chemical modification of enclave magma by post emplacement crystal fractionation, diffusion and metasomatism. Contrib. Min. Pet., 104, 47-55.

Ellis, A. J.; Mahon, W. A. J. (1964): Natural Hydrothermal systems and experimental hot-water/rock reactions. Geo. et Cosmo. Acta., 28, 1323-1358.

Exley, C.S.; Stone, M. (1964): The granitic rocks of south west England. Trans R. Soc. Cornwall, 131, 131-184.

Farrand, M. G. (1960): Trace elemnets across four xenoliths. Geol. Mag., 97, 488-493.

Faure, G. (1986): Principles of Isotope Geology. J.Wiley & Sons, Chichester.

Fenn, P. M. (1977): The nucleation and growth of alkali feldspars from hydrous melts. Can. Mineral., 15, 135-161.

Firman, R. J. (1957): Fissure metasomatism in volcanic rocks adjacent to the Shap granite, Westmorland. Quat. J. Geol Soc. Lond., 113, 205-221.

Firman, R. J. (1978): Intrusions: in, The Geology of the Lake District. Yorks. Geol. Soc. Occasional Pub. No. 3.

Forland (1972): reported in, **Smith, J.V. (1974):** Feldspar Minerals, Vol. 2. Chemical and Textural Properties. Springer-Verlag, Berlin.

Flood, R.H.; Vernon, R.H. (1988): Microstructural evidence of orders of crystallization in granitoid rocks. Lithos, 21, 237-245.

Flood, T. P.; Schuraytz, B. C.; Vogel, T. A. (1988): Magma mixing due to disruption of a layered magma body. J. of Volcan. Geotherm. R., 36, 241-255.

Fourcade, S.; Allégre, C.J. (1981): Trace elements behavior in granite genesis: A case study the calc alkaline plutonic association from the Querigut Complex (Pyrénées, France). Contrib. Min. Pet., 76, 177-195.

Fuhrman, M. L.; Lindsley, D. (1988): Ternary-feldspar modeling and thermometry. Amer. Min., 73, 201-215.

Giletti, B.J. (1991): Rb and Sr diffusion in alkali feldspars, with implications for cooling histories of rocks. Geo. et Cosmo. Acta, 55, 1331-1343.

Grantham, D.R. (1926): The petrology of the Shap Granite. Proc. Geol Assoc., 39, 299-331.

Gribble, C.D.; Hall A. J. (1985): A Practical Introduction to Optical Mineralogy. George, Allen and Unwin, London.

Hall, A. (1987): Igneous Petrology. Longman, Singapore.

Hall, A.; Jarvis, K. E.; Walsh, J. N. (1993): The variation of cesium and 37 other elements in the Sardinian granite batholith, and the significance of cesium for granite ptrogenesis. Contrib. Min. Pet., 114, 160-170.

Harker, A.; Marr, J.E. (1891): The Shap Granite, and associated igneous and metamorphic rocks. Q. J. Geol. Soc. Lond., 47, 266-328.

Heald, M.T. (1950): Structure and petrography of the Lovewell Mountain Quadrangle, New Hampshire. Bull. Geol Soc. Amer., 61, 43-89.

Hibbard, M.J. (1991): Textural anatomy of twelve magma mixed granitoid systems. In: Enclaves in granite petrology. Elsevier, Amsterdam.

Hibbard, M.J.; Watters, R.J. (1985): Fracturing and diking in incompletely crystallized granitic plutons. Lithos, 8, 1-12.

Hogan, J. P. (1993): Monomineralic megacrysts: Textural evidence for mineral resorption during crystallization of igneous rocks. J. Geol., 101, 531-540.

Holden, P.; Halliday, A. N.; Stephens, W. E. (1987): Neodymium and strontium isotope content of microdiorite enclaves points to mantle input to granitoid production. Nature, 330, 53-56.

Holden, P.; Halliday, A. N.; Stephens, W. E.; Hennev, P. J. (1991): Chemical and isotopic evidence for major mass-transfer between mafic eclaves and felsic magma. Chem. Geol., 92, 135-152.

Houghton, H. F. (1980): Refined techniques for staining plagioclase and alkali feldspars in thin section.

Hutchison, C. S. (1974): Laboratory Handbook of Petrographic Techniques. Wiley, New York.

Jans, R. H.; Tuttle, O. F. (1963): Layerd pegamtite-aplite intrusions. Special Paper, Min. Soc. Amer., 1, 78-92.

Johannes, W. (1980): Metastable Melting in the Granite System Qz-Or-Ab-An-H_2O. Contrib. Min. Pet., 72, 73-80.

John, B. E.; Blundy, J. D. (1993): Emplacement-related strain deformation of granitoid magmas, southern Adamello Massif, Italy. Geol. Soc. Amer. Bull., 105, 1517-1541.

Kawachi, Y.; Sato, T. (1978): Orthoclase megacrysts in the Yakushima granite, southern Kyushu, Japan. Neus Jahrb. Mineral. Abh., 132, 136-152.

Keith, H. D.; Tuttle, O. F. (1952): Significance of variation in the high-low inversion of quartz. Amer. Jour. Sci., (Bowen Vol.), 203-224.

Kleeman, A.W. (1937): The nature and origin of the so-called diorite inclusions in the granite of the Granite Island. Trans. R. Soc. S. Aust., 61, 207-220.

Kroll, H.; Knitter, R. (1991): Al, Si exchange kinetics in sanidine and anorthoclase and modeling of rock cooling paths. Amer. Min., 76, 928-941.

Laves, F. (1952): Phase relations of the alkali feldspars. Jour. Geol., 59, 436-441.

Langmuir, C.; Vocke, R.D.; Hanson, G. N. (1978): A general mixing equation with applications to Icelandic basalts. Earth. Planet. Sci. Lett., 37, 380-392.

Le Bas, M.J. (1982): The Caledonian granites and diorites of England and Wales. Igneous rocks of the British Isles. Wiley, Chichester.

Lee, M. K. (1984): The three-dimensional form of the Lake district granite batholith. Investigation of the geothermal potential of the U.K. British Geological Survey, Edinburgh.

Luth, W. C.; Jahns, R. H.; Tuttle, O. F. (1964): The granite system at preassures of 4 to 10 kilobars. J. of Geophy. R., 69, 759-773.

MacKenzie, W. S.; Donaldson, C. H.; Guilford, C. (1987): Atlas of igneous rocks and their textures. Longman, New York.

Manning, D. C. and Slavin, W. (1962): Lithium isotope analysis by atomic absorption spectrophototmetry. At. Absorption Newsletter, Perkin-Elmer Corp., 8, 1-5.

Mariano, A. N.; Ito, J.; Ring, P. J. (1973): Cathodoluminescence of plagioclase feldspars. Geol. Soc. Amer. Abastracts. 5, 726.

Mariano, A. N.; Roeder, P. L. (1983): Kerimasi: a neglected carbontite volcano. J. of Geol., 91, 449-455.

Marshall, D.J. (1988): Cathodoluminescence of geological materials. Unwin Hyman, Boston, pp. 1-145.

Mason, R. A. (1982): Trace element distributions between the perthite phases of alkali feldspars from pegmatites. Min. Mag., 45, 101-106.

McCarthy, T.S.; Cawthorn, R.G. (1980): Changes in initial 87Sr/86Sr ratio during protracted fractionation of igneous complexes. J. of Petrol., 21, 245-264.

Mehnert, K.R. (1968): Migmatites. Elsvier, Amsterdam.

Mehnert, K.R.; Busch, W. (1981): The Ba content of K feldspar megacrysts in granites: a criterion for their formation. Neus Jarbh. Mineral. Abh., 140, 221-252.

Millward, D.; Moseley, F.; Soper, N. J. (1978): The Eycott and Borrowdale volcanic rocks: in, The Geology of the Lake District. Yorks. Geol. Soc. Occasional Pub. No. 3.

Mineral Powder Diffraction File, (Minerals) Data Book (1980): J. C. P. D. S. International Centre for Diffraction Data, Pennsylvania.

Morozova, I. M.; Alferovski, A. A. (1974): Fractionation of lithium and potassium isotopes in geological processes. Geokhimia. 1, 30-38.

Moseley, F. (1978): The Geology of the English Lake District, An introductory Review: in, The Geology of the Lake District. Yorks. Geol. Soc. Occasional Pub. No. 3.

Moseley, F. (1983): The Volcanic Rocks of the Lake District. MacMillan, London.

Mysen, B. (1992): Peralkalinity, Al-Si substitution, and solubility mechanisms of H_2O in aluminosilicate melts. Jour. of Petrol., 33, 347-375.

Newbury, D. E.; Joy, D. C.; Echlin, P.; Fiori, C. E.; Goldstein, J. I. (1987): Adavanced Scanning Electron Microscopy and X-ray Microanalysis. Plenum, New York and London.

O'Brien, C. (1985): The geochemisry, metasomatism nad petrogenesis of the granites of the English Lake District. J. Geol. Soc. Lond., 142, 1139-1157.

Ono, A. (1982): Quartz solid solution in the system Li_2O-Al_2O_3-SiO_2-H_2O. J. of Japan. Assoc. of Miner., Petrol. and Econ. Geologists, 74, 417-420.

Parsons, I. (1978): Feldspars and fluids in cooling plutons. Min. Mag., 42, 1-17.

Paterson, S. R.; Vernon, R. H.; Tobisc, O. T. (1989): A review of criteria for the identification of magmatic and tectonic foliations in granitoids. J. of Struc. Geol., 11, 349-363.

Pearce, T.H.; Clark, A. H. (1989): Normarski interference contrast observations of textural details in volcanic rocks. Geology, 17, 757-759.

Perrin, R. (1954): Granitization, metamorphism and volcanism. Amer. J. Sci., 252, 449-465.

Pin, C. (1991): Sr-Nd isotopic study of ineous and metasedimentary enclaves in some Hercynian granitoids from the Massive Central, France. In: Enclaves in granite petrology. Elsevier, Amsterdam.

Pitcher, W.S.; Berger, A.R. (1972): The geology of Donegal: a study of garnite emplacement and unroofing. Wiley, New York.

Pitcher, W. S. (1991): Synplutonic dykes and mafic enclaves. In: Enclaves in granite petrology. Elsevier, Amsterdam.

Poli E. G.; Tommasini, S. (1990): Model for the Origin and Significance of Microgranular Enclaves in Calc-alkaline Granitoids. Jour. of Petrol., 32, 657-666.

Putnis, A.; Fernandez-Diaz, L.; Prieto, M. (1992): Experimentally produced oscillatory zoning in the (Ba, Sr)SO_4 solid solution. Nature, 358, 743-745.

Read, H.H. (1942): Rocks showing feldspar porphyroblasts and nodes from Unst, Shetland. Proc. Geol Assoc., 53, 107.

Read, H.H. (1957): The Granite Contoversy. Murby, London.

Rollinson, H. (1993): Using geochemical data: evalution, presentation, interpretation. Longman, New York.

Rundle, C. C. (1979): Ordovician intrusions in the English Lake District. J. Geol. Soc. Lond., 136, 29-38.

Smith, J. V.; Brown, W. L. (1988): Feldspar minerals, Vol. 1. Springer, New York.

Smith, J.V. (1974): Feldspar Minerals, Vol. 2. Chemical and Textural Properties. Springer-Verlag, Berlin.

Smithson, S.B. (1962): Symmetry relations in alkali feldspars of some amphibole facies rocks from the southern Norway Precambrian. Norsk Geol. Tidsskr., (Feldspar Volume) 42.

Soper, N. J.; Moseley, F. (1978): Structure: in, The Geology of the Lake District. Yorks. Geol. Soc. Occasional Pub. No. 3.

Spears, D. A. (1961): The distribution of alpha radioactivity in a specimen of Shap granite. Geol Mag., 68, 483-487.

Stimac, J. A. ; Wark, D. A. (1992): Plagioclase mantles on sanidine in silicic lavas, Clear Lake, California: Implications for the origin of rapakivi texture. Bull. Geol. Soc. Am., 104, 728-744.

Stolper, E. (1982): The speciation of water in silicate melts. Geo. et Cosmo. Acta., 46, 2609-2620.

Stone, M.; Austin, G.C. (1961): The metasomatic origin of the potash feldspar megacrysts in the granites of Southwest England. J. Geol., 69, 464-472.

Svec, H. J.; Anderson A. R. Jnr (1965): The absolute abundance of the lithium isotopes in natural sources. Geo. et Cosmo. Acta., 29, 633-641.

Sylvester, A.G. (1964): The Precambrian rocks of the Telmark area in south central Norway, III. Geology of the Vardal granite. Norsk Geol. Tidsskr., 44, 445-482.

Swanson, S.E. (1977): Relation of nucleation and crystal growth to the development of granitic structures. Amer. Min., 62, 966-978.

Taylor, H. P.; Epstein, S. (1963): $^{18}O/^{16}O$ ratios in rocks and coexsisting minerals of the Skaergaard Intrusion, East Greenland. J. of Petrol., 4, 51-74.

Taylor, H. P.; Sheppard, S. M. F. (1986): Processes of isotopic fractionation and isotope systematics. Rev. in Min., 16, 227-271.

Taylor, H. P. Jnr. (1968): The oxygen isotope geochemisry of igneous rocks. Contrib. Min. Pet., 19, 1-17.

Taylor, T. I.; Urey, H. C. (1938): Fractionation of the lithium and potasium isotopes by chemical exchange with zeolites. J. Chem. Phy. 6, 429-438.

Thomas, H.H.; Smith, W.C. (1932): Xenoliths of igneous origin in the Tregastel-Ploumananac'h Granite, Cotes du Nord, France. Q. J. Geol. Soc. Lond., 88, 274-296.

Thirlwall, M. F.; Fitton, J. G. (1983): Sm-Nd garnet age of the for the Ordovician Borrowdale Volcanic Group, English Lake District. J. Geol. Soc. Lond., 140, 511-518.

Turner, F.J.; Verhoogan, J. (1960): Igneous and Metamorphic Petrology. McGraw-Hill, New-York, N.Y.

Tuttle, O. F.; Bowen, P. (1958): Origin of granite in the light of experimental studies in the system $NaLaSi_3O_8$-$KAlSi_3O_8$-SiO_2-H_2O. Mem. Geol. Soc. Amer., 74, 153.

Valley, J. W.; O'Neil, J. R. (1984): Fluid heterogeneity during granulite facies

metamorphism in the Adirondacks: stable isotope evidence. Contrib. Min. Pet., 85, 158-173.

Vernon, R.H. (1968): Microstructures of high grade metamorphic rocks at Broken Hill. Australian J. Petrol., 9, 1-22.

Vernon, R.H. (1983): Restite, xenoliths and microgranitoid enclaves in granites. J.Proc R. Soc. N.S.W., 116, 77-103.

Vernon, R.H. (1986): K feldspar megacrysts in granites Phenocrysts, not porphyroblasts. Earth Sci. Reviews, 23, 1-63.

Wark, D. A.; Stimac, J. A. (1992): Origin of mantled (rapakivi) feldspars: experimental evidence of a dissolution- and diffusion-controlled system.

Wadge, A. J.; Gale, N. H.; Beckinsale, R. D.; Rundle, C. C. (1978): A Rb-Sr isochron for the Shap granite. Proc. Yorks. Geol. Soc., 42, 297-305.

Wedepohl, K. H. (1978): Handbook of Geochemistry, (II-1, H-Al). Springer-Verlag, Berlin.

Whitney, J.A. (1975): The effects of pressure, temperature, and X_{H2O} on phase assemblages in four synthetic rock compositions. J. Geol., 83, 1-31.

Whitney, J.A. (1988): The origin of granite: The role and source of water in the evolution of granitic magmas. Bull.Geol.Soc.Amer., 100, 1886-1897.

Wintsch, R.P. (1975): Feldspathization as a result of deformation. Bull. Geol. Soc. Amer., 86, 35-38.

Worden, R. H.; Walker, D. F.; Parsons, I.; Brown, W. L. (1989): Developement of microporosity, diffusion channels and deuteric coarsening in perthitic alkali feldspars. Contrib., Min., Pet., 104, 507-515.

Yardley, B. W. D. (1989): An Introduction to Metamorphic Petrology. Longman, New York.

York, D. (1967): The best isochron. Earth Planet.Sci.Lett., 2, 479-482.

York, D. (1969): Least squares fitting of a straight line with correlated errors. Earth Planet.Sci.Lett., 5, 320-324.

Zaidel, A. N.; Korennoi, E. P. (1961): Spectral determination of the isotope composition and concentration of lithium in solutions. Opt. Spectry., 10, 299-302.